

DESIGN AND FABRICATION OF HIGH CAPACITY LITHIUM-ION  
BATTERIES USING ELECTRO- SPUN GRAPHENE MODIFIED VANADIUM  
PENTOXIDE CATHODES.

A Thesis

Submitted to the Faculty

of

Purdue University

by

Amirhossein Ahmadian

In Partial Fulfillment of the

Requirements for the Degree

of

Master of Science in Mechanical Engineering

August 2019

Purdue University

Indianapolis, Indiana

**THE PURDUE UNIVERSITY GRADUATE SCHOOL**  
**STATEMENT OF COMMITTEE APPROVAL**

Dr. Mangilal Agarwal, Chair

Department of Mechanical and Energy Engineering

Dr. Jian Xie

Department of Mechanical and Energy Engineering

Dr. Hamid Dalir

Department of Mechanical and Energy Engineering

**Approved by:**

Dr. Sohel Anwar

Chair of the School Graduate Program

To my parents and my sister.

## ACKNOWLEDGMENTS

I would like to extend my sincerest gratitude to my advisor Prof. Mangilal Agarwal for his supervision, enthusiastic support, and many valuable suggestions and comments throughout my masters study and related research. Completion of this work would not have been possible without the support and nurturing of Prof. Mangilal Agarwal.

My sincere thank also goes to Prof. Jian Xie as my thesis committee member and Dr. Yadung Liu. As both provided me an opportunity to join their weekly brainstorming meetings and who gave access to research facilities.

Besides that, I would like to thank the rest of my thesis committee: Dr. Dalir and Dr. Nejat for their perceptive comments which encouraged me to broaden my research from various perspectives.

Also, my sincere thank goes to Dr. Chini, as my University of Tehrans advisor, for his selfless effort through the course of my masters degree at the University of Tehran. Also, my best wishes go to Integrated Nano-systems Development Institute (INDI) and its director, Prof. Mangilal Agarwal, that provided me an opportunity to join their team as a research assistant, and who gave access to laboratories and research facilities.

My thanks are also due to all the colleagues who provided me with a friendly and enjoyable working environment. In particular, I am grateful to Dr. Nojan Aliahmad for supporting me throughout the course of this study.

Last but not least, I am grateful to my family: my dear parents, Prof. Alireza Ahmadian and Mehrandokht Emamnayeri, to my precious sister, Hanieh, and to my kind-hearted grandmother and grandfather, Esmat Dehghan and Hedayat Emam, for supporting me spiritually throughout writing this thesis and throughout every step of my life.

## TABLE OF CONTENTS

	Page
LIST OF FIGURES . . . . .	viii
ABSTRACT . . . . .	xi
1 INTRODUCTION . . . . .	1
1.1 Lithium-ion Batteries . . . . .	1
1.1.1 A Review on Lithium-ion Batteries and Current Battery Technologies . . . . .	1
1.1.2 Theory . . . . .	2
1.1.3 Lithium-ion Batteries Electrochemical Process . . . . .	5
1.2 Vanadium Oxides as a Cathode Material . . . . .	9
1.2.1 Vanadium Pentoxide $V_2O_5$ . . . . .	14
1.2.2 Hydrated Vanadium Pentoxide Synthesis ( $V_2O_5 \cdot nH_2O$ ) . . . . .	18
1.2.3 Graphene Modified Vanadium Pentoxide Prepared Through Sol-gel Synthesis . . . . .	22
1.3 Electrospinning . . . . .	25
1.3.1 Overview of Nano-fiber Bundles Fabrication Methods and Electrospinning . . . . .	25
1.3.2 Review on Electrospinning and Electrostatic Phenomenon . . . . .	26
1.3.3 Electrospinning Categories . . . . .	27
1.3.4 Electrospinning Process and Principles . . . . .	28
1.3.5 Fiber Deposition . . . . .	31
1.4 Solution-based Electrospinning and Related Effective Parameters . . . . .	31
1.4.1 Concentration . . . . .	33
1.4.2 Solvent . . . . .	35
1.4.3 Voltage and Electric Field . . . . .	36
1.4.4 Flow Rate . . . . .	36

	Page
1.4.5	Collecting Distance . . . . . 37
1.4.6	Polarity . . . . . 37
1.4.7	Humidity . . . . . 37
1.4.8	Temperature . . . . . 38
1.5	Common Polymers in Electrospinning . . . . . 38
1.6	Applications of Electrospinning and its Role in Energy Storage Systems 39
1.6.1	Electro-spun Vanadium Pentoxide . . . . . 42
2	EXPERIMENTAL . . . . . 43
2.1	Optimized Sol-gel Synthesis of Vanadium pentoxide ( $V_2O_5$ ) Suitable for Electrospinning . . . . . 43
2.2	Fabrication and Formation of Nanostructured $V_2O_5/GO$ Hybrid . . . . 43
2.3	Centrifuging . . . . . 45
2.4	Synthesis of $V_2O_5/GO$ Mixed with Polymer . . . . . 47
2.5	Electrospinning . . . . . 47
2.6	Thermal annealing . . . . . 50
2.7	Electrode Fabrication . . . . . 51
2.8	Battery Assembly . . . . . 53
2.9	Cell Testing . . . . . 55
3	RESULTS AND DISCUSSION . . . . . 57
3.1	Fabrication of a Polymerized Nanostructured $V_2O_5/GO$ Hybrid for Electrospinning . . . . . 57
3.2	Morphology of Electro-spun Fibers . . . . . 61
3.3	Vanadium Oxide-based Cathode and Lithium Cells . . . . . 70
3.4	Electrochemical Characterization . . . . . 71
3.4.1	Galvanostatic Charging/Discharging Curves . . . . . 71
3.4.2	Coulombic Efficiency . . . . . 72
3.4.3	TGA Analysis . . . . . 75
3.4.4	Mercury Porosimetry . . . . . 76
3.4.5	BET Specific Surface Area . . . . . 79

	Page
3.4.6 XRD Analysis . . . . .	79
4 CONCLUSION . . . . .	81
5 FUTURE RECOMMENDATION . . . . .	83
REFERENCES . . . . .	84

## LIST OF FIGURES

Figure	Page
1.1 Ragone chart of specific power vs. specific energy in different battery types vs. different current rates [7]. . . . .	2
1.2 Schematic of a typical Li-ion battery in action [21]. . . . .	6
1.3 Electrode reactions in the most common Li-ion cell [13]. . . . .	6
1.4 Schematic of the electrochemical process within a Li-ion battery [13]. . . . .	7
1.5 The colorful oxidation states of vanadium from lowest oxidation state to highest oxidation states. . . . .	11
1.6 Vanadium species coordination geometries [35]. . . . .	13
1.7 Pourbaix diagram of vanadium species [36]. . . . .	14
1.8 Crystal structure of $V_2O_5$ . . . . .	16
1.9 Comparison of specific capacity and capacity retention of vanadium-oxide based. cathode materials as a function of cycle count and current density with our proposed method [39, 59–75]. . . . .	21
1.10 Molecular structures of graphene, GO, and rGO [78]. . . . .	22
1.11 TEM images of the frozen $HVO_3$ and $HVO_3/GO$ solutions in different aging timings. 1) $HVO_3$ : (a) 0 min, (b) after 1 h, (c) after 1 h 30 min and (d) after 2 weeks. 2) $HVO_3/GO$ : (e) after 30 min, (f) after 2 h, (g) after 6 h and (h) after 3 weeks [39]. . . . .	24
1.12 Nanofiber bundles. . . . .	26
1.13 General electrospinning setup. . . . .	28
1.14 Deformations of the prolate droplet and Taylor cone by increasing the electric field captured in different timings and ultimately, the formation of the jet [114]. . . . .	30
1.15 (a) solid beads vs.(b) porous beads produced by electrospinning [147]. . . . .	35
2.1 Ion-exchange column for vanadium pentoxide synthesis. . . . .	44
2.2 Yellowish $HVO_3$ solution, which brings about $V_2O_5$ formation. . . . .	44
2.3 Dark brown bath sonicated GO (2%) dispersed in $HVO_3$ solution. . . . .	45

Figure	Page
2.4 Dark red 2 weeks old $V_2O_5/GO$ : signifying the completion of the formation of a 3D network of $V_2O_5$ hydrogel. . . . .	46
2.5 Dark brown $V_2O_5/GO + PVA$ hybrid. . . . .	47
2.6 Electrospinning setup. . . . .	48
2.7 Solution inside the BD 10 ml syringe with a needle gauge size of 25G. . . . .	48
2.8 Electro-spun [ $V_2O_5/GO + PVP$ ] (0.45:4). . . . .	49
2.9 Final electro-spun [ $V_2O_5/GO + PVA$ (3:20 in water)] (10:4). . . . .	50
2.10 Annealed electro-spun $V_2O_5/GO + PVA$ (0.25g) at 400 °C . . . . .	51
2.11 Blade coated cathode material on Aluminum foil with a thickness of 30-35 $\mu m$ under IR light for 2-3 hours. . . . .	54
2.12 Arbin BT2000 battery cycle general setup. . . . .	56
3.1 Left Picture: $V_2O_5$ hydrogel PH level before mixing with GO Right Picture: $V_2O_5$ hydrogel PH level after mixing with GO. . . . .	58
3.2 Dark brown bath sonicated GO (2%) dispersed in $HVO_3$ solution. . . . .	58
3.3 Dark red $V_2O_5/GO$ after 2 weeks of aging bringing about the formation of completed network of $V_2O_5$ hydrogel. . . . .	59
3.4 50X magnification microscope pictures of centrifuged $v_2O_5/GO$ at speeds of a) not centrifuged; b) 2500 rpm; c) 6000 rpm; d) 10000 rpm; e)12000 rpm; f)14000 rpm. . . . .	60
3.5 An example of individual beads of electro-spun $V_2O_5$ (polymerized after 7hr; 1:4) + GO + PVP. . . . .	62
3.6 An example of beads on strings of electro-spun $V_2O_5$ (polymerized after 7hr; 1:4) + GO + PVP. . . . .	63
3.7 An example of uniform electro-spun $V_2O_5/GO$ (polymerized after 7 hours with PVP). . . . .	64
3.8 $V_2O_5r/GO + PVP$ (polymerized after 7hrs)): after annealing in $N_2$ (@ 400°C ). . . . .	65
3.9 An example of uniform electro-spun $V_2O_5/GO$ (polymerized after 2 weeks with PVA). . . . .	66
3.10 $V_2O_5/rGO + PVA$ (polymerized after 2 weeks)): after annealing in $N_2$ (@ 400°C ). . . . .	67
3.11 Electro-spun $V_2O_5/GO + PVP$ in $H_2O_2$ and water. . . . .	68

Figure	Page
3.12 Electro-spun $V_2O_5/GO + PVP$ in DMF and water. . . . .	69
3.13 Galvanostatic charge/discharge curve of $V_2O_5/GO + PVP$ for the 1st cycle. . . . .	72
3.14 Galvanostatic charge/discharge curve of $V_2O_5/GO + PVP$ for the 2nd cycle. . . . .	73
3.15 Galvanostatic charge/discharge curve of $V_2O_5/GO + PVP$ for the 10th cycle. . . . .	74
3.16 Coulombic efficiency for $V_2O_5/GO + PVP$ vs. charge capacity. . . . .	75
3.17 TGA analysis of PVP (Sigma Aldrich, $M_w = 1.3M$ ). . . . .	76
3.18 TGA analysis of PVA ( <i>Mowiol</i> <sup>R</sup> 8-88, $M_w = 67k$ ). . . . .	77
3.19 Powdered $V_2O_5/GO$ mercury porosimetry results (prepared through sol-gel method). . . . .	78
3.20 Electro-spun $V_2O_5/GO$ mercury porosimetry results (prepared through sol-gel method). . . . .	78
3.21 XRD patterns of the $V_2O_5/GO + PVP$ . . . . .	80
3.22 XRD patterns of the $V_2O_5/GO + PVA$ . . . . .	80

## ABSTRACT

Ahmadian, Amirhossein. M.S.M.E., Purdue University, August 2019. Design and Fabrication of High Capacity Lithium-Ion Batteries Using Electro- Spun Graphene Modified Vanadium Pentoxide Cathodes.. Major Professor: Mangilal Agarwal.

Electrospinning has gained immense interests in recent years due to its potential application in various fields, including energy storage application. The  $v_2o_5/GO$  as a layered crystal structure has been demonstrated to fabricate nanofibers with diameters within a range of  $\sim 300$  nm through electrospinning technique. The porous, hollow, and interconnected nanostructures were produced by electrospinning formed by polymers such as Polyvinylpyrrolidone (PVP) and Polyvinyl alcohol (PVA), separately, as solvent polymers with electrospinning technique.

In this study, we investigated the synthesis of a graphene-modified nanostructured  $v_2o_5$  through modified sol-gel method and electrospinning of  $V_2O_5/GO$  hybrid. Electrochemical characterization was performed by utilizing Arbin Battery cycler, Field Emission Scanning Electron Microscopy (FESEM), X-ray powder diffraction (XRD), Thermogravimetric analysis (TGA), Mercury Porosimetry, and BET surface area measurement.

As compared to the other conventional fabrication methods, our optimized sol-gel method, followed by the electrospinning of the cathode material achieved a high initial capacity of  $342 \text{ mAhg}^{-1}$  at a high current density of  $0.5C$  ( $171 \text{ mA}g^{-1}$ ) and the capacity retention of  $80\%$  after 20 cycles. Also, the prepared sol-gel method outperforms the pure  $v_2o_5$  cathode material, by obtaining the capacity almost two times higher.

The results of this study showed that post-synthesis treatment of cathode material plays a prominent role in electrochemical performance of the nanostructured

vanadium oxides. By controlling the annealing and drying steps, and time, a small amount of pyrolysis carbon can be retained, which improves the conductivity of the  $v_2o_5$  nanorods. Also, controlled post-synthesis helped us to prevent aggregation of electro-spun twisted nanostructured fibers which deteriorates the lithium diffusion process during charge/discharge of batteries.

# 1. INTRODUCTION

## 1.1 Lithium-ion Batteries

### 1.1.1 A Review on Lithium-ion Batteries and Current Battery Technologies

The pioneering work on Lithium batteries began in 1912 under the leadership of G. N. Lewis. The primary non-rechargeable lithium batteries gained entry into the market in the 1970s. Lithium was preferred because the metal is the lightest, provides the most significant energy density, and presented a remarkable level of electrochemical potential. However, it could not be used in manufacturing batteries due to its instability, especially during charging. Researchers found that Lithium batteries could explode during charging, presenting various safety issues [1]. Lithium batteries could work but recharging them became a significant challenge. Thus, experts abandoned work on lithium batteries in favor of other solutions, including non-metallic options. Researchers found that using lithium ions was an effective way of replacing lithium batteries [2,3]. Lithium-ion batteries have become a popular source of energy for consumer electronics, including mobile phones, computers (laptops), cameras, and personal digital assistants (PDA). In 1991, Sony Corporation became the first company to commercialize lithium-ion batteries. Currently, many companies have joined the production of lithium-ion batteries. Manufacturers of consumer electronics prefer Li-ion batteries because of their high energy density, lower rates of self-discharge, low maintenance, and safety [4,5].

Lithium ions, however, possess lower energy density compared to lithium metals. Using the ions, however, was safer and also met both charging and recharging requirements. Compared to other metals like Nickel-cadmium, lithium ions had twice

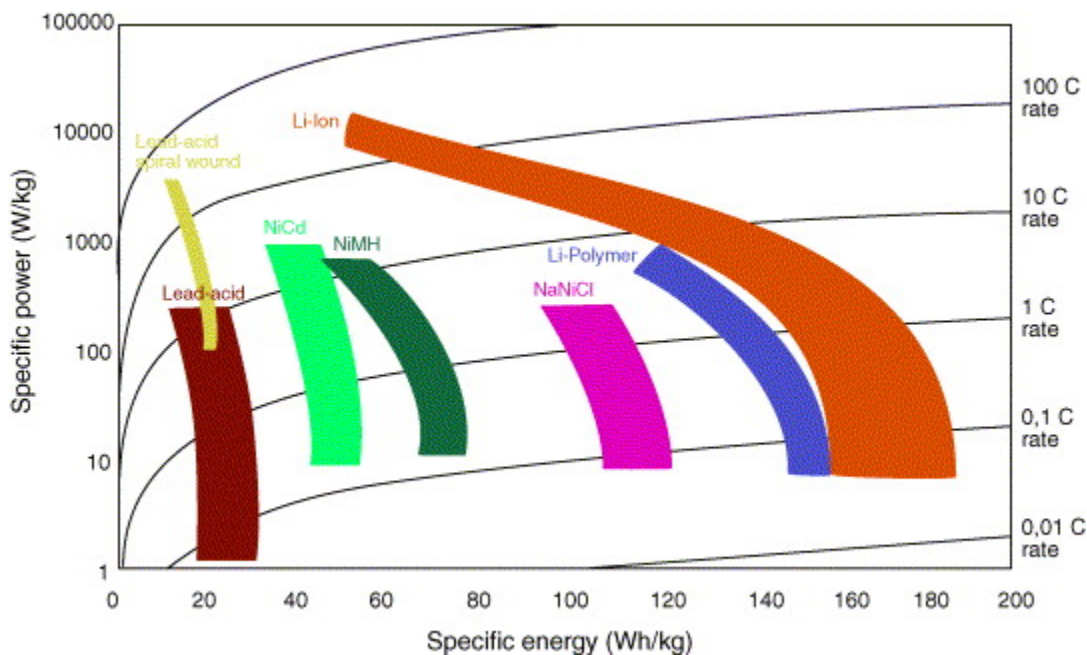


Fig. 1.1. Ragone chart of specific power vs. specific energy in different battery types vs. different current rates [7].

higher energy density making them preferable [6]. The relationship between the specific power and specific energy of different types of batteries is shown in Figure 1.1 in different current rates. As shown, lithium-ion batteries provide the highest specific power and specific density in all current rates among all the other types of batteries [7]. The primary purpose of this thesis is to fabricate high capacity lithium-ion batteries using electro-spun graphene-modified vanadium pentoxide cathodes.

### 1.1.2 Theory

Although there are various rechargeable batteries, Li-ion batteries have received more attention due to their applicability for both consumer and industrial purposes due to their high-power density and energy. In fact, among all metal-based batteries, Li-ion batteries are considered to have the highest gravimetric, volumetric, and energy density [8]. This has been linked to lithium's small ionic radius of about 0.76

and low atomic weight of  $6.94 \text{ g.mol}^{-1}$ . Moreover, it has a relatively low density of approximately  $0.53 \text{ g.cm}^{-3}$ . Lithium also has a meager redox potential,  $-3.041 \text{ V}$ , and this helps in providing electromotive force. Contrary to a disposable battery, Li-ion can be rechargeable allowing the transfer of mass and charge within the electrodes. The amount of stored energy and released energy is governed by the thermodynamics and kinetics of active electrode processes. The reaction can also be assessed using a half cell, where lithium acts as a reference electrode. It can also be investigated as a full cell, where electrons produced at the cathode are consumed at the anode and conserved if there were no side reactions [9, 10].

Lithium-ion battery consists of four major components, including cathode, anode, electrolyte, and separator. Every part of the battery is essential because all the other parts cannot function if one is missing: The anode or negative electrode acts as the reducing or fuel electrode. During the electrochemical reaction within the cell, it loses electrons to the external circuit and will be oxidized in the end. In the other side of the battery, the cathode or positive electrode performs as the oxidizing electrode. During the electrochemical process, it gains electrons from the external circuit and will be reduced in the end. In between anode and cathode inside the battery, the electrolyte or the ionic conductor provides the medium for transfer of ions. It dissolves salts, acids, or alkalis to facilitate ionic conductivity. In general, the electrolyte is in a liquid form, such as water or other solvents, However, in some other cases, solid electrolytes or gel-type polymer electrolytes can be utilized. Cathode and anode have to be kept from coming into contact, thereof the separator or the barrier takes this role. A cathode is the source of lithium ions and determines the average capacity or voltage of the battery. According to Sun, Sun, Xie, and Liu (2016), the lithium-ion battery generates electrical energy through chemical reactions occurring on the surface of the lithium metal [11]. Thus, the insertion of the lithium metal into the battery is through the cathode. However, lithium is unstable in its elemental form, and experts must combine it with other chemicals to gain stability [12]. The cathode must be an efficient and stable oxidizing agent, while in contact with the

electrolyte and having a useful working voltage at the same time [13]. In the case of lithium-ion batteries, oxygen is used to stabilize the lithium metal. Oxygen combines with lithium to form lithium oxide, also described as an active material [14]. Cathode plays a significant role in determining the capacity of the battery [15]. A large lithium metal, for instance, is likely to produce more energy than small lithium metal.

An anode is the part of the battery which stores and releases lithium-ions from the cathode, allowing currents to pass through, and completes the electrical circuit. Practically, metals are chiefly utilized as anode material. Zinc has been a primary anode because it has these desirable properties [13,16]. Also, the anode is manufactured using graphite coated with an active material. In this case, the active material is lithium oxide. Graphite is mainly preferred for the anode because it is more stable and does not react to the chemicals present inside the battery. Lithium, as the lightest metal, with a high value of electrochemical likeness, has gained entry as a promising anode material. With the development of intercalation electrodes, lithiated carbons are considered to be promising candidates in lithium-ion battery technology. Lithium alloys are also developed and fabricated in lithium-ion batteries acting as an anode [17].

An electrolyte is the component of the battery, which allows the flow of lithium ions from the anode to the cathode. The materials used in making electrolyte is expected to have higher conductivity of electrons. In order to prevent internal short-circuiting, the electrolyte must have a proper ionic conductivity but not be electronically conductive [13]. In most cases, the electrolyte consists of salts, solvents, and additives. Solvents are liquids that allow salts to dissolve and form a liquid, which enables the flow of ions. However, the addition of additives to the electrolyte may be necessary depending on the needs of the manufacturer. For instance, if a manufacturer requires a higher capacity battery within a limited space, additives may be included in the battery to speed up the flow of ions. Electrolytes may come in different types depending on the materials used in the manufacturing process [18]. Besides, the type of electrolytes also determines the speed of the flow of ions from the anode to the

cathode. Some manufacturers try to modify the electrolyte using additives or solvents to achieve the desired purpose. Electrolyte plays a significant role in determining the safety of the battery. For instance, it allows the ions to flow and not the electrons. If electrons flow through an electrolyte, issues such as overheating and subsequent explosion may occur [19].

Separator provides a barrier that prevents cathode and anode from coming into contact. The separator also prevents the direct flow of electrons by allowing only ions to pass through the microscopic holes. The electrons are then forced to flow through the conducting wire in external circuit while the ions flow through the electrolyte [13]. Allowing both electrons and ions to flow through the electrolyte may cause serious safety issues. The separator must be from the materials that do not react with the chemicals present in the electrolyte. In most cases, synthetic resins such as polypropylene and polyethylene make the separator. Both electrolyte and separator play a critical role in maintaining the safety of the battery [19, 20].

### 1.1.3 Lithium-ion Batteries Electrochemical Process

In Li-ion cell charging process, the active, positive electrode material is oxidized, and the active negative electrode material is reduced. As illustrated in Figure 1.3, lithium ions are deintercalated from the cathode and intercalated into anode. In the following reactions,  $LiMO_2$  is representing cathode, a metal oxide like  $LiCoO_2$ . Also, C represents the anode, a negative carbonaceous material such as graphite. In Figure 1.3, x and y are selected based on the molar capacities of the electrode materials for lithium. In regular occasions, x is about 0.5, and y is about 0.16. Therefore x/y is equal to 3 [13].

The reverse occurs on discharge due to the lack of metallic lithium inside the cell. As compared to Lithium batteries, Li-ion batteries are chemically less reactive, safer, and offer longer cycle life. The charge-discharge electrochemical process in a Li-ion cell is depicted graphically in Figure 1.4. In this figure, the layered active materials, as

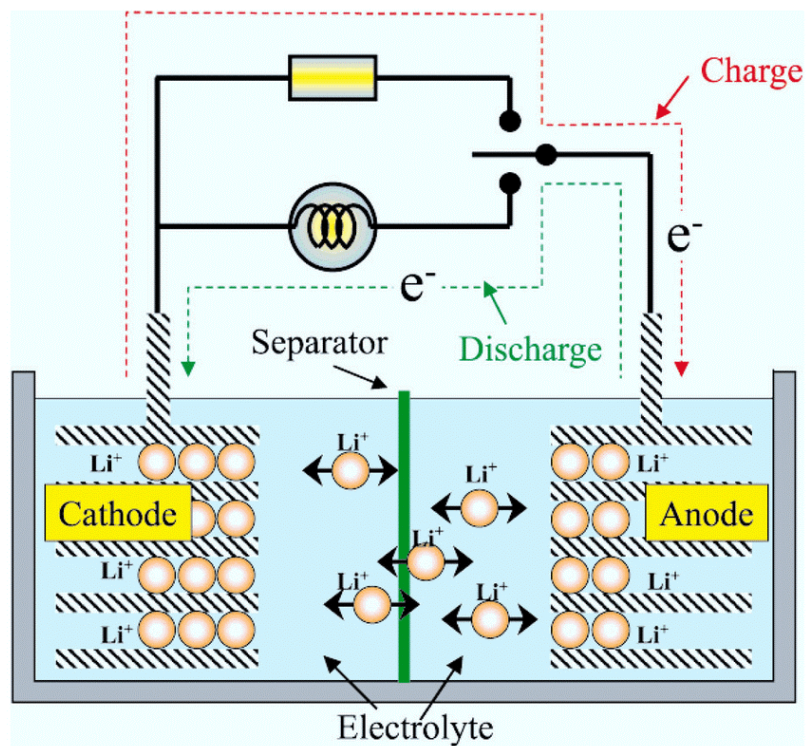


Fig. 1.2. Schematic of a typical Li-ion battery in action [21].

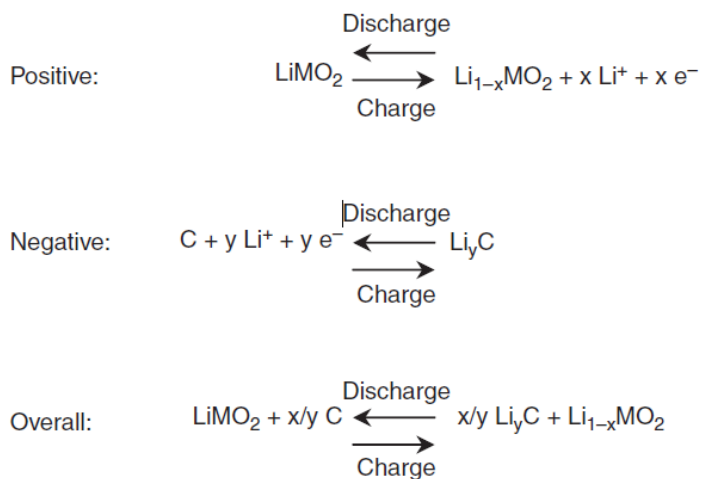


Fig. 1.3. Electrode reactions in the most common Li-ion cell [13].

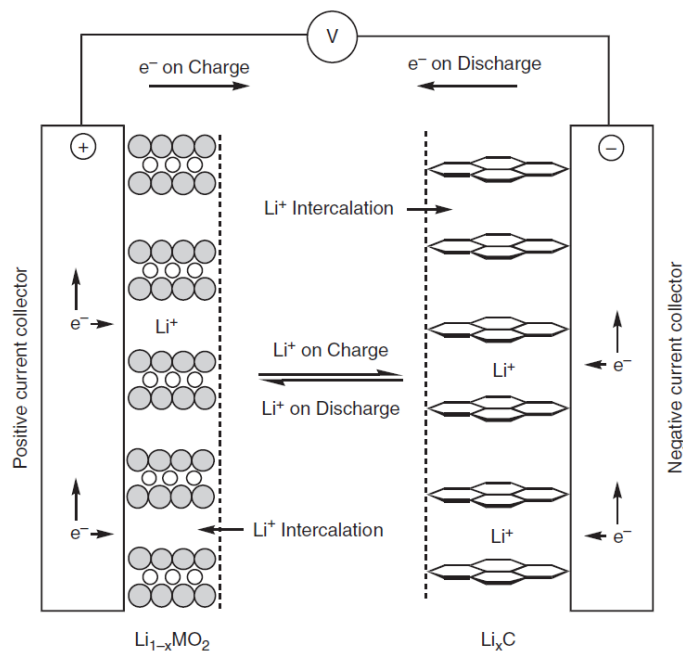


Fig. 1.4. Schematic of the electrochemical process within a Li-ion battery [13].

a promising candidate material for cathodes are shown on metallic current collectors [13]. The electrons are transferred throughout the external circuit from the positive current collector as the ion transfer happens within the cell.

### Ficks Law of Diffusion in Li-ion Batteries

The high surface to volume ratio of fibers, can be accomplished by incorporating the electrospinning method in energy storage applications [22, 23]. In a way that it can provide more physical contact and gap for the lithium de/intercalation process allowing more penetration depth for  $\text{Li}^+$  into the electrode which is determined by the diffusion length. Diffusion length depends on many properties including the material property and the surface morphology [24, 25]. In this regard, a theoretical study on the Li-ion diffusion rate is carried out:

It states that the flux travels from regions of high concentration to regions of low concentration, with a magnitude that is proportionate to the concentration gradient.

The ions in the electrolyte diffuse due to the minor changes in the electrolyte concentration. In Ficks first law, linear diffusion is only a matter of concern. The alteration in concentration,  $c$ , as a function of time ( $t$ ), and distance ( $x$ ) is:

$$\frac{\partial c}{\partial t} = -\frac{D}{\epsilon} \frac{\partial c}{\partial x} \quad (1.1)$$

The negative sign indicates the flux of ions flowing from high concentration to low concentration regions. In this equation,  $D$  is the diffusion coefficient for the lithium-ion which has the value of  $7.510^{10}m/s$  in the  $LiPF_6$  electrolyte. The value for  $\epsilon$  or the porosity of the electrolyte, is 0.724. Counting on approximation, equation (1.1) becomes:

$$\frac{\partial c}{\partial t} = \frac{c_2 - c_1}{l} \quad (1.2)$$

where  $l$  is the length between the electrodes. Plugging Equation (1.2) into Equation (1.1):

$$\frac{\partial c}{\partial t} = -\frac{D}{\epsilon} \frac{c_2 - c_1}{l} \quad (1.3)$$

The concentration at the anode is  $c_1$  and at the  $Li_xV_2O_5$  cathode is  $c_2$ . However, Fick's second law postulates how diffusion results in the concentration change concerning time. Mathematically, a second-order differential equation is used to describe this concentration change in Li-ion batteries. Therefore, Equation 1.10 becomes [26]:

$$\frac{\partial c}{\partial t} = -\frac{D}{\epsilon} \frac{\partial^2 c}{\partial x^2} \quad (1.4)$$

## Migration in Li-ion Batteries

Another predominant factor involved in the movement of the  $Li^+$  ions is concerned with voltage change, which influences the movement of ions in the electrolyte. Hence, Ficks first law takes the form of the following:

$$\frac{\partial c_1}{\partial t} = -\frac{zfc_0D}{RT\epsilon} \frac{\partial \phi}{\partial x} \quad (1.5)$$

The negative sign indicates the ions transfer is happening from high voltage to low voltage. In equation (1.5), the concentration at the anode is  $c_0$ , and  $z$  is the charge of

the ion. In this case,  $z$  equals +1 for  $Li^+$ . The Faradays constant (F) has a value has a value of  $9.6485310^4$  C/mol. The initial electrolyte concentration is denoted by  $c_0$ . Also, the diffusion coefficient denoted as  $D$  continues to be  $7.5 * 10^{10}$ . The ideal gas constant (R) has the value of  $8.3145$  J/(mol.K). The temperature, T, is the standard temperature of 298 K. The value for  $\epsilon$ , the porosity of the electrolyte, and diffusion coefficient denoted as  $D$  remain the same. The change in voltage as a function of the position is  $\frac{\partial \phi}{\partial x}$ . If the voltage( $\phi$ ), is considered constant, then the equation can be expressed as:

$$\frac{\partial c}{\partial t} = -\frac{z f \phi D}{RT \epsilon} \frac{\partial c}{\partial x} \quad (1.6)$$

In order to simplify the calculation, the linearized equation following the same scheme has been presented here. Using the following equation, the concentration change due to voltage is [26].

$$\frac{\partial c}{\partial t} = -\frac{z f \phi D}{RT \epsilon} \frac{c_2 - c_1}{l} \quad (1.7)$$

As a simple way to calculate concentration change, transference number is used as followed by the below equation [26]:

$$\frac{\partial c}{\partial t} = -\frac{D}{\epsilon} \frac{\partial c}{\partial x} + (1 - t_+) \quad (1.8)$$

where  $t_+$  is 0.364 for  $Li^+$  in this battery. The structural change occurs after electrospinning when the morphology becomes more porous as verified by a mercury porosimeter. We have demonstrated through our porosimeter results that the electrospun  $V_2O_5$  nanotubes help to improve the Li diffusion as the diffusion length decreases significantly due to the formation of nanostructured  $V_2O_5$ . This can be seen and verified by the above equation as the diffusion length decreases; the lithium intercalation rate increases proportionally.

## 1.2 Vanadium Oxides as a Cathode Material

There has been extensive research over the past years on cathode materials; However, lack of a suitable cathode material has remained to be a hindrance towards an

improved battery performance. On the other hand, anode materials possess stable capacities that are factors better compared to cathode counterparts. Cathode materials are innately limited to a significantly low intercalation capacity as well as degradation during long-term cycles. In other words, cathode performance has become a hindrance to further capacity improvement in Li-ion batteries; there has been extensive research focused on such electrode [27]. However, there is an ongoing exploration of alternative cathode materials in an effort to increase the intercalation capacity of currently used cathode materials. The most popular battery electrode material candidates are layered intercalation compounds, which are mostly comprised of metal oxides. The first category of these layered compounds is those comprised of the layered compounds with nearly close-packed lattice with electro-active transition metal ion in within the alternating layers, while lithium occurring in the unoccupied layers. The second class consists of layered metal oxide compounds consist of open structure; for example, layered vanadium oxides and tunneled manganese dioxide [28].

Also, there is a growing interest in research on vanadium oxides on its applications as a cathode material for alkali ion batteries. Recently, we have seen an increasing interest in alkali-ion technologies. Oxides of transition metals have also been studied extensively due to their technological and fundamental aspect. However, vanadium oxides have received much attention due to their ability to create many compounds with oxygen that exhibit varying chemical, optical, and structural properties [29]. There is an extensive literature in the suitability of vanadium-based cathode in battery systems [30]. Different forms of vanadium oxide structures can be obtained via the facile distortion of the V-O octahedral as well as its ability to exist in different oxidation states ( $V^{2+}$ ,  $V^{3+}$ ,  $V^{4+}$ ,  $V^{5+}$ ) distinguished by colors as displayed in Figure 1.5. Vanadium-oxygen is a layered material with different V-O polyhedron constitute a layered framework. There are only five stable vanadium oxides, and they include a  $VO_2$ ,  $V_2O_3$ ,  $V_3O_5$ ,  $V_3O_7$ , and  $V_2O_5$ . Different other phases can be formed when cations intercalate into the framework [31].

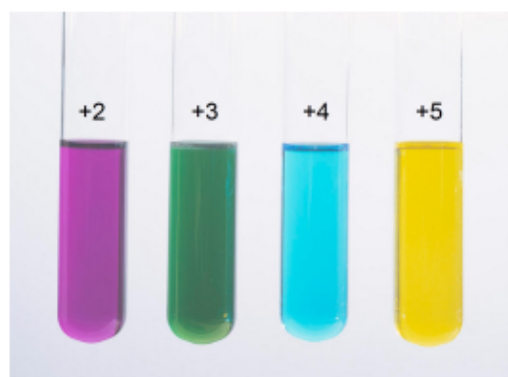


Fig. 1.5. The colorful oxidation states of vanadium from lowest oxidation state to highest oxidation states.

Vanadium occurs naturally in rock deposits such as titaniferous magnetite, and uraniferous sandstone and siltstone, however, it only constitutes the diminutive amount of the host rock [32]. For battery applications, vanadium oxide offers several benefits ranging from ease of synthesis, cheap, high energy densities, etc. as a result, it has attracted many interests as it also fulfills the electrode material criteria as discussed above [33].

The principal oxides of vanadium happen as single valence in different oxidation states ranging from  $V^{2+}$  to  $V^{5+}$ , in the form of  $VO$ ,  $V_2O_3$ ,  $VO_2$ , and  $V_2O_5$ . The ability to have different oxidation state creates meaningful differences that determine other properties such as wider variation range as well as increased specific capacity, especially when cations intercalate these vanadium materials. In addition, it has been proven that vanadium has the ability to change the oxidation state as a way of achieving stability of crystal structure as well as increase multivalent cations can help achieve local electroneutrality [31]. The d-orbital of the vanadium atom is not entirely occupied, and this can affect the size of the structural change. In an octahedral environment, a significant change can occur if the nonbonding orbitals are filled, but if they are completely filled, there is a significant change in the volume [34]. Since vanadium has several unoccupied nonbonding orbitals, its compounds can be considered to be a suitable candidate for materials in multivalent batteries.

Vanadium is an element in the first row of transition elements. Its atomic number and atomic weights are 23 and 50.9415 amu, respectively. Vanadium is a redox element and exists in several oxidation states ranging from -1 to +5, and for this reason, vanadium can exist in several coordination numbers and geometries. Figure 1.6 below shows the coordination polyhedral from coordination number 4 to 8; However, vanadium complex coordination geometries are slightly distorted. Unlike other transition metals, vanadium has the ability to adopt a host coordination geometry as while others have a single coordination geometries [35].

In addition, acid-base equilibrium is important as it tells as vanadium redox behavior. Figure 1.7 below shows vanadium ions redox behavior in an aqueous solution

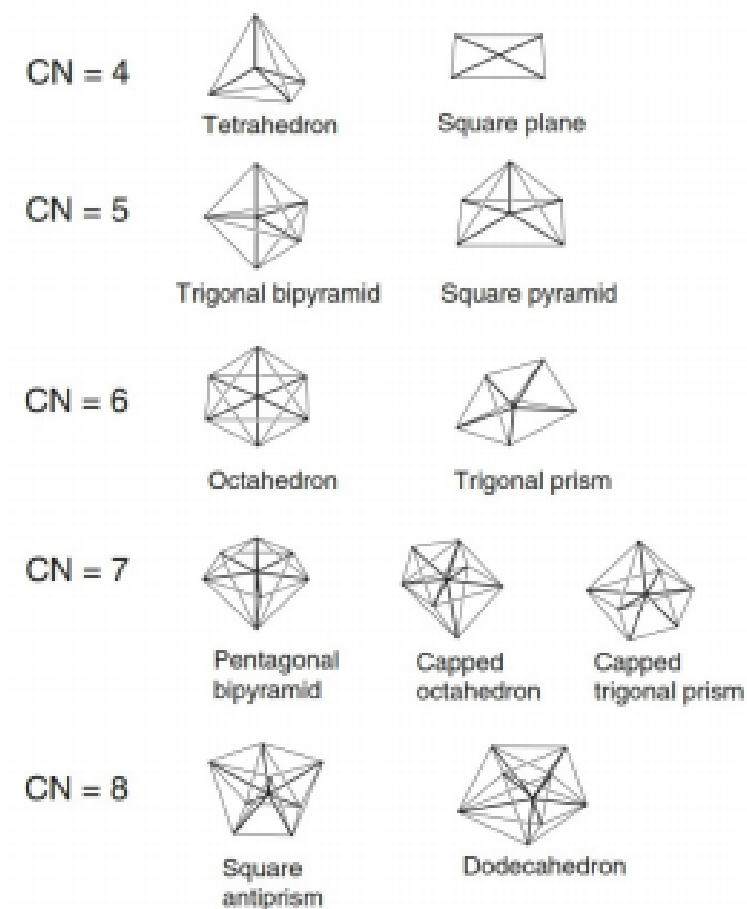


Fig. 1.6. Vanadium species coordination geometries [35].

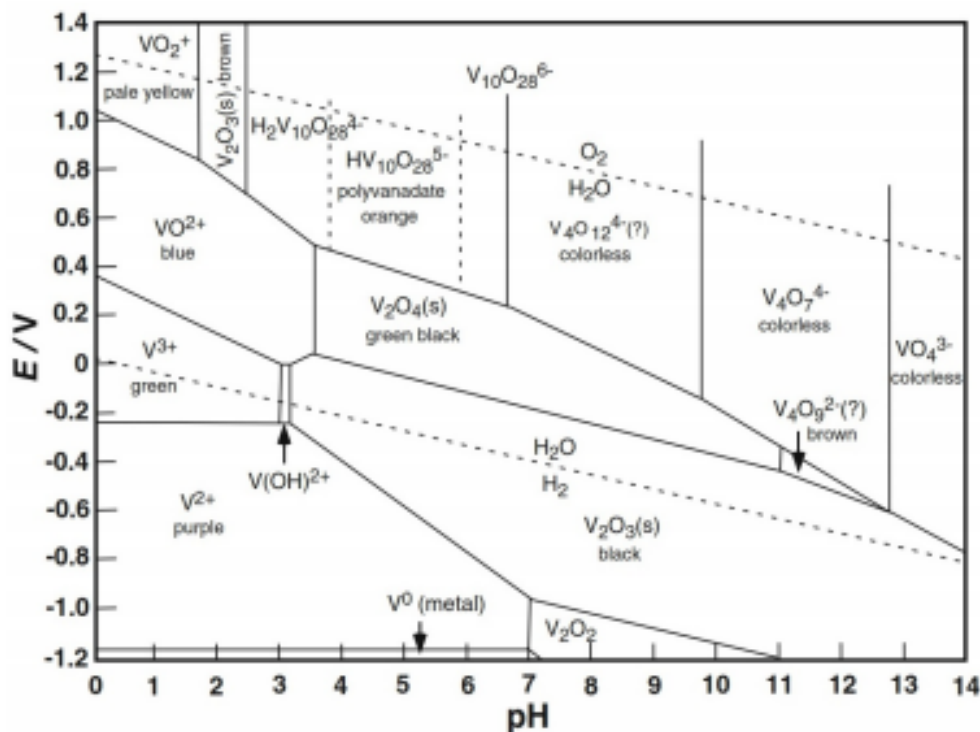


Fig. 1.7. Pourbaix diagram of vanadium species [36].

that is affected by PH. For examples,  $V^{4+}$  and  $V^{5+}$  species are prevalent in alkaline solutions around 0V, whereas  $V^{3+}$  exists in acidic conditions [36].

### 1.2.1 Vanadium Pentoxide $V_2O_5$

Researchers have made many suggestions regarding potential solutions that will increase the energy density of the batteries. For instance, some researchers have suggested the use of lithium metal as an anode and searching for a higher voltage cathode [37]. One of the materials that can be used to obtain a higher capacity and higher voltage cathode is vanadium pentoxide. Unlike lithium metal, vanadium pentoxide does not produce lithium ions. However, it has the highest reversible capacity among the available materials used for making cathode [38]. Moreover, vanadium pentoxide

has the ability to change phases from  $V^{5+}$  to  $V^{2+}$ , which makes it a promising and the most prevalent oxide among all other vanadium oxides. In a sense that, by changing oxidation state, theoretically, it enables lithium intercalation/deintercalation process to be accomplished entirely by facilitating to approach the theoretical value of  $443 \text{ mAhg}^{-1}$  [39].

Researchers also believe that vanadium pentoxide can be used to solve other limitations associated with lithium-ion batteries. For instance, the use of vanadium pentoxide can prolong the lifespan of the lithium-ion batteries making them durable and safe. Future research on the lithium-ion batteries may favor the use of vanadium pentoxide over lithium-ions [40, 41].

### **Vanadium Pentoxide $V_2O_5$ Chemical Structure**

Vanadium pentoxide is considered to be the most stable and prevalent compound among another vanadium oxide. Also, it has a high oxygen concentration. It is formed through corner-sharing and edge-sharing  $VO_6$  octahedra, and when in a crystal form, it forms an orthorhombic structure [42]. It is placed in pmnm space group, and its lattice parameters are as follows  $a = 11.510 \text{ \AA}$ ,  $b = 3.563 \text{ \AA}$ ,  $c = 4.369 \text{ \AA}$ , where the coordinate a, b, and c are interchangeable [40]. The vanadium pentoxide stoichiometry is perceived to be a deformed octahedral  $VO_6$ , which is crucial in building the structure. The octahedra are irregular in vanadium pentoxide, five of the V-O distances ranges between  $1.585 \text{ \AA}$  and  $2.021 \text{ \AA}$ , while the 6th V-O is approximately  $2.79 \text{ \AA}$ . These deformed  $VO_6$  octahedra are shared by adjacent octahedra. This structure exhibits that the layers are connected by weak Van der Waals interaction. Therefore, vanadium pentoxide crystal structure is layered where each layer is  $4.4 \text{ \AA}$  apart with an easy cleavage along (001) plane. Its orthorhombic crystal structure of  $V_2O_5$  can be regarded as layers of trigonal bipyramids of  $V_2O_5$  that share edges and zigzag double chains, as seen in Figure 1.8 [43].

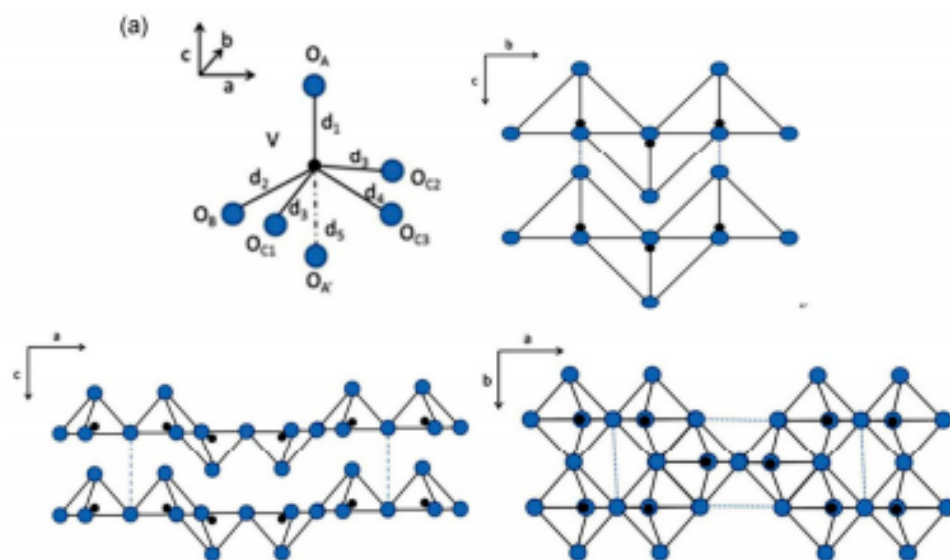


Fig. 1.8. Crystal structure of  $V_2O_5$ .

A single vanadium atom can form six V-O bonds using oxygen atoms, producing a distorted trigonal by-pyramids around the vanadium atoms. These by-pyramids are connected since they share corners in a and b-coordinate and c-coordinate. The sixth vanadium-oxygen bond consists of weak van der Waals forces, and this enables the insertion of ions within the layers. It is difficult for Lithium-ion insertion and electronic transport to occur through c-axis layers as compared to along the a-b plane. There are different combinations of the vanadium-oxygen bond; the O atoms can be classified into three categories:  $O_A, O_C(O_{C1}, O_{C2}, O_{C3})$  and  $O_B$ . The length of the strongest bond of the three is  $VO_A(d1)$  bond is 1.58 Å. The  $O_B$  atoms then forms two bonds: ( $VO_B(d1) = 1.77$  Å) with the angle  $VO_BV$  of  $125^\circ$ , while the  $O_C$  atoms forms three bonds ( $VO_{C1,2}(d3) = 1.88$  Å) with bond angles  $104^\circ$ ,  $VO_{C3}(d4) = 2.02$  Å) with bond angle  $143^\circ$ . The  $VO_{A'}$  interlayer force band has a length of 2.78 Å. The lithium-ion intercalation and de-intercalation process are expressed as follows [44]:  $V_2O_5 + xLi \rightarrow Li_xV_2O_5$  The phase transformation occurs when lithium ion is inserted in the vanadium pentoxide layers. Theoretically, the intercalation process of the lithium ion can be categorized in several steps, and different phases of the  $Li_xV_2O_5$  can be formed in every phase. X, in this case, denotes the amount of lithium, and thus, the five phases are [34, 35]:

Phase 1:  $\alpha-V_2O_5$  ( $x < 0.01$ )

Phase 2:  $\epsilon-Li_xV_2O_5$  ( $0.35 < x < 0.7$ )

Phase 3:  $\delta-Li_xV_2O_5$  ( $x = 1$ )

Phase 4:  $\gamma-Li_xV_2O_5$  ( $x < 2$ )

Phase 5:  $\omega-Li_xV_2O_5$  ( $x > 2$ )

Among the five phases of  $Li_xV_2O_5$ , phase 1 has a little significant impact on the  $V_2O_5$  structure, and phase 2 is formed, and there was increased puckering of vanadium oxide layers. This phase occurs when lithium is equal to 1. As a result of intercalation of lithium-ion, there occur slight structural modifications like increment of the interlayer spacing and puckering of the layers; however, the basic layer structure does not change. However, if more than one lithium ions are an intercalated phase,

is transformed into phase 4 through irreversible reconstruction mechanism. However, phase 5 ( $\omega\text{-Li}_x\text{V}_2\text{O}_5$ ) itself can be reversibly cycled in the range of  $0 < x < 2$ ) at the same time maintain the  $\gamma$ -type structure. With continuous intercalation of lithium ions, a rock salt structure of  $\omega\text{-Li}_x\text{V}_2\text{O}_5$  is formed via the irreversible process. Research has shown that discharging  $\text{V}_2\text{O}_5$  to the  $\omega\text{-Li}_x\text{V}_2\text{O}_5$  phase can lead to a rapid capacity loss and increased cycling, and this is not a desirable process for a cathode material. Rather, discharging phase 1 to phase 2 does not have a significant impact on the vanadium-oxygen bonds, and these phases are reversible [38,45]. The intercalation of one lithium-ion is approximate to a specific capacity of  $147 \text{ mAhg}^{-1}$ , while for two lithium-ion intercalation corresponds to the specific capacity of  $294 \text{ mAhg}^{-1}$  for  $\text{V}_2\text{O}_5$  in the voltage range of 2.0-4.0 V vs.  $\text{Li}/\text{Li}^+$ . The value of two lithium-ion intercalation is much higher than the theoretical capacity of the commercial cathode materials such as  $\text{LiMn}_2\text{O}_4$  ( $148 \text{ mAhg}^{-1}$ ),  $\text{LiFePO}_4$  ( $170 \text{ mAhg}^{-1}$ ),  $\text{Li}_3\text{V}_2(\text{PO}_4)_3$  ( $197 \text{ mAhg}^{-1}$ ) and  $\text{LiCoO}_2$  ( $274 \text{ mAhg}^{-1}$ ) [46].

### 1.2.2 Hydrated Vanadium Pentoxide Synthesis ( $\text{V}_2\text{O}_5 \cdot n\text{H}_2\text{O}$ )

Vanadium pentoxide  $\text{V}_2\text{O}_5$  is a red crystalline powder, which may sometimes appear yellowish. It is slightly soluble in water but has a higher density than water [47]. Vanadium pentoxide is potentially irritant to the eyes, skin, and mucous membranes. Recently, there has been a revitalized interest in the use of vanadium pentoxide in the production of lithium-ion batteries [48]. One of the reasons behind this renewed interest is the desire to increase the energy density of the lithium-ion batteries.

$\text{V}_2\text{O}_5 \cdot n\text{H}_2\text{O}$  means hydrated vanadium pentoxide. Vanadium pentoxide in this form has been linked with a higher intercalation capacity. Hydrated vanadium pentoxide can reversibly host cations due to its short diffusion length and the large interlayer space [39,49]. Recently, in their study, Moretti and Passerini provided a comprehensive review on bi-layered nanostructured hydrated vanadium pentoxide for metal batteries, which demonstrated that there are renewed interests on hydrated

vanadium pentoxide for energy storage.  $V_2O_5 \cdot nH_2O$  can be obtained from aerogel or xerogel depending on the method of drying used. Hydrated vanadium pentoxide xerogel has the capability of intercalation about to 3 equivalent of lithium ions, however without irreversible lattice formation, only up to 1 equivalent of lithium-ion can be intercalated. The structure of the vanadium pentoxide xerogel is ribbon-like and exhibits a lamellar arrangement. The water molecules function as pillars between vanadium pentoxide layers, and this result in lithium-ion intercalation of approximately 1.4 times higher than that of orthorhombic  $V_2O_5$ . The interlayered water molecules in the distorted square-pyramidal ligand facilitate the electron and lithium-ion transfer [50]. Intercalation materials in xerogel offer benefit such small diffusion distance leading to rapid injection and removal of the guest species. The electrochemical interaction rate of lithium-ion is, however, hindered by the host solid diffusion. Also, the high surface area supports overall reaction rates [51–53].

Wang et al. synthesize several hydrated vanadium pentoxide molecules ( $n = 0.3, 0.6, \text{ and } 1.6$ ) xerogel by reacting vanadium pentoxide with hydrogen peroxide followed by thermal annealing. The hydrated vanadium pentoxide ( $n = 0.3$ ) obtained at  $250^\circ\text{C}$  had the best electrochemical performance, the initial capacity was  $275 \text{ mAhg}^{-1}$  and stabilized at the capacity of  $185 \text{ mAhg}^{-1}$  at a current density of  $100 \mu\text{Acm}^{-2}$  [54].

In order to attain hydrated vanadium pentoxide molecules, sol-gel processing technique is implemented to synthesis vanadium pentoxide xerogel. Sol-gel processing is used to prepare inorganic materials, and it involves two reactions: hydrolysis and condensation that begin with organo-metallic compounds and inorganic salts. Vanadium pentoxide can be synthesized by the sol-gel method, and thus making it an attractive process for large-scale industrial utilization [31, 55]. One of the methods of synthesizing is ion exchange of alkaline vanadate. Alkaline vanadate ( $\text{NaVO}_3$ ) is passed through the cation exchange column to acidify the solution and remove unwanted sodium ions. The acidified solution then undergoes gelation and polymerization [56–58]. As shown in the following figure sol-gel method, almost stands out among other cathode materials prepared through other methods in terms of specific

capacity. According to Qi Liu et al. graphene modified vanadium pentoxide fabricated through sol-gel method retains a specific capacity of  $354 \text{mAhg}^{-1}$  at 0.5C. Also, optimized sol-gel method for electrospinning purposes provides high initial capacity of  $342 \text{mAhg}^{-1}$  for a high current density of  $171 \text{mAhg}^{-1}$  (0.5C) and the capacity retention of 80% after 20 cycles. As compared to pure  $V_2O_5$  capacity is almost two times higher. However, there are some limitations for the fabrication of this type of battery such as time-consuming sol-gel synthesis, difficult electrospinning process, and complicated annealing procedure. In the following, specific capacity and capacity retention of vanadium oxide-based cathode materials as a function of cycle count and current density are listed (modified from [59]). Synthesized xerogel through ion-exchange presents a layered structure that is necessary for the intercalation process without the transformation of its basic structure during the reaction. Furthermore, its conductivity enables its use as a rechargeable cathodic material, electrochemical sensors, as well as electrochromic devices [76]. The conduction occurs via thermally activated electrons that are continuously hopping from one metallic component to another in diverse oxidation state: these electrons are unpaired. These gels are a form of hydrated oxides, and thus their overall conduction is facilitated by their ionic contribution of protons that moving between the layered structure of vanadium pentoxide xerogel. The intercalated water content can also be used to determine conductivity with xerogel. Regarding its application, vanadium pentoxide xerogel are considered appropriate because they allow the lithium ions intercalation to ensure that the electroneutrality is maintained since there is the production of an electron during the process. However, lithium insertion into the vanadium oxide structure is hindered by steric hindrance that causes a decrease in charge-discharge capacity, solvent exchange, and changes in mechanical stress and volume [77].

Synthesis Method	Cathode Composition	Current density (mA/g)	Capacity (cycle #)	mAh/g	Capacity retention (%)
Heat treatment	LiCoO <sub>2</sub>	47	180(1)→150(50)		83
Surface and chemically modified	LiMn <sub>2</sub> O <sub>4</sub>	50	140(1)→131(50)		93
Hydrothermal	LiV <sub>3</sub> O <sub>8</sub>	120	213(1)→152(18)		72
Flame pyrolysis	LiV <sub>3</sub> O <sub>8</sub> nanoparticles	100	271(1)→180(90)		66
Solution process	LiVO-PP composite	40	184(1)→183(50)		99
Spray drying	Li <sub>1.1</sub> V <sub>3</sub> O <sub>8</sub>	116	260(2)→220(60)		84
Hydrothermal	LiV <sub>3</sub> O <sub>8</sub> nanorod	100	247(1)→236(100)		96
Surfactant-assisted polymer precursor	LiV <sub>3</sub> O <sub>8</sub> nanorod	120	182 (2)→180(60)		99
Soft chemistry	LiV <sub>3</sub> O <sub>8</sub> nanorod	100	320(2)→250(100)		78
Chelating and PEG modifying	LiV <sub>3</sub> O <sub>8</sub> nanosheets prepared at different temperatures	100	262(2)→260(100)		99
Hydrothermal	Li <sub>x</sub> V <sub>2</sub> O <sub>5</sub> nanobelts > 15nm thickness	100	400(5)→370 (25)		92
Solid state reaction	Li <sub>x</sub> V <sub>3</sub> O <sub>8</sub> nanobelts > 20nm thickness	100	234(1)→195.5(30)		84
Hydrothermal	Li <sub>x</sub> V <sub>3</sub> O <sub>7</sub> .H <sub>2</sub> O (x=4.32); nanobelts > 30 nm thickness	100	340(1)→240(20)		71
Hydrothermal	V <sub>3</sub> O <sub>7</sub> .H <sub>2</sub> O nanobelts > 20nm thickness	30	253(1)→229(50)		90
Sol-gel	Li <sub>1.2</sub> V <sub>3</sub> O <sub>8</sub>	60	281(2)→200(4)		71
Sol-gel	Li <sub>0.96</sub> Ag <sub>0.04</sub> V <sub>3</sub> O <sub>8</sub>	150	328(1)→253(50)		77
Sol-gel	Li <sub>x</sub> V <sub>2</sub> O <sub>5</sub>	87	173(1)→144(20)		83
Sol-gel	Li <sub>x</sub> V <sub>2</sub> O <sub>5</sub> /GO	177	354(1)→ 283(150)		80
<b>Optimized sol-gel and electrospinning</b>	<b>Li<sub>x</sub>V<sub>2</sub>O<sub>5</sub>/GO nanorods &gt; 300nm thickness</b>	<b>170</b>	<b>342(1)→277(20)</b>		<b>80</b>

Fig. 1.9. Comparison of specific capacity and capacity retention of vanadium-oxide based. cathode materials as a function of cycle count and current density with our proposed method [39, 59–75].

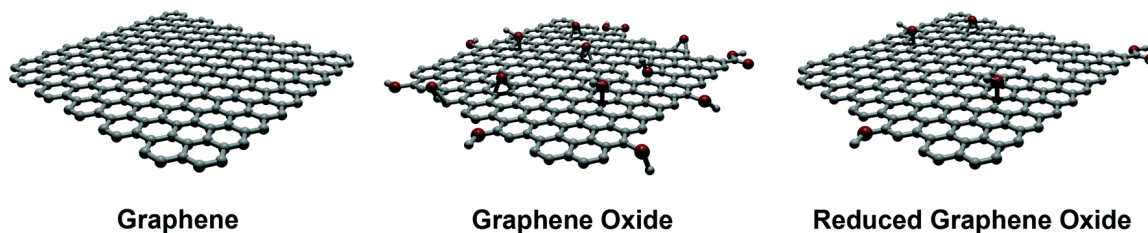


Fig. 1.10. Molecular structures of graphene, GO, and rGO [78].

### 1.2.3 Graphene Modified Vanadium Pentoxide Prepared Through Sol-gel Synthesis

Graphene is a single-atomic-layer of  $sp^2$ -bonded carbon atoms arranged in a honeycomb crystal structure as shown in, which provides excellent electrical conductivity of  $6.29 * 10^7 S.cm^{-1}$ , the mechanical fracture strength of  $\sim 130$  GPa), and thermal properties of  $\sim 3,000$  W/m.K in the plane. However, exfoliated graphene sheets are extremely hydrophobic, and they tend to aggregate. Simply put, they own a low water dispersibility. In order to attain dispersion of graphene in water, graphene oxide due to its excellent water dispersibility and vibrant surface chemistry is used. In general, graphene can be prepared using either the chemical reduction or thermal reduction of graphene oxide (GO); It owns as a layered stack of oxidized graphene sheets with different functional groups and represents the hydrophilic derivative of graphene. It is worth to mention that GO can be easily handled and dispersed in the water as the form of single sheet layers at low concentrations [39, 78]. Graphene oxide (GO) and reduced graphene oxide (rGO), two popular members of the graphene family are represented in Figure 3.1.

Despite the many plus points of GO, this nanomaterial is structurally defective, in a sense that it is considered to be electrically insulating and mechanically weaker than graphene [79]. In order to improve its electrical and mechanical properties, the thermal or chemical reduction of GO (in order to remove oxygen functional groups

and regenerate the  $sp^2$  network) has been widely studied, resulting in the formation of reduced graphene oxide or rGO. In terms of electrical properties, rGO is an intermediate structure between the ideal graphene honeycomb sheet and the highly-oxidized GO, consequently maintaining some properties and losing some others over to graphene [80]. In fact, Graphene, in general, is given due consideration as one of the most ideal conducting materials to improve the electrical conductivity of  $V_2O_5$  and its structure [39,56,58,81–85]. In simple physical mixing under regular circumstances, high graphene loadings is required which brings about a significant improvement on the rate performance and cycle life. However it is shown that it can deteriorate the specific capacity. In this regard, the amount of graphene has to be optimized in the sol-gel processing method which is believed to be within the range of 2-3% [39].

In the sol-gel processing method, once  $NaVO_3$  is passed through the ion exchange column,  $HVO_3$  aqueous solution is formed. After the formation of  $HVO_3$  and mixing with graphene oxide, the graphene-modified vanadium pentoxide ( $V_2O_5/GO$ ) nucleation process happens immediately (0 min). Then, a few minutes later, small  $V_2O_5$  ribbons start to form into  $\sim 100$  nm long ribbons, as verified and shown in the 60-min picture (Figure 1.9). This continuation of  $V_2O_5$  ribbons growth, leads to the fast growth in one direction as observed after 90 min. Finally, after two-three weeks, the  $V_2O_5$  hydrogel 3D network is shaped with a similar length as before, but with a much larger width than the  $V_2O_5$  ribbons [39]. Single-layered GOs, create gaps between  $V_2O_5$  ribbons i.e they are sandwiched between the graphene sheets as shown in the following pictures. However, the proper timing for the growth of  $V_2O_5$  hydrogel network for the electrospinning purposes is estimated to be between 7-12 hours. In the following TEM images, the vanadium oxide ribbon growth in different aging times, for both pure  $HVO_3$ , and  $HVO_3/GO$  is shown.

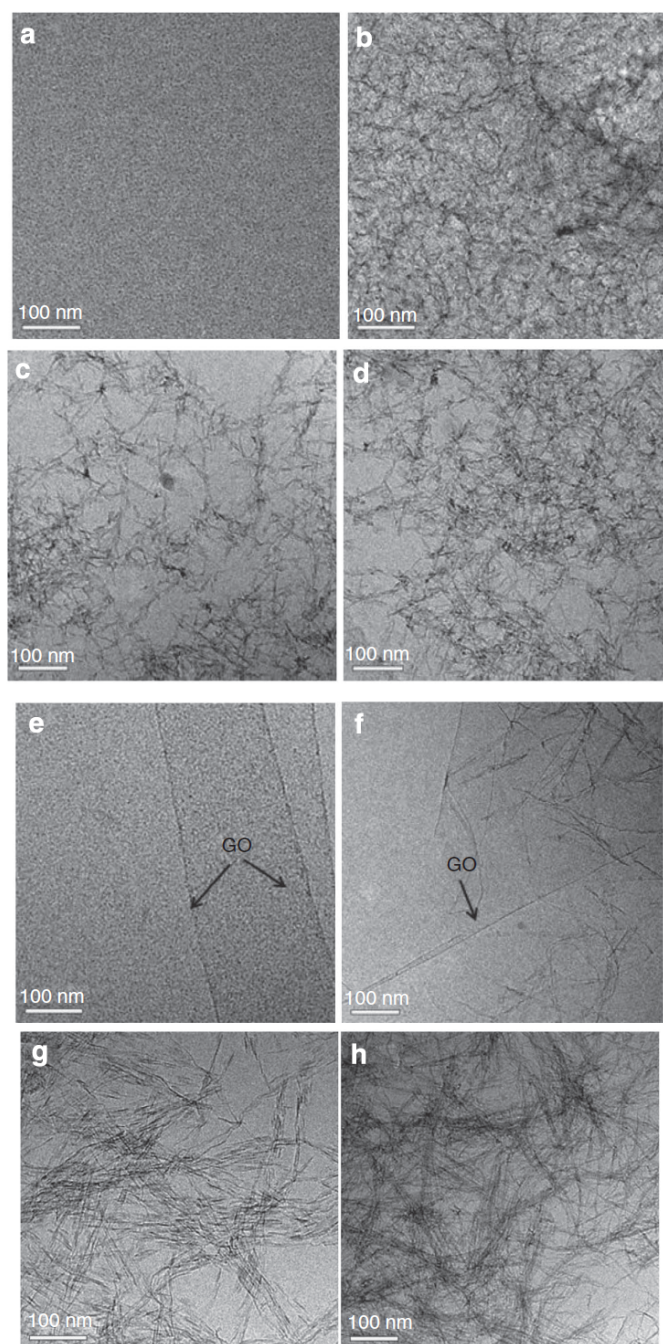


Fig. 1.11. TEM images of the frozen  $HVO_3$  and  $HVO_3/GO$  solutions in different aging timings. 1)  $HVO_3$ : (a) 0 min, (b) after 1 h, (c) after 1 h 30 min and (d) after 2 weeks. 2)  $HVO_3/GO$ : (e) after 30 min, (f) after 2 h, (g) after 6 h and (h) after 3 weeks [39].

### 1.3 Electrospinning

#### 1.3.1 Overview of Nano-fiber Bundles Fabrication Methods and Electrospinning

Nanofibers refer to fibers that have a diameter of less than 1000nm; they can be developed using various processing techniques [86,87]. So far the nano-fiber making techniques include direct drawing [88–90], magneto-spinning [91], extrusion [92,93], melt-blowing [94], hard templating [95], soft-templating [96], self-assembly [96,97], lithography [98,99], centrifuge spinning [100,101], hydrothermal/solvothermal [102], ball milling [103], chemical vapor deposition [104,105], and electrospinning [12,106–108]. Among thereof fabrication methods, electrospinning outperforms due to its many advantages such as controllable fiber diameter (from tens of nanometer to a few microns), covering fabrication of wide range of materials (natural and synthetic polymers, metals, ceramics, composites, sol-gels), versatile fiber morphologies (porous, dense, core-sheath, hollow, spiral, side-by-side, nanoparticles, nanorods, nanowires, nanosheets, and nanobelts), and capable of large scale production [86,87,109–111].

Nano-fibers formation stems from the electrostatic force along with the spinning force resulting in the continuous splitting of polymer droplets. Nanofibers deposit on the metal collector plate, layer upon layer, thus resulting in the formation of a nanofibrous mat [112–114]. The extrinsic parameters of the electrospinning process significantly impact the nanofiber structural morphology. Extrinsic parameter comprises of the working distance, viscosity, conductivity, polymer solution, humidity, temperature, as well as the applied voltage. To attain a uniform nanofiber mat, it is crucial to optimize the extrinsic parameters. When the nano-fibrous mat is uniform, it results in the formation of the bead-containing fibrous structure and continuous fibrous structure (nanofiber yarns). Nanofiber yarns are defined as entangled continuous fiber bundles possessing two intrinsic features: continuous length and interlocked twisted structure [115].



Fig. 1.12. Nanofiber bundles.

The correlation between extrinsic electrospinning parameters and relative abundance of different fiber morphologies leads to the formation of different nanofiber bundles forms. In general, nanofiber bundles can be categorized as the following [116]:

### 1.3.2 Review on Electrospinning and Electrostatic Phenomenon

In the early 1930s, Formhals employed electrospinning fabrication method as a fiber spinning technique. In 1934, the invention was patented, titled as process and apparatus for preparing artificial threads which developed spinning techniques. However, some practical issues such as fiber drying and collection had remained until he initiated his first patent overcoming spinning difficulties at the time. A movable thread was applied to collect the threads in a stretched condition. In his patent, he reported the spinning of cellulose acetate fibers utilizing acetone as the solvent [117,118].

Electrostatic phenomena arise from the ability of electrons to move with relative ease in various materials. Electrostatics comprises of two general classes including conduction and induction. Induction refers to a temporary state where electrons in a substance are either attracted to the repelled by the nearby charged object [119]. Conduction, on the other hand, occurs when a charged object comes into actual contact with a neutral object. The excess electrons move from a charged object to a neutral object; thus, when the objects are separated, the objects acquire the

same charge [120]. Electrostatic charges exert forces calculated using Coulombs law  $F = k \frac{Q_1 Q_2}{d^2}$  between opposite charges causing water droplet deformation [121]. In general, electrospinning refers to the production of fibers by means of electric current to draw charged threads of polymer solutions. The fibers produced using this process usually has a thickness of hundreds of nanometers. The electrospinning process shares the characteristics of conventional dry spinning as well as electro-spraying of fiber [122]. The process is highly suitable for the production of complex and large molecules as the process does not involve the use of chemistry coagulation or the application of the high temperatures [86, 87, 109–111, 123].

### 1.3.3 Electrospinning Categories

Nanofibers production by means of electrospinning technique may occur in two ways needle-less and needle-based. Needle-based electrospinning constitutes starting with a polymer solution in a tightly closed reservoir as these limits as well as prevents solvent evaporation. The needle-based system is essential as it allows for the processing of a wide range of materials, including highly volatile solvents [124]. Needle-based electrospinning has the following advantages process flexibility where it has the capacity to process various structures such as multi-axial and core-shell fibers. The distinction between the two fibers enables the incorporation of Active Pharmaceutical Ingredients (API) to be incorporated in the fiber. Another advantage is that the needle-based method has tightly controlled flow rate, minimizes solution waste, and has a limited number of jets [125]. The Numerous advantages have made the needle-based method immensely popular.

On the other hand, needle-less electrospinning allows for the large-scale production of materials. A Starting polymer solution inside an open vessel is utilized to generate nanofibers using a rotating or stationary platform [126]. However, the needle-less electrospinning method cannot carry out versatile fiber production. Also various process parameter cannot be controlled, including the flow rate [127].

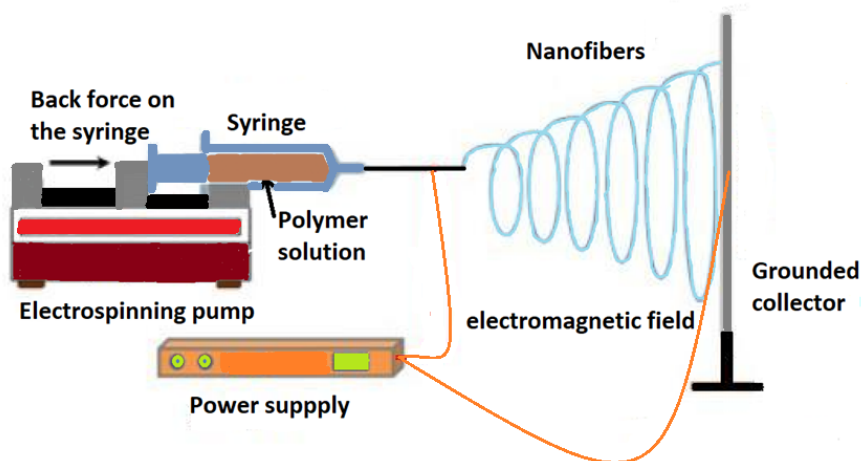


Fig. 1.13. General electrospinning setup.

#### 1.3.4 Electrospinning Process and Principles

Electrospinning refers to a process used to develop a nonwoven fabric that is impermeable using submicron fiber when a liquid jet that is a millimeter in diameter is pushed through a nozzle that has an electric field. In general, the fiber formation process in electrospinning can be observed and classified into three different stages: Deformation of the prolate droplet (Taylor cone) and jet initiation, whipping or bending instability, and fiber deposition. The general setup for electrospinning is depicted in Figure 1.12. The electrostatic charging at the tip of the nozzle is crucial to the formation of a Taylor cone where a single jet of fluid ejects [113]. The acceleration and thinning of the jet in the electric field and radial charge repulsion causes the primary jet to split into multiple filaments; this is referred to as Splaying. The size of the resultant fibers depends on the number of the subsidiary jets formed. Under normal conditions, the fluid jet whipping in electrospinning is immensely fast as this condition is essential for the production of nanofibers [128]. In general, the fiber

formation process in electrospinning can be observed and classified into three different stages: Deformation of the prolate droplet (Taylor cone) and jet initiation, whipping or bending instability, and fiber deposition.

### **Taylor Cone**

In 1964, Geoffrey Taylor initially described the cone. Taylor's primary interest was in determining how water droplets behave within strong electric fields, for instance, thunderstorms. Exposing a small volume of a liquid that is electrically conductive to an electric field results in shape distortion due to surface tension. Increase in voltage increases the impact of the electric field, as the electric field exerts a magnitude force on the droplet similar to the surface tension, resulting in the formation of a cone shape. On reaching a given threshold voltage, the rounded tip inverts and then releases a jet of liquid. The cone-jet commences the start of the electro-spraying process achieved at a voltage higher than the threshold. The Taylor cone refers to the theoretical limit of a cone-jet when the electro-spraying process commences. For a perfect cone to be achieved, there needs to be a semi-vertical angle of 49.3 degrees, the cone surface needs to be equipotential, and the cone ought to exist in a steady-state equilibrium [129]. Taylor cone formation is an essential part of the electrospinning process. Symmetrical vortices arising within the Taylor cone are likely to increase the velocity of the solution. Beads that occur in cone-jet results in the formation of beaded nanofiber [130].

In Figure 1.13, the formation of a Taylor cone captured in different timings can be observed.

### **Whipping and Jet Instability**

A strong electric field is likely to deform a liquid of finite electric conductivity into a conical shape arising from the balance between the surface tension and electric stresses. Conversely, close to the apex of the cone, the structure is unstable and the

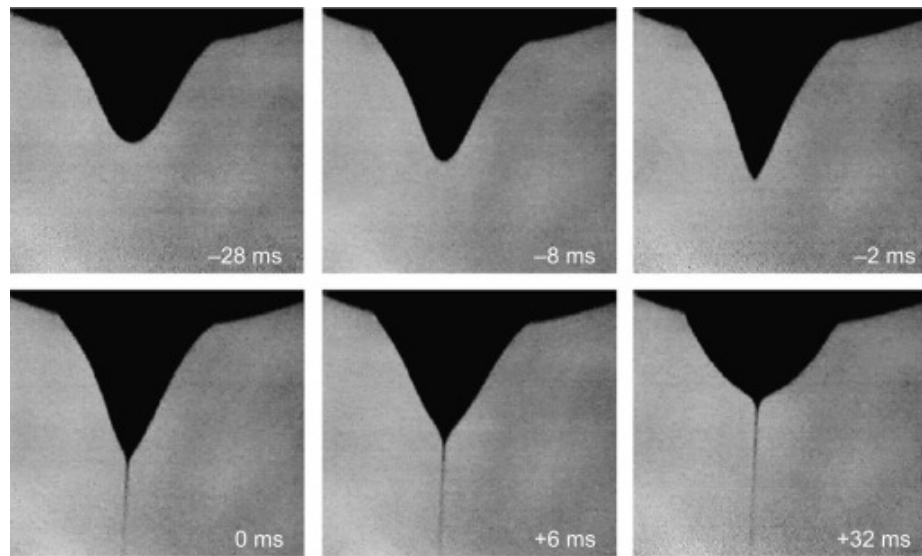


Fig. 1.14. Deformations of the prolate droplet and Taylor cone by increasing the electric field captured in different timings and ultimately, the formation of the jet [114].

thin jet structure replaces the associated singularity. The electrospay arises from the imposed flow rate of the liquid of the cone-jet structure that has stability within certain applied voltage values arising from the cone-jet structure breaking into spherical droplets due to axisymmetric instabilities. However, a lateral instability causes the jet to bend off its axis arising from electrostatic repulsion between the straight and the bent parts of the jet. In the instance that the whipping instability growth rate is larger than the one associated with a jet breakup; thus, the jet off-axis movement becomes a significant aspect of its evolution [131].

Replacing a liquid with a polymer solution where the solvent evaporates prior to a drop breakup taking place results in polymer fiber formation. The existence of lateral instability within the electrospinning application results in the formation of thinner fibers as the bending continues to stretch and along with thinning the jet. However, in most experiments carried out, the whipping is noticeably chaotic, thus making it difficult to have an in-depth understanding of its properties and structure [86,87,131].

### **1.3.5 Fiber Deposition**

Nano-fibers formation emanates from the electrostatic force accompanied by the spinning mechanical force resulting in the continuous splitting of polymer droplets. Nanofibers deposit on the metal collector plate, layer upon layer, thus resulting in the formation of a nanofibrous mat [112–114].

## **1.4 Solution-based Electrospinning and Related Effective Parameters**

Solution-based electrospinning needs a solvent to solubilize a given polymer. Consequently, identifying the correct solvent plays a vital role in attaining a homogeneous polymer solution. The solution parameter is lucrative in determining a suitable solvent for a given polymer. Solubility parameter takes into consideration the various molecular interactions in a given mole of material including such as polar interaction,

dispersion forces, as well as specific interaction, including hydrogen bonding [132]. Cohesive energy is given as

$$E = \Delta H - RT \quad (1.9)$$

Where:  $\Delta H$  is Latent heat of vaporization,  $T$  is Absolute temperature, and  $R$  is Universal gas constant.

Later, Charles M. Hansen extended the Hildebrand solubility theory to Hansen Solubility Parameters (HSP) 21, which estimates the relative miscibility of polar and hydrogen bonding systems as [133]:

$$\delta_i^2 = \delta_d^2 + \delta_p^2 + \delta_h^2 \quad (1.10)$$

where:  $\delta_i$  is Hansen solubility parameter,  $\delta_d$  is Dispersive component,  $\delta_p$  is the polarity, and  $\delta_h$  is the hydrogen bonding. A suitable solvent for a particular polymer ought to have a solubility parameter close to that of the polymer. Therefore, calculating the Hansen solubility parameter where the polymer-solvent ought to have a small value of  $R_a$  [134].

$$Ra^2 = 4(\delta_{d1} - \delta_{d2})^2 + (\delta_{p1} - \delta_{p2})^2 + (\delta_{h1} - \delta_{h2})^2 \quad (1.11)$$

Additionally, a suitable solvent ought to have a relative energy difference (RED) of less than one. And  $RED = Ra/R_o$  Where  $R_o$  refers to the radius of a sphere [134]. where:

$RED < 1$  the molecules are similar and dissolve,  $RED = 1$  the molecules partially dissolve, and  $RED > 1$  the molecules do not dissolve.

Nanofibers fabrication could be affected by many factors which lead to different morphologies such as uniform or ordered pattern structure with a round cross-section, beads-on-string structures, or individual beads. These crucial factors such as polymer type, polymer molecular weight, polymer distribution, polymer concentration [135, 136], solution conductivity, solution surface tension, solution viscosity, and solvent properties. Solvent properties contain boiling point, volatility, and dielectric

properties [137]. Operating factors are another key parameter in final fiber morphology, which including applied voltage, collecting distance, the flow rate of the polymer solution [138]. Last but not least, external conditions or ambient conditions for intense humidity, ambient temperature, and addition flow are also effective parameters on electrospinning [86, 87, 107, 139].

#### 1.4.1 Concentration

The electrospinning process depends on polymer concentration as the most crucial factor. Such that changing in polymer concentration leads to a change in solution viscosity. As the polymer concentration increases, the viscosity increases first at a steady rate and thereafter at a much higher rate [140]. The solution viscosity is extremely governed by intermolecular interactions between polymer-polymer, polymer-solvent, and solvent-solvent within the polymer solution. Electrospinning a dilute polymer solution is analogous to an electro-spraying process. On the other hand, the polymer intermolecular distance within the solution is so considerable that the interaction is considered to be very weak. Therefore, the viscoelastic force in the polymer jet is minute to form a uniform fibrous structure. In this process, the jet splits into separate charged sections as the voltage is applied. Gradually these charged sections turn into droplets or individual beads as a result of high surface tension caused by solvent evaporation while spinning. Similarly, an increase in the polymer concentration leads to higher viscoelastic force and more difficult for the jet to be split. In lieu of breaking the like-charged sections, electrostatic repulsion within the solution elongates the links between charged sections, consequently forming thinner filaments. Relatively thicker sections stretch thinner although to the links between charged sections. As the solvent evaporates while spinning, due to the surface tension, filaments tend to take the shape of beads-on-string morphology. Accordingly, a further increase in the polymer concentration, brings about uniform elongation of and formation of the jet, resulting in homogeneous fiber morphology [86, 87, 140, 141].

critical concentration ( $c^*$ ) is defined to distinguish whether predominant intermolecular interaction will happen or not leading to a chain entanglement [142]. In this regard, the following formula has been utilized to describe solution entanglement. The following formula calculates the ratio of polymer molecular weight to the solution entanglement molecular weight [143, 144]:

$$(n_e)_{solution} = \frac{M_W}{(M_e)_{solution}} = \frac{\phi M_W}{M_e} \quad (1.12)$$

where:  $M_e$  is entanglement molecular weight,  $M_W$  is polymer weight average molecular weight, and  $\phi$  is polymer volume fraction.

if  $(n_e)_{solution} < 2$ : polymer chains do not entangle and individual beads structure is formed.

if  $2 < (n_e)_{solution} < 3.5$ : insufficient polymer chain entanglement and beads-on-string structure is resulted.

if  $(n_e)_{solution} > 3.5$ : sufficient polymer chain entanglement and beads-on-string structure is shaped.

In general, throughout electrospinning, the solution viscosity can be increased by using a concentrate polymer solution or increasing the weight of the molecular polymer. For instance, polylactide solution doped with polyethylene oxide that has a high molecular weight increases viscosity of the polymer solutions [145]. Increased viscosity improves the jet stability allowing for the construction of multi-filament yarn, individual fiber, and aligned unidirectionally across a large area or enabling the individual filaments the develop an ordered pattern. Introducing a fiber-forming agent resulted in the formation of an elongated stable jet suitable for the collecting arrays of aligned fibers [146]. Research has shown that using the polymers with a higher molecular weight and increasing viscosity by increasing the concentration of the electrospinning solution results in a stable jet [139].

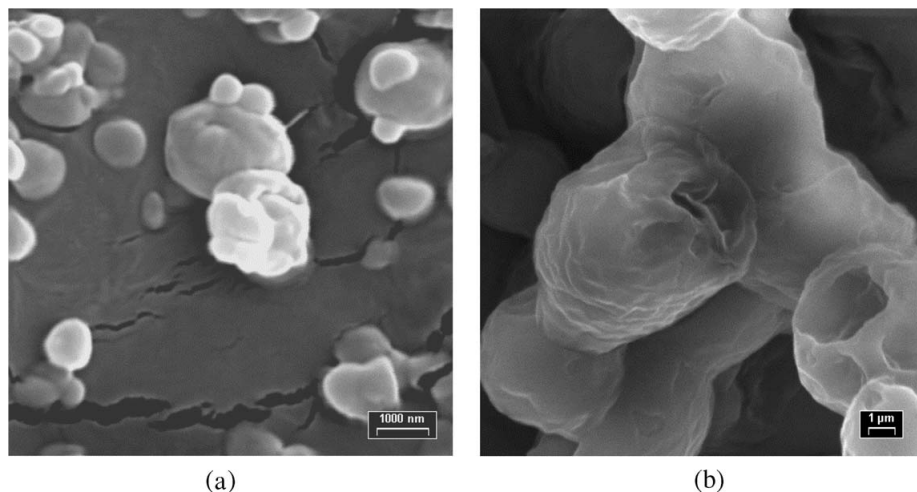


Fig. 1.15. (a) solid beads vs.(b) porous beads produced by electrospinning [147].

#### 1.4.2 Solvent

Selecting a proper solvent plays a prominent role in the electrospinning process. Since solutions conductivity, viscosity and surface tension are affected by a handful of solvents characteristics including solvents conductivity, boiling point, vapor pressure, polarity, dipole moment, dielectric constant, etc.

Solvent volatility ought to match up with the jets traveling time, i.e., solvents with low volatility result in wet web structure in the end. In the same manner, rapid evaporation of highly volatile solvents is accompanied with cooled down and frozen filament surface leading to a porous surface on the web structure [147].

Electro-spinnability of a solution can be enhanced by doping a solution using salt, using a solvent that has a high dielectric constant and higher conductivity as this increases the spinning jet charge density. However, these same factors result in a shortened length jet that ought to be avoided if one has an objective of attaining acquitting a stable jet with a greater length. Doping polyethylene oxide with salt illustrates higher conductivity minimizing the length of the stable jet. However, the chloroform system the critical conductivity between the bending instability and the long stable jet is estimated to be as low as  $0.6 \mu S/cm$  [148].

### 1.4.3 Voltage and Electric Field

Conventionally, in the electrospinning process, an increase in the voltage leads to an increase in the length of a stable jet. The elevation in length stems from a larger tangential electric field from starting from the needle tip as well as lower static charge density to stabilize the electrospinning jet. However, the conventional effect does not cater to all solutions. The inconsistency may be due to a variety of factors such as dielectric property and conductivity of the solution. These factors have more influence on jet stability [149].

The bending and stretching stability of the jet are affected by applied voltage in the sense that uniform patterned web could result at higher voltages in some cases. However, the applied voltage is not the only principal element, and other elements such as flow rate and jet traveling speed, and density have to be compromised at the same time [150].

Typically, the electrospinning process uses direct-current (DC) voltage; however, alternating-current (AC) has been reported in a few papers which are not considered as safe as DC voltage, particularly in high voltage circumstances [151–153]. The reason for taking advantage of AC could be witnesses when highly aligned fibers are sought. In this sense, highly aligned web structure is collected on a rotating mandrel when the AC power source is applied [154].

### 1.4.4 Flow Rate

The solution flow rate has to be reached at a minimum certain point at which the spinning jet can compensate for the solution evaporation rate in order to maintain the continuous flow of the fibers [155]. If the flow rate is higher than needed, the solution will accrue at the tip of the needle resulting in a formation of large droplets hindering the formation of normal Taylor cone, and ultimately solution dripping off the tip. Sometimes also blockage of the needle or nozzle happens, which is due to the rapid evaporation of the solvent, causing solidification of the droplet inside the needle or nozzle [156, 157].

#### 1.4.5 Collecting Distance

The collecting distance is proportional to the electric field intensity in the sense that solution traveling time can be affected directly. In some circumstances, less collecting distances can be helpful meaning that stronger electrostatic force is applied to the jet consequently shorter time for the jet to travel. A stronger electrostatic force can be either efficacious due to the effective stretching of the jet hence the formation of finer fibers on the collector. However, shorter distance may cause reverse effects, i.e., incomplete solvent evaporation, thereafter formation of wet fiber webs. Similarly, increasing the distance can lead to a weaker electric field and dripping of the jet in the half-way towards the collector [87, 138, 155, 156].

#### 1.4.6 Polarity

The electrospinning process with high voltage electrode applied to the nozzle causes more strong and concentrated electric field on the nozzle such that when the jet travels the distance from the high charged needle to the collector, it experiences a reducing electrostatic force. This facilitates the chaotic whipping instability, which brings about a large fiber deposition area. Contrary, a higher voltage applied to the collector leads to a more intense electric field near to the collector, i.e., it strengthens the jet movement toward the collector. This suppresses the whipping movement [86].

#### 1.4.7 Humidity

Electro-spun fiber morphology is influenced by ambient humidity, i.e., interaction between jet solution and moisture. Humidity can affect fiber diameter by means of modifying the solvent evaporation rate. The average diameter of nanofibers decreases with humidity increase. At relatively high humidity environments, beaded fibers start to form. Conversely, at relatively lower humidity level, the evaporation rate of the solvent could be high due to a difference in pressure between vapor and ambient air

inside the electrospinning chamber. As a result, fibers happen to solidify thereafter producing coarse fibers as compared to fibers generated in relatively higher humidity levels [158].

Humidity also affects the surface structure in such a way that, in fast evaporation circumstances caused by low humidity, porous fibers start to form. This could be explained by the fact that evaporation takes heat energy out of the jet surface, resulting in a reduction on surface temperature to a level that can initiate tiny ice formation on the filament surface. These tiny ices are preserved until the deposited fibers on the surface of collector exchanges heat with the ambient air and reaches the ambient condition [159].

#### **1.4.8 Temperature**

Temperature is considered to be in a close relationship with polymer properties affecting crystallinity and molecular chain orientations [86]. According to Yang et al., the surface tension and the viscosity of the electrospinning solution decreases with increasing the ambient temperature. However, an extra increase in temperature causes rapid evaporation of the solvent, which can disrupt the electrospinning process. Therefore, a balanced temperature point shall be found in order to gain the most desired fiber quality [158, 160].

### **1.5 Common Polymers in Electrospinning**

Polymers used in electrospinning can be natural, synthetic, or copolymer depending on the needs of the manufacturers as well as the availability of the materials. Examples of natural polymers include collagen, chitosan, and fibrinogen [87]. Natural polymers have some advantages over synthetic polymers due to their immunogenicity and biocompatibility. Natural polymers such as collagen and gelatin can provide solutions used in the electrospinning process. In circumstances where synthetic fibers are readily available, natural fibers may not suffice. Some of the synthetic

polymers include polyvinyl alcohol (PVA), Polyvinylpyrrolidone (PVP), polylactide (PLA), polyglycolide (PGA), poly-D-lactide (PLDA), and polylactide-co-glycolide (PLGA) [140]. Combining either natural or synthetic fibers or combining several synthetic fibers can produce copolymers [142].

The aim is to develop polymers that can withstand various limitations, including heat and degradation. Copolymers are usually developed to overcome the limitations of a given natural or synthetic polymer [143]. For example, adding poly (glycolide) can minimize the stiffness or rigidity of poly (ethylene-co-vinyl alcohol) (PEVA) [144]. Most copolymers provide a variety of features needed by manufacturers to develop suitable nanofibers.

## **1.6 Applications of Electrospinning and its Role in Energy Storage Systems**

Electro-spun fiber size may exist within the nanoscale while the fibers may have the nanoscale surface texture that results in various modes of interaction in comparison with the macroscale materials. The ultra-fine fibers arising from electrospinning have two significant properties, such as a large surface to volume ratio and a structure that is relatively free from defects at a molecular level. A high surface to volume ratio makes electro-spun materials suitable for undertaking activities that require a higher physical contact, including providing a site for a chemical reaction as well as the filtration of small-sized physical materials. Also, minimal defects at a molecular level allow electro-spun fibers to attain maximum strength, thus can attain high mechanical performance for composite materials [56].

There are various applications of electro-spun fiber can act as filters; for instance, the Lycopodium moss spores have a diameter of 60 micrometers, thus can only be captured by an electro-spun polyvinyl alcohol fiber. Nanofibers webs may act as an efficient filtering medium as the nanofibers have small London-Van Der Waals forces that are crucial for adhesion among the fiber that captures materials. Nanofibers

in textile manufacturing provide an opportunity of developing seamless non-woven garments that may have a variety of functions including environmental, flame, and chemical protection. Electrospinning can combine various coatings and fibers in order to develop three-dimensional shapes, for instance, clothing that consists of different layers of polymers [76].

Medical application of nanofibers involves tissue engineering where electro-spun scaffold may be penetrated with cells that treat or replace biological targets. Also, wound dressing using nanofibers have an excellent capability to separate the wound from microbial infections [77]. Electrospinning is essential in the development of medical textile materials or diverse fibrous treatment delivery system comprising of transdermal patches and implants. Electrospinning can ensure the establishment of a continuous manufacturing system within the pharmaceutical industry. Synthesized liquids can be turned into a tablet using electrospinning [78].

Electrospinning is a feasible process that can be suitable for the manufacture of elongated composite materials within a stipulated timeframe. The process has the potential to produce fibers in sufficient quantities within a reasonable period. Research has illustrated that electrospinning is the most cost-effective way to manufacture the various medical fibers such as medical implants, scaffolds, wound dress for artificial human tissues. Scaffolds function similarly like an extracellular matrix found in natural tissues [79]. Biodegradable fibers are used as an extracellular matrix and may be coated with collages in order to promote cell attachment. The last application of electro-spun fibers is that they act as catalysts, where they act as a surface where enzymes are immobilized. The enzyme can be vital in breaking down toxic chemicals from the environment [80]. The role of electrospinning is to produce fibers used in energy conversion and storage. The electrospinning process produces fibers with diameters ranging from nanometers to micrometers [161]. The fibers provide sufficient storage space and also plays a critical role in converting the stored energy into electrical currents. A general spinning setup consists of a high voltage power supply, a grounded collector, and a syringe with a metallic needle [162].

In most cases, the supply of the voltage is either a melt or a solution. As the heating continues, a pendant droplet forms beneath the syringe. The pendant droplet is subjected to electrostatic repulsion to turn it into a cone-shaped material known as Taylor cone. As the electrostatic propulsion continues, the conical droplet discharges polymer solution at the tip of the needle [163]. The interaction between the electric field and surface tension eventually forces the solvent to evaporate, leaving behind a long, thin filament which solidifies into a uniform fiber. Electrospinning began in the 1930s, and experts have used it in the development of fibers used in storing and conversion of energy inside the lithium-ion batteries [164]. Many adjustments have been made to the process to make it less energy consuming and more productive.

Some of the advantages of electrospinning include flexible temperatures, short production cycle, and little pressure. Besides, nanofibers synthesized from the hydrothermal method have a lower aspect ratio, which is critical in the transfer of energy [165]. In other words, fibers made from electrospinning are likely to provide more efficient energy transfer compared to other methods such as electro-spun NWs [166]. However, electrospinning also has various limitations, including difficulties in preparing inorganic nanofibers and limited quantity or variety of polymers used in the process. Limited variety of polymers restricts manufacturers to the use of available materials which may not reach the desired energy capacities [167]. Besides, the performance of nanofibers made from the inorganic materials is likely to decline after calcination. Manufacturers are also silent about the aging process which renders many batteries inefficient. The aging process drains the energy capacity of various cells and reduces the performance of lithium-ion batteries. According to Zhang, Tan, Kong, Xiao, and Fu (2015), much research is ongoing to determine the cause of aging and develop appropriate measures [81].

### 1.6.1 Electro-spun Vanadium Pentoxide

Although other fabrication methods have resulted in significant enhancement of the electrochemical performance, the processes are time-consuming and complex. Among these methods of preparing one-dimensional nanomaterials, electrospinning is considered to be the most versatile and promising synthesizing process for producing nanofibers in large scale [168]. Compared to these synthesizing methods, electrospinning facilitates the generation of thin fibers can have a relatively wide range of used as a result of its feasibility in generating nanofibers in large quantities with well-defined surface morphology at relatively low cost and less time [169].

Cheah et al. (2011) synthesized one-dimensional vanadium pentoxide nanofibers by electrospinning of vanadium precursor consisting of polyvinylpyrrolidone and vanadyl acetylacetonate [170,171]. Vanadium pentoxide nanotube has also been synthesized by electro-spinning using vanadium precursor containing vanadium (iv) acetylacetonate to obtain excellent electrochemical performance [54,172].

However, currently at present preparations of vanadium pentoxide nanomaterials utilizes organic vanadium precursors which are toxic, expensive, and easily hydrolyzed. Therefore, obtaining a low-cost and straightforward synthesis of one-dimensional vanadium pentoxide materials with excellent performance has remained a challenge. The renewed interest in vanadium Pentoxide arises from the need to have rechargeable batteries as well as higher-density batteries on Lithium-ion batteries. Lithium metal is used as the anode while vanadium pentoxide as the cathode. Vanadium pentoxide has the largest reversibility compared to other cathode materials. Nanostructures on lithium batteries provide improved capacities for performance by availing a large effective contact area to ensure diffusion of Lithium-ion and minimal resistance in regards to charge transfer. The layered phases availed contributes to its capacity of greater than 3 volts region with an enhanced specific energy of 726 Watt-hour per kilogram [169].

## 2. EXPERIMENTAL

### 2.1 Optimized Sol-gel Synthesis of Vanadium pentoxide ( $V_2O_5$ ) Suitable for Electrospinning

The  $V_2O_5$  xerogel was prepared by a straightforward, modified ion-exchange method. A 0.1 M solution of  $NaVO_3$  (Sigma, 99.5%) was eluted through a column loaded with a proton-exchange resin (Dowex-50-WX2, 100200 mesh). It is worth to mention those different solution concentrations of 0.1M, 0.15 M and 0.2 M were tested and the best outcome was resulted from 0.1 M. In a practical sense, seeking reason is that higher concentration solution can lead to more non-homogenous and more coagulated solution which deteriorates electro-spinnability of the solution. Also, different proton-exchange resin with mesh sizes of 50-100, 100-200, and 200-400 were tested, and the optimum obtained solution suitable for electrospinning was found to be Dowex-50-WX2, 100200 mesh. Other exchange resins were not suitable to obtain mature homogenous hydrogels. In the following, 0.1 M  $NaVO_3$  synthesis procedure is as follows:

### 2.2 Fabrication and Formation of Nanostructured $V_2O_5/GO$ Hybrid

After completion of  $HVO_3$  synthesis for almost lasting for almost 2-4 hours, 2-3 % GO was added to the obtained yellowish hybrid of  $HVO_3$  solution right away and bath sonicated for 30 min in order to achieve more uniform and well-dispersed GO in  $HVO_3$  solution (Figure 2.3). Then, the  $V_2O_5/GO$  hybrid was aged from a few hours to a few weeks, and the  $V_2O_5$  growth on GO sheets was carefully observed as the  $V_2O_5/GO$  hydrogel starts to form. The solution gradually changes color from yellow to dark brown during first few days, and ultimately after 12 weeks to dark red,

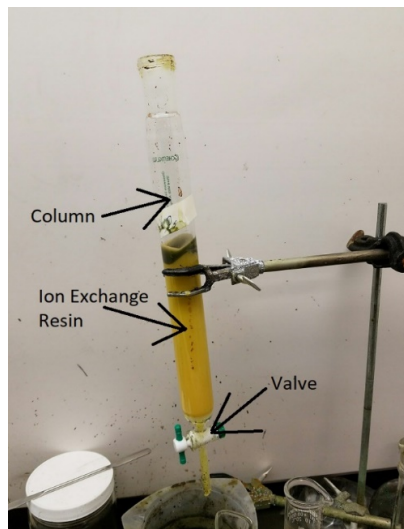


Fig. 2.1. Ion-exchange column for vanadium pentoxide synthesis.



Fig. 2.2. Yellowish  $HVO_3$  solution, which brings about  $V_2O_5$  formation.

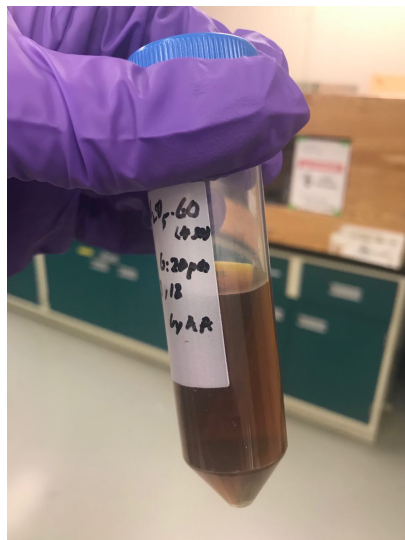


Fig. 2.3. Dark brown bath sonicated GO (2%) dispersed in  $HVO_3$  solution.

signifying the completion of the nucleation process, leading to a three-dimensional network of  $V_2O_5$  hydrogel Figure 2.4. Concerning synthesis  $V_2O_5/GO$  suitable for the electrospinning,  $V_2O_5$  ribbons dispersed in GO (2%) are let to grow for at least 7 hours to form the minimum required ribbons for the sake of fabrication of high capacity cells.

### 2.3 Centrifuging

The resulting suspension ( $V_2O_5/GO$ ), before electrospinning, was centrifuged to remove the unreacted acids and salts. The obtained hybrid, was centrifuged at the speed of 2500rpm with a centrifuging duration of almost 5 min. Higher speeds causes precipitation of GO and  $V_2O_5$  ribbons and forms two-phase solution, which is not desirable for electrospinning,  $V_2O_5$  ribbons and graphene oxide flakes.



Fig. 2.4. Dark red 2 weeks old  $V_2O_5/GO$  : signifying the completion of the formation of a 3D network of  $V_2O_5$  hydrogel.



Fig. 2.5. Dark brown  $V_2O_5/GO + PVA$  hybrid.

## 2.4 Synthesis of $V_2O_5/GO$ Mixed with Polymer

$V_2O_5/GO$  hybrid was mixed with a proper amount of PVA or PVP in order to make the solution electro-spinnable [83,173–177]. The nucleation immediately (0 min) occurs once the  $HVO_3$  solution is formed right after  $NaVO_3$  passes through the ion exchange column. Finally, after two weeks, the 3D network of  $V_2O_5/GO$  hydrogel is completely shaped. However, the proper timing for the growth of  $V_2O_5/GO$  hydrogel network for the electrospinning purposes is estimated to be between 7-12 hours. After mixing with polymer, the obtained dark yellow colloid solution was kept in a glass on a magnetic stirring plate to attain a homogeneous hydrogel for 24 hours (Figure 2.5).

## 2.5 Electrospinning

Vanadium pentoxide-based fibers with smooth surfaces were prepared by electrospinning from a clear dark red solution containing 0.45:4  $V_2O_5$  sol-gel precursors and PVP. In the following pictures, solutions mixed with PVP during the electrospinning process and the final electro-pun sample (Figure 2.9) can be observed. Also, the general electrospinning setup and a replete syringe used for spinning are shown in the following pictures (Figure 2.7, Figure 2.8).

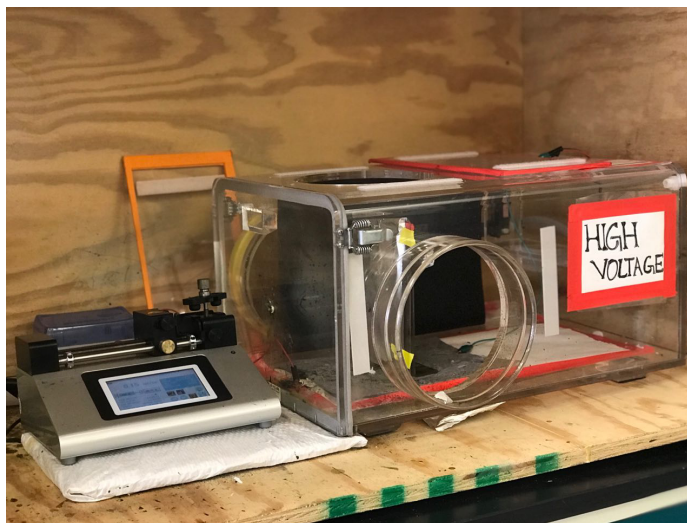


Fig. 2.6. Electrospinning setup.



Fig. 2.7. Solution inside the BD 10 ml syringe with a needle gauge size of 25G.

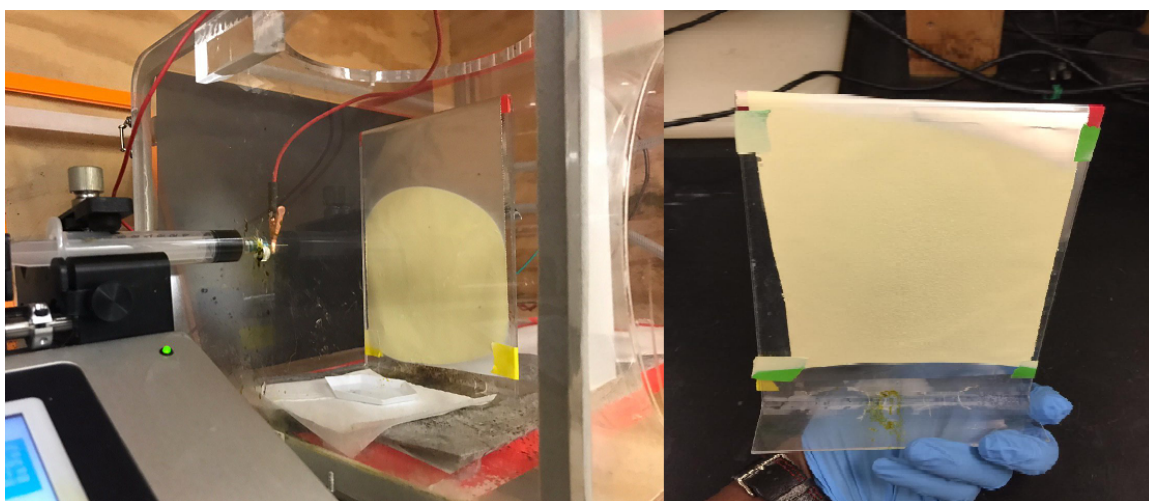


Fig. 2.8. Electro-spun [ $V_2O_5/GO + PVP$ ] (0.45:4).

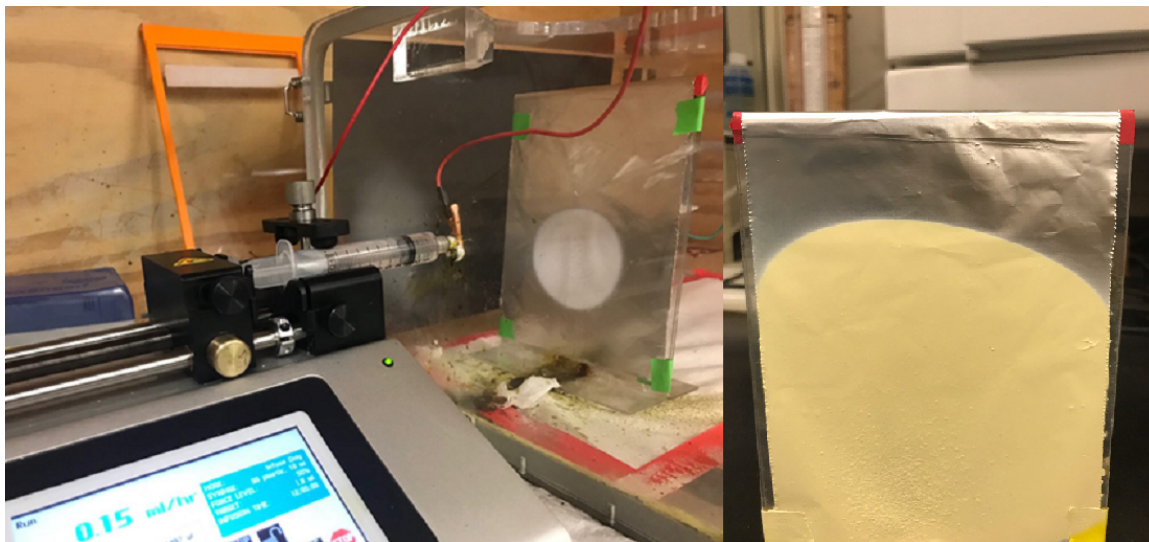


Fig. 2.9. Final electro-spun [ $V_2O_5/GO + PVA$  (3:20 in water)] (10:4).

Also, Vanadium pentoxide-based fibers with smooth surfaces were prepared by mixing PVA in clear dark red solution containing 4 (PVA in water): 10 ( $V_2O_5$  sol-gel precursors) (Figure 2.10). PVA requires to be dispersed in hot water, i.e., 90 °C as the PVP and water mixture maintained at around waters boiling temperature for almost 3 hours. This will result in a homogeneous PVA mixture which later can be well mixed with  $V_2O_5$  xerogel.

Once the electrospinning is finished, the achieved fibers could be scrapped off from the aluminum collector.

## 2.6 Thermal annealing

Polymer removal from the electro-spun samples is a critical part. If the whole amount of the polymer (here PVP and PVA, electro-spun separately) remains in the electro-spun samples, it can act as an insulator during Lithium intercalation and deintercalation procedures. We have observed that post-synthesis treatment conditions



Fig. 2.10. Annealed electro-spun  $V_2O_5/GO + PVA$  (0.25g) at 400 °C .

play a prominent role in electrochemical performance of the fabricated cells. It is critical, to find an optimal drying and annealing temperatures of electrodes to be rest assured that an efficient water is removed from the crystal structure of synthesized material. Specially, in this case, when the fibers are fabricated with thermoplastic polymers such as PVA and PVA. By controlling the annealing and drying time and steps, a small amount of pyrolysis carbon can be retained, which could improve the conductivity of the  $V_2O_5$  nanorods. Also, controlled post-synthesis helped us to prevent aggregation of electro-spun twisted nanostructured fibers which deteriorates the lithium diffusion process during charge/discharge of batteries. In this regard, the formed  $V_2O_5/GO$  hydrogel was heated and annealed under  $N_2$  at different rates and timings. After several endeavours, a rate of  $5C.min^{-1}$  and a holding temperature of 400 °C for 6 hours, was found to own the best outcome. During which the GO is reduced to graphene, and the graphene-modified  $V_2O_5$  hybrid is formed.

## 2.7 Electrode Fabrication

The electrodes were cast with a slurry of 70%  $V_2O_5/rGO$ , 10% polyvinylidene difluoride (PVDF), and 20% carbon black onto a 10-mm-thick sheet of aluminum

(Al) foil. Active materials are coated on a conductive surface (here Al.) which acts as a current collector. Active material crystals are required to be attached to the aluminum surface. In this regard, a binder comes to use and is mixed with the active material and deposited over the current collector. Binder is mostly an ionic conductive polymer like PVDF, which is dissolvable in a solvent such as acetone, ethanol, or *n*-methyl-2 pyrrolidone (NMP). In this case, NMP has been used as a binder. This binder can produce enough adhesion between the particles and the conductive surface, whereas it can transfer ions from interior layers of the active material layer to the outer surface.

NMP is widely used in electrode fabrication owing a low boiling point, being non-reactive in contact with the conductive microfiber paper, and acting as a better solvent for the binder. To have a complete active material slurry, some highly conductive particles such as carbon black, SuperP Carbon, SuperP Lithium (from Timcal) or  $KS_6$  must be added to the solution active material. These highly conductive materials increase the conductivity of the active material layer and transfer the electron from the middle layers to the current collector. These can also produce different conductive layers between the active materials. SuperP Carbon or Lithium is highly conductive carbon compound with the particle size of about 40 nm while  $KS_6$  is a graphite compound with around 1 to 3  $\mu m$  size. SuperP is used to provide particle to particle connection, electrolyte absorption, and dispersed in the binder.  $KS_6$  also can provide more significant conductive paths with a porous structure.

Lithium salts are the primary materials of each electrode. Other highly conductive materials which are not reacting with lithium and their particle size are in nano, or some micrometer could be used as well such as carbon black, or graphite. The as-prepared slurry of binder and active materials are deposited over the current collector using different methods such as blade coating or spray method and form electrodes. The prepared electrodes were placed in a vacuum oven and allowed to dry at 80°C for 24 h. All the materials of the electrode paste are mixed and ground, before adding the NMP solvent. This solvent dissolves the PVDF and improves the adherence of the

electrode materials. This mixture needs to stir for overnight to become completely uniform. Overnight stirring is needed due to the low dissolution rate of PVDF in the solvent. The final paste is coated over the current collector films with spray coating and blade coating methods. Although blade coating is a standard method of making electrodes, spray coating can produce better results. Spray coating is using a lower amount of binder in the paste mixture.

Furthermore, this method can also provide thinner and more efficient electrodes. The thickness of the active material layer is related to the number of sprays over the substrate and the concentration of the solution. The maximum thickness of the active material layer reaches to 50  $\mu\text{m}$ . The electrodes then dry inside a vacuum oven for 12 hours with the temperature from 80 to 90°C . After the drying process, the electrodes must be rest inside the vacuum oven for cool down process. Polymer binder can absorb moisture when it is warm and reduce the quality of the electrode. This drying process is necessary to remove the solvent and water particles from the electrode.

## 2.8 Battery Assembly

The half-cell was prepared by using a working electrode to assemble a half-cell configuration inside a dry glove box with Li metal as an anode,  $\text{LiPF}_6$  1 M in an EC/DEC (1:1 by volume, purchased from Novolyte) as an electrolyte, and a Celgard PP membrane as a separator. Using Arbin BT-200 Battery Tester, the cell was electrochemically cycled at room temperature. A field emission scanning electron microscope was used to determine the morphology of the electrodes before cycling.

The cell fabrication process must be held inside an argon-filled glove box to avoid any possible damages to the cell, the  $\text{V}_2\text{O}_5/r\text{GO}$  cathodes have to be cut into circular shapes with a diameter of 0.58 cm, and Li metal anodes are cut into circular shapes which are not allowed to exceed the diameter of the coin cells. Then, the cathodes are kept inside a vacuum oven with a set temperature of °C for 24 hours in order

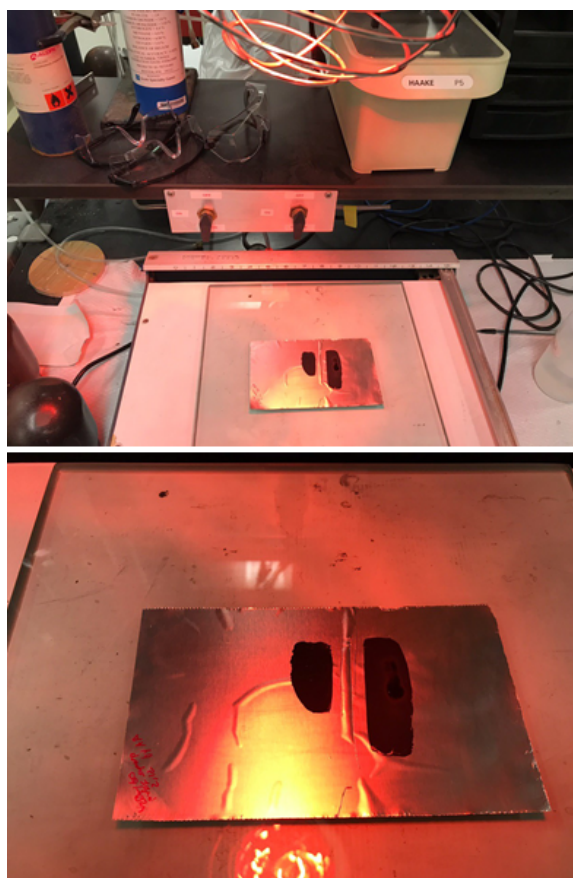


Fig. 2.11. Blade coated cathode material on Aluminum foil with a thickness of 30-35  $\mu m$  under IR light for 2-3 hours.

to remove the excess water from them. The Li anodes have to be kept inside the glovebox all the time. Lithium powder can be highly reacted due to its large surface area. Sometimes chunks of lithium metal are soaked in oil or kept with some other hydrocarbon to avoid any possible incidents since lithium possess highly flammable nature. While using a glove box and handling lithium, in case safety equipment should be kept close to hand, to extinguish any possible lithium fire.

The CR2016 coin cell configuration with a stainless steel spacer and spring or a nickel foam are used to encapsulate electrodes and separator within the cell. The  $V_2O_5/rGO$  cathode electrode is already deposited on Aluminum (Al) surface which the Al foil is in touch with the lower bottom of the coin cell to perform as a current collector for the battery. Next, a Celgard PP separator film separates the cathode from Li anode on top. Then, stainless still spacer with a spring or nickel foam is placed on top of Lithium, which keeps a distance from the outer shell of the coin cell. The battery assembly is soaked in  $LiPF_6$  1M in an EC/DEC electrolyte solution (1:1 by volume, purchased from Novolyte), pressed, and encapsulated in a coin cell. The CR2016 coin cell indicates a cell diameter of 20 mm with 1.6 mm in height. After all, the fabricated coin cell is kept undisturbed for 24 hours, allowing it to reach a stable state by thoroughly soaking the electrode materials and the separator with the electrolyte solution.

## 2.9 Cell Testing

After battery assembly, fabricated coin cells are stored in a proper container in order to allow them to rest for 24 hours to reach the optimum and most stable statues of the battery. This helps the cell the electrode and separator to be completely soaked in the electrolyte solution.  $V_2O_5/rGO$  half cells are tested using Arbin BT200 battery testing system. Two types of experiments were conducted for these cells. The first type of experiment is the galvanostatic charge/discharge test, and the second type is the self-discharge tests. From galvanostatic charge and discharge experiments, the



Fig. 2.12. Arbin BT2000 battery cycle general setup.

working voltage and current of the testing cell should be set. The voltage is related to the lithium salts were used inside each cell, and the current is related to the internal resistance and time of the experiments. Due to testing the cycle life of the cell, each battery is set to be tested between 15 to 50 cycles to observe the factors such as degradation, short circuit current, and safety issues such as high temperature or explosive reactions. During all of the experiments, the voltage range, the number of cycles, the safety margins, and the testing current is set separately regarding the active materials of each test [178].

### 3. RESULTS AND DISCUSSION

#### 3.1 Fabrication of a Polymerized Nanostructured $V_2O_5/GO$ Hybrid for Electrospinning

An optimized sol-gel method has been developed to synthesis  $V_2O_5/GO$ . Different solution concentrations of 0.1 M, 0.15 M and 0.2 M were tested and the best outcome was resulted from 0.1 M concentration. Higher concentration solutions can lead to more non-homogenous and more coagulated solution which deteriorates electrospinnability of the solution. The optimum obtained solution suitable for electrospinning was found to be Dowex-50-WX2, 100200 mesh. After completion of  $HVO_3$  synthesis for almost lasting for almost 2-4 hours, 2-3% GO was added to the obtained yellowish hybrid of  $HVO_3$  solution right away and bath sonicated for 30 min in order to achieve more uniform and well-dispersed GO in  $HVO_3$  solution (Figure 3.2). Also, for better understating, the PH level of  $HVO_3$  solution before and after mixing with GO is shown (Figure 3.1), which represents that PH scale remains pretty much the same at nine.

Then, the  $V_2O_5/GO$  hybrid was aged from few hours to few weeks, and the  $V_2O_5$  growth on GO sheets was carefully observed as the  $V_2O_5/GO$  hydrogel starts to form. The hybrid gradually changes color from yellow to dark brown during first few days, and eventually after 12 weeks to dark red, signifying the completion of the formation of a 3D network of  $V_2O_5$  hydrogel Figure 3.3.

Concerning synthesis of the electro-spinnable  $V_2O_5/GO$ ,  $V_2O_5$  ribbons dispersed in GO (2%) are let to grow for at least 7-12 hours to form the minimum required ribbons for the sake of fabrication of high capacity cells. However, it is worth to mention that aging  $V_2O_5$  ribbons more than a day will result in the formation of non-homogenous gels on most occasions, which is not desirable and applicable for the

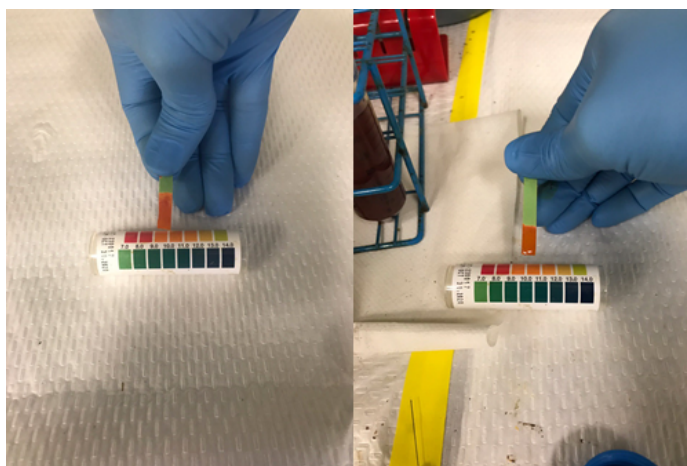


Fig. 3.1. Left Picture:  $V_2O_5$  hydrogel PH level before mixing with GO Right Picture:  $V_2O_5$  hydrogel PH level after mixing with GO.

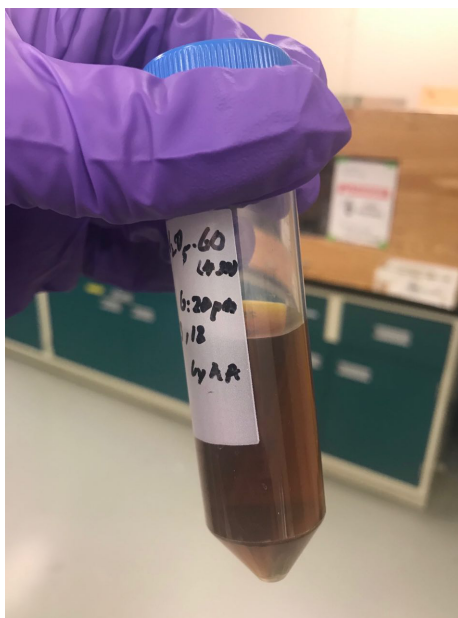


Fig. 3.2. Dark brown bath sonicated GO (2%) dispersed in  $HVO_3$  solution.



Fig. 3.3. Dark red  $V_2O_5/GO$  after 2 weeks of aging bringing about the formation of completed network of  $V_2O_5$  hydrogel.

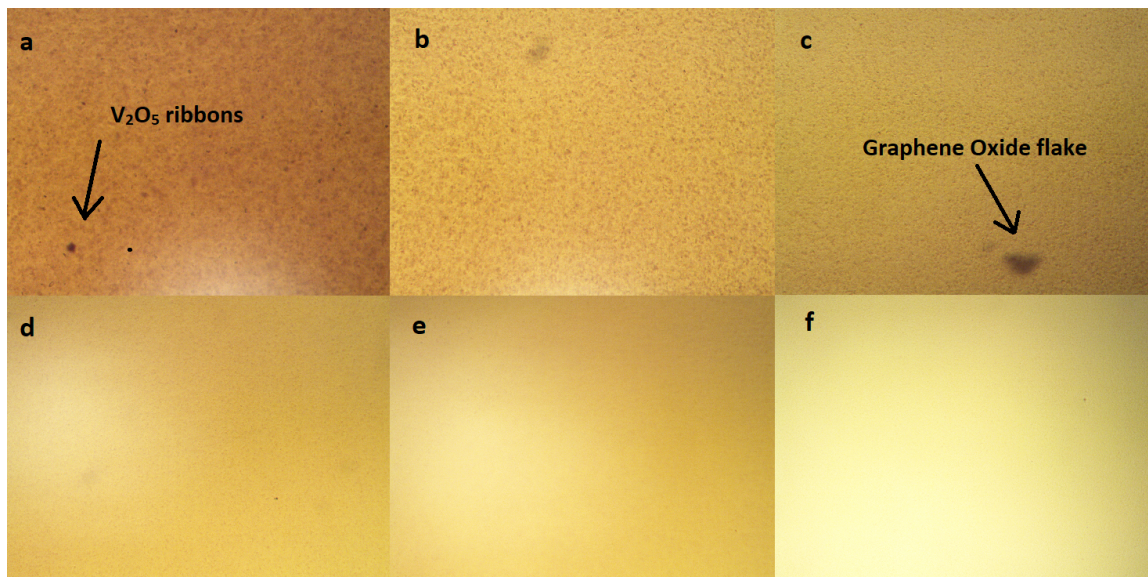


Fig. 3.4. 50X magnification microscope pictures of centrifuged  $V_2O_5/GO$  at speeds of a) not centrifuged; b) 2500 rpm; c) 6000 rpm; d) 10000 rpm; e)12000 rpm; f)14000 rpm.

electrospinning process. In order to be rest assured that the formed hybrid is perfectly suitable for electrospinning, the hybrid was centrifuged. A case study on the speed and duration of the centrifuging process of the prepared solution was conducted. After several times of trying, the speed of 2500rpm with a centrifuging duration of almost 5 min was found to be the sweat-spot in this process. It can be perceived from the microscope pictures that centrifuging at higher speeds causes precipitation of GO and  $V_2O_5$  ribbons and forms two-phase solution, which is not desirable for electrospinning.  $V_2O_5$  ribbon and graphene oxide flakes observed under the microscope are depicted in Figure 3.4.

However in a few occasions, under the careful synthesis of homogenous 0.1 M  $NaVO_3$  and subsequently careful synthesis of  $V_2O_5$  sol-gel through the cleaned column with a proper resin mesh size, homogenous  $V_2O_5$  gel will result after two weeks which is the optimum timing for the formation of fully grown  $V_2O_5$  network on GO sheets.

PVP was mixed with such a gel after two weeks but it could not form a well-dispersed and homogenous solution. In this regard, PVA was introduced and mixed with a two weeks old  $V_2O_5/GO$  gel, and the quality of the final colloid solution was satisfying and homogenous, thus spinnable. After mixing with polymer, the obtained dark yellow colloid solution was kept in a glass on a magnetic stirring plate to attain a homogeneous hydrogel for 24 hours.

However, PVA requires to be dispersed in hot water, i.e.,  $90^\circ\text{C}$  as the PVP and water mixture are maintained at waters boiling temperature for almost 3 hours. This will result in a homogeneous PVA mixture which later can be well mixed with  $V_2O_5$  xerogel. It should be bared in mind that the  $V_2O_5$  sol-gel cannot be heated up due to its sensitivity to temperature, resulting in a non-homogenous and gel-like shape. Although with PVA, not with PVP, 2-3 weeks old homogeneous vanadium oxide hydrogel could be spun, a large amount of water is required. For the  $V_2O_5$  xerogel, abundant water may react with the lithium to form  $Li_2O$ , which deteriorates intercalation performance, consequently, lowers the capacity to around  $100\text{ mAhg}^{-1}$ . Therefore, better results was attained with PVP mixed with the hybrid after 7-12 hours, since it could be mixed directly in  $V_2O_5$  hybrid.

### 3.2 Morphology of Electro-spun Fibers

The electrospinning process is dependent on polymer concentration as the most crucial factor. This dependency emanates from the fact that change in polymer concentration leads to a change in solution viscosity. Having said that, as the polymer concentration increases, the viscosity increases, too, but at a steady rate at first and after that at a much higher rate [140]. The solution viscosity is extremely governed by intermolecular interactions between polymer-polymer, polymer-solvent, and solvent-solvent within the polymer solution. Electrospinning a dilute polymer solution is analogous to an electro-spraying process, and the polymer intermolecular distance within the solution is so considerable that the interaction is considered to be very

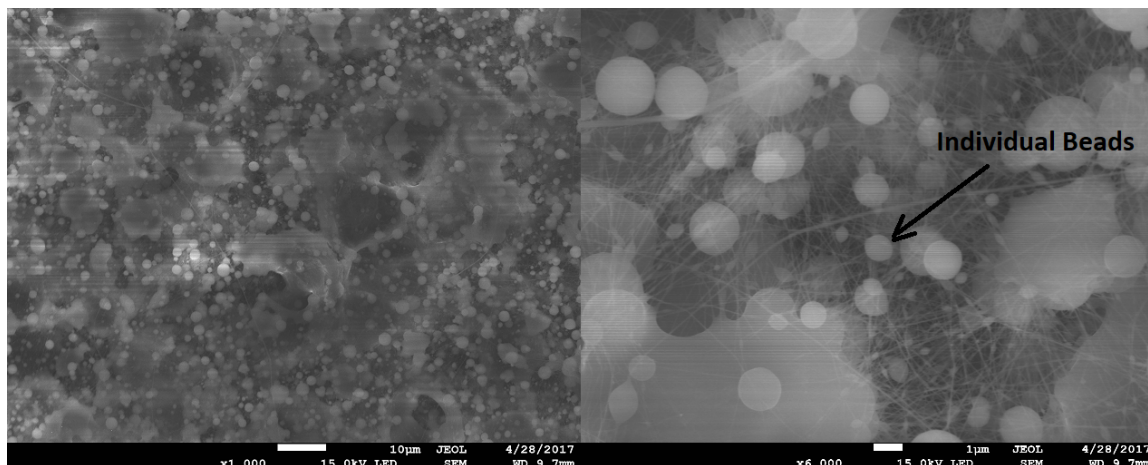


Fig. 3.5. An example of individual beads of electro-spun  $V_2O_5$  (polymerized after 7hr; 1:4) + GO + PVP.

weak. Therefore, the viscoelastic force in the polymer jet is minute to form a uniform fibrous structure. In this process, the jet splits into separate charged sections as the voltage is applied. Gradually these charged sections turn into droplets or individual beads as a result of high surface tension caused by solvent evaporation while spinning Figure 3.5. Similarly, an increase in the polymer concentration leads to higher viscoelastic force and more difficult for the jet to be split. In lieu of breaking the like-charged sections, electrostatic repulsion within the solution elongates the links between charged sections, consequently forming thinner filaments. Relatively thicker sections stretch thinner although to the links between charged sections. As the solvent evaporates while spinning, due to the surface tension, filaments tend to take the shape of beads-on-string morphology Figure 3.6. Accordingly, a further increase in the polymer concentration, brings about uniform elongation of and formation of the jet, resulting in homogeneous fiber morphology Figure 3.7 [86, 87, 140, 141].

In this regard, both PVP and PVA in different concentration and aging timing were mixed with  $V_2O_5/GO$  hydrogel. After several attempts, the optimized amount for both polymers were found. It is believed that, 0.45 (PVP): 4 ( $V_2O_5/GO$ ) and 4

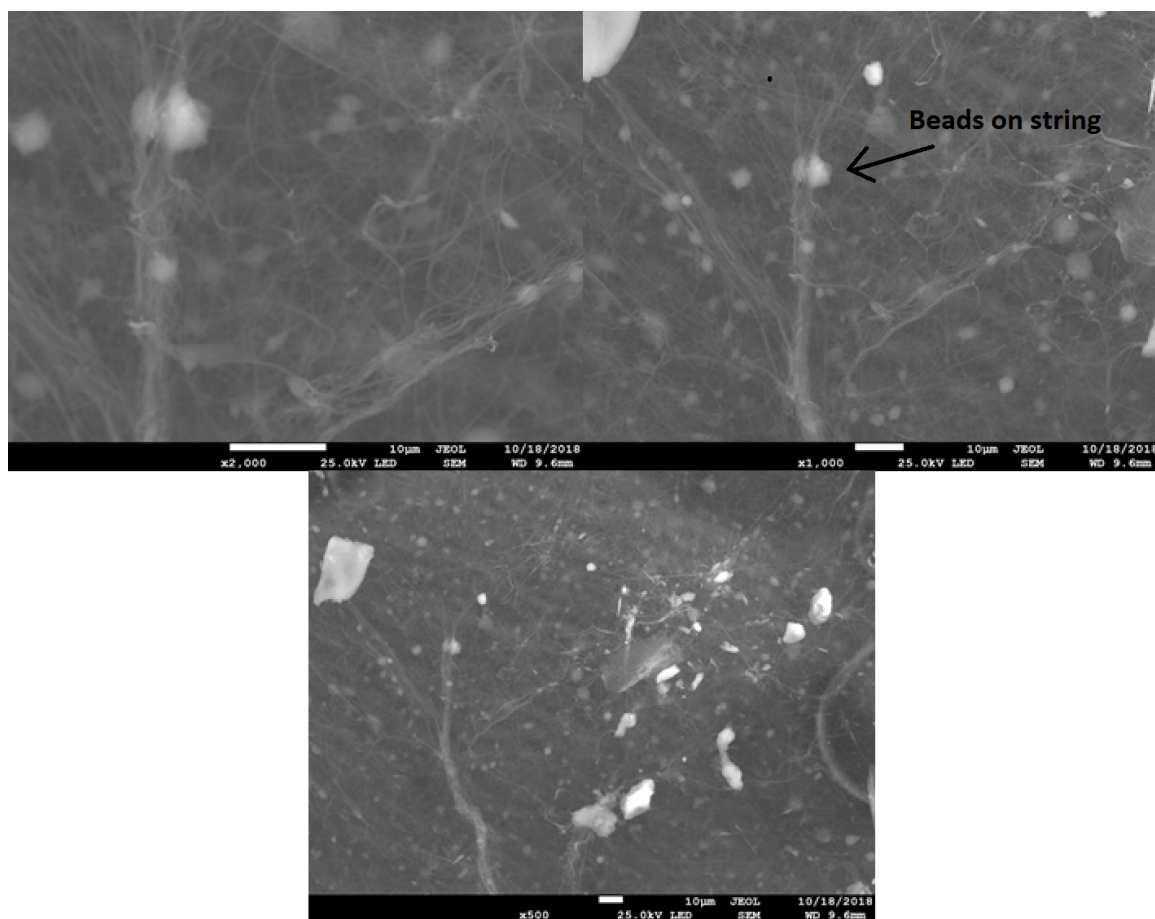


Fig. 3.6. An example of beads on strings of electro-spun  $V_2O_5$  (polymerized after 7hr; 1:4) + GO + PVP.

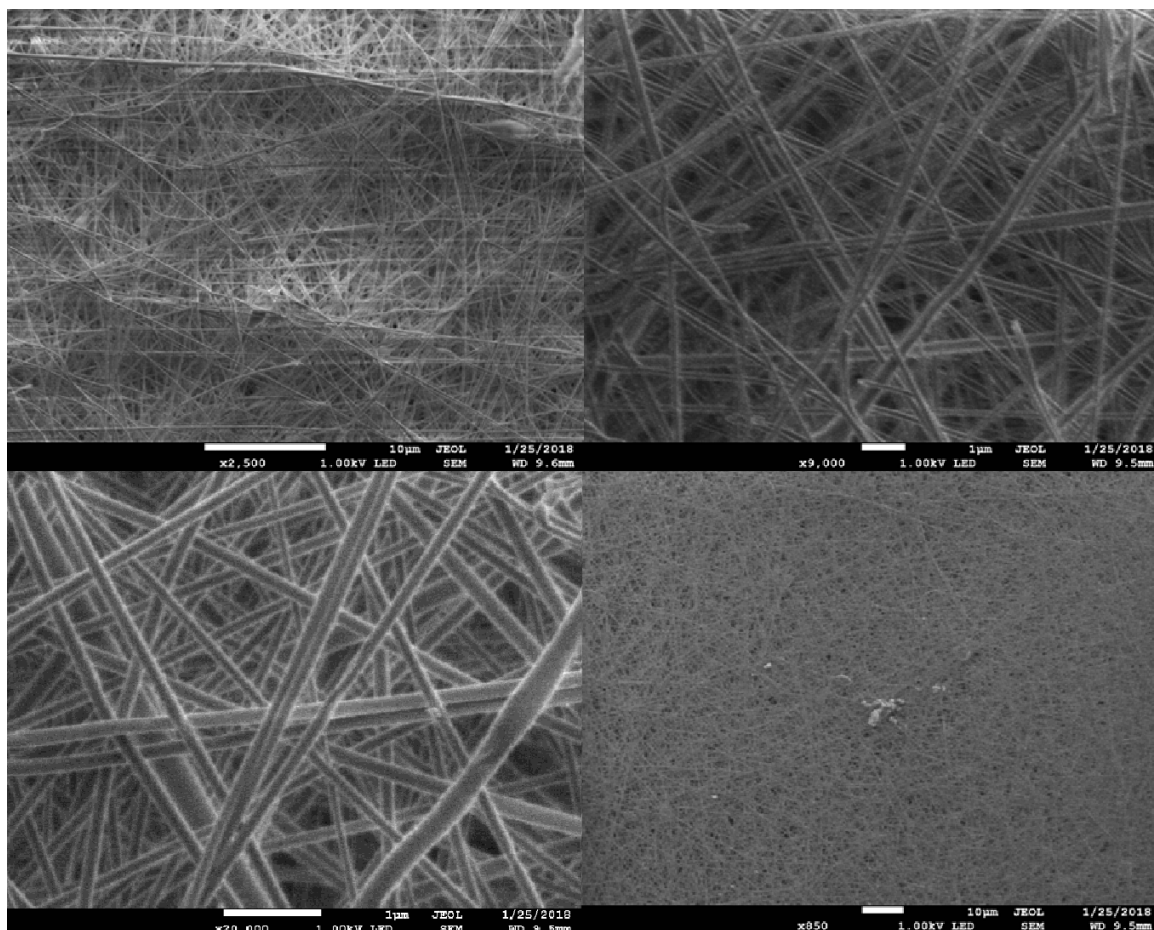


Fig. 3.7. An example of uniform electro-spun  $V_2O_5/GO$  (polymerized after 7 hours with PVP).

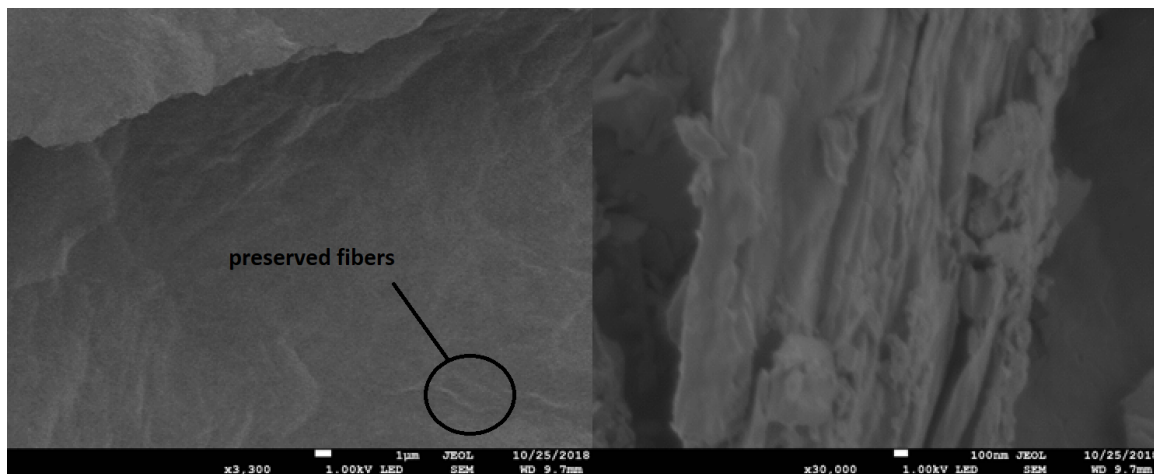


Fig. 3.8.  $V_2O_5r/GO + PVP$  (polymerized after 7hrs): after annealing in  $N_2$  (@  $400^\circ C$ ).

(PVA in water): 10 ( $V_2O_5/GO$ ) are the suitable ratios for electrospinning purposes. Also, annealed electro-spun fibers are provided (Figure 3.8, Figure 3.10), and the preserved regions of fibers have been shown. Due to the thermoplastic behavior of PVA and PVA, and carbonized polymer at  $\sim 400^\circ C$ , some electrospun fibers has been aggregated, leading to an amorphous structure in some regions. However, some preserved region of fibers are shown in the following pictures.

Selecting a proper solvent plays a prominent role in the electrospinning process. Since solutions conductivity, viscosity and surface tension are affected by a handful of solvents characteristics including solvents conductivity, boiling point, vapor pressure, polarity, dipole moment, dielectric constant. In most cases, water is selected to be as a solvent for PVA and PVP. However, in many incidents, it was observed that the resulted polymerized  $V_2O_5$  xerogel forms a two-phase non-homogenous colloid solution. To tackle this problem, hydrogen peroxide ( $H_2O_2$ ) was used to breakdown the non-homogenous hydrogel. In most case, the resulted solution viscosity was not enough for electrospinning purposes as it changes the sol-gel to a runny liquid solution. In a few cases, after several attempts,  $V_2O_5/GO + PVP$  diluted in water and ( $H_2O_2$ )

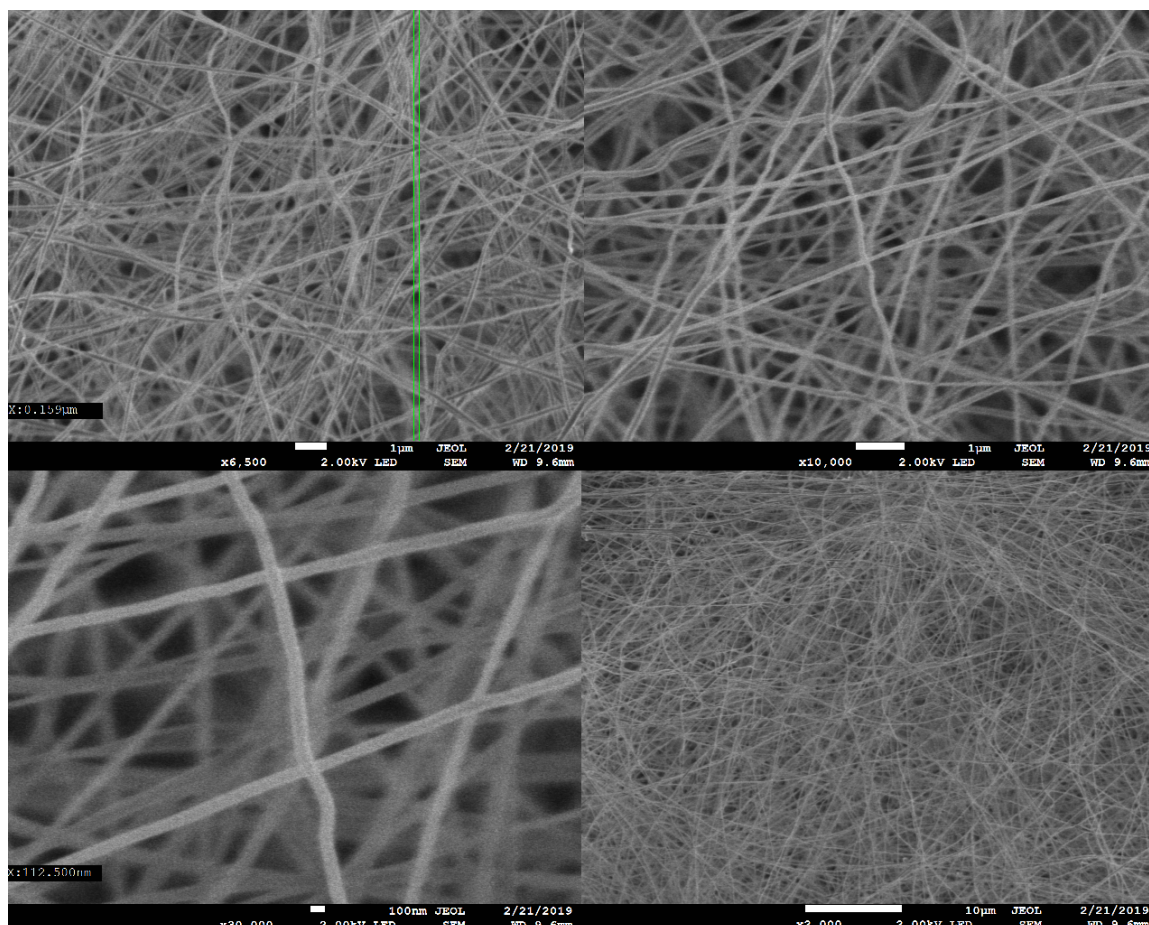


Fig. 3.9. An example of uniform electro-spun  $V_2O_5/GO$  (polymerized after 2 weeks with PVA).

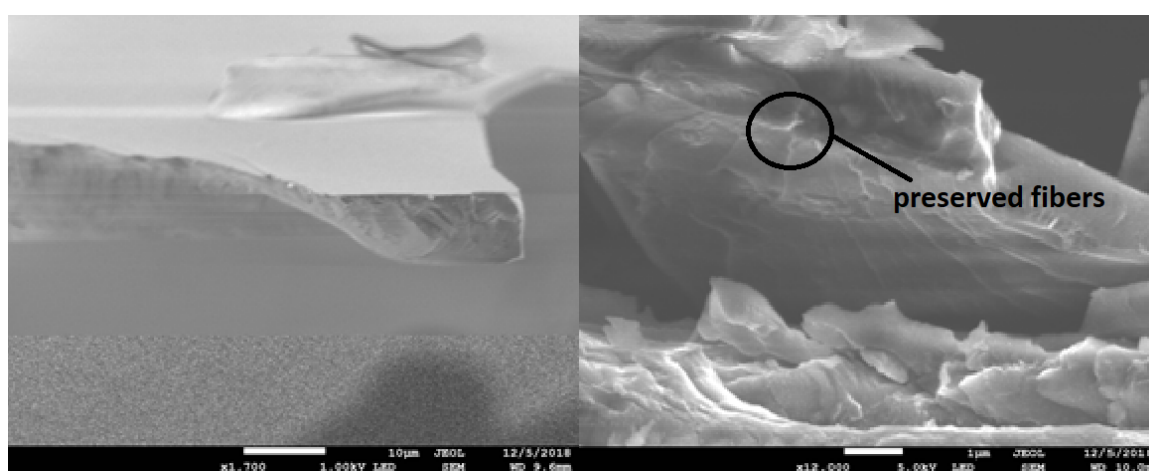


Fig. 3.10.  $V_2O_5/rGO + PVA$  (polymerized after 2 weeks): after annealing in  $N_2$  (@  $400^\circ C$ ).

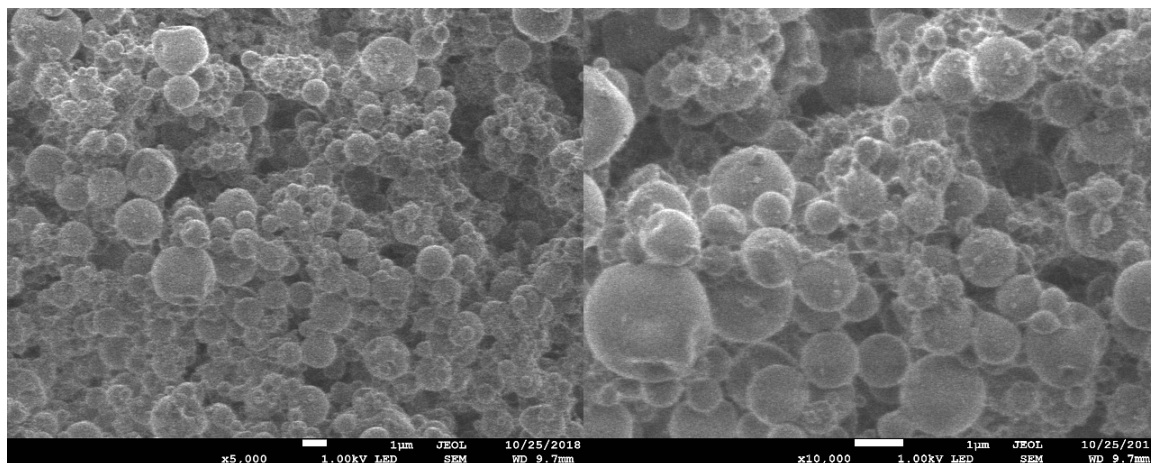


Fig. 3.11. Electro-spun  $V_2O_5/GO + PVP$  in  $H_2O_2$  and water.

could be electrospun as shown by the following figure (Fig 3.11). As shown in the picture, there is no sign of formation of a nanofibrous structure which is believed to be the remnants of ( $H_2O_2$ ) as it could not be evaporated during the electrospinning process.

As a result of this, dimethylformamide (DMF) was tried out to overcome the aforementioned problem as a solvent. In this regard, DMF was mixed with the hydrogel in different ratios. The outcoming fibers were not desirable as it obviously can be perceived that no fibers are not shaped (Fig 3.12).

In the end, in cases of  $V_2O_5/GO + PVP$  and  $V_2O_5/GO + PVA$ , it was testified by several experiments, by synthesizing  $V_2O_5/GO$  xerogel in different ratios of water, DMF, and ( $H_2O_2$ ), that the achieved electrospun morphology could not lead into an interconnected nonfibrous structure. As we keep the hydrogel more intact and less complicated, the electrospinning process is more facilitated. In a sense that, the solution inside a syringe possesses more viscous properties and the excess solvent could be evaporated more easily while spinning.

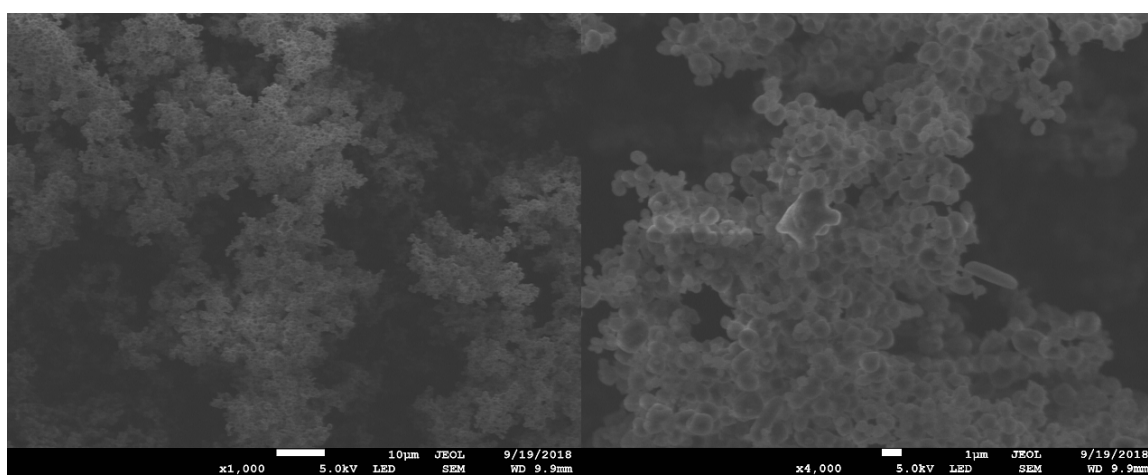


Fig. 3.12. Electro-spun  $V_2O_5/GO + PVP$  in DMF and water.

### 3.3 Vanadium Oxide-based Cathode and Lithium Cells

Most of the current cathode materials in lithium-ion batteries exhibit a specific capacity meaningfully lower than  $200 \text{ mAhg}^{-1}$  (e.g.,  $140 \text{ mAhg}^{-1}$  for  $\text{LiCoO}_2$ ). One exception is vanadium-based materials (e.g.,  $\text{VO}$ ,  $\text{Li}_x\text{VO}_2$ ,  $\text{V}_2\text{O}_5$ ,  $\text{Li}_x\text{V}_2\text{O}_5$ ,  $\text{V}_3\text{O}_8$ ,  $\text{Li}_x\text{V}_3\text{O}_8$ ,  $\text{Li}_x\text{V}_3\text{O}_7$ ,  $\text{V}_4\text{O}_9$ ,  $\text{Li}_x\text{V}_4\text{O}_9$ ,  $\text{V}_6\text{O}_{13}$ ,  $\text{Li}_x\text{V}_6\text{O}_{13}$ , their derivatives, their doped versions, and combinations thereof, wherein  $0.1 < x < 5$ ) that exhibit extraordinary specific capacity due to their ability to incorporate more than one lithium ion per Vanadium atom. A theoretical specific discharge capacity of  $443 \text{ mAhg}^{-1}$  can be achieved when three lithium ions intercalate into  $\text{V}_2\text{O}_5$  [69]. D.A. Semenenko et al. reported an ultra-high capacity of  $490 \text{ mAhg}^{-1}$  attributed to  $\text{Li}_x\text{V}_2\text{O}_5$  nano-belts with the  $\delta$ -type crystal structure. The enhanced electrochemical properties of this battery is attributed to the sophisticated post synthesis treatment of the single-crystalline  $\text{Li}_x\text{V}_2\text{O}_5$  nanobelts [70]. However, vanadium-oxide based batteries are not vastly commercialized due to the following reasons:

1) Electrochemical properties, including specific capacity, capacity retention, rate capability, and long-term cyclability, are profoundly affected by fabrication conditions, including pre-synthesis and post-synthesis circumstances.

2) In most cases of high initial capacity, i.e., higher than  $300 \text{ mAhg}^{-1}$ , the specific capacity usually drops by a large amount over repeated charge and discharges. However, in cases of lower capacity, i.e., less than  $250 \text{ mAhg}^{-1}$ , capacity retention is found to be rational. However, this amount is by long shot lesser than theoretical discharge capacity ( $443 \text{ mAhg}^{-1}$ ) and the highest reported capacity ( $490 \text{ mAhg}^{-1}$ ). Seldom, one can find a vanadium oxide-based lithium battery with both high specific capacity, and reasonable capacity retention needs to be met. To overcome this problem, in this research, graphene-modified vanadium-based cathodes prepared through optimized sol-gel method has been investigated to meet thereof needs. The synthesized  $\text{V}_2\text{O}_5/\text{rGO}$  also exhibits improved cycling stability. This half cell achieved 87% initial after 10 cycles and 79% initial after 10 cycles at 0.5 C.

3) Higher current rates have a considerable effect on specific capacity while charging/discharging. Even though in some literature, nano-structure morphology, i.e., nanoparticles, nanorods, nanowires, nanosheets, and nanobelts have been synthesized, vanadium-based cathodes still fall short in terms of providing a good capacity at a high rate (i.e., they exhibit poor rate capability). Concerning this issue, the initial capacity of  $342 \text{ mAhg}^{-1}$  has been reported at 0.5 C, which is considered to be a high current density for battery testing. It is worth to mention that due to their nanostructured morphology, electro-spun  $\text{Li}_x\text{V}_2\text{O}_5$  nanorods demonstrate significantly high specific capacities at high current densities. The high capacity values of  $\text{Li}_x\text{V}_2\text{O}_5$  nanofibers can be accomplished as a result of the large surface area and short diffusion length typical of nanostructured materials.

We have observed that post-synthesis treatment conditions play a prominent role in electrochemical performance of the fabricated cells. It is critical, to find an optimal drying and annealing temperatures of electrodes to be rest assured that an efficient water is removed from the crystal structure of synthesized material. Specially, in this case, when the fibers are fabricated with thermoplastic polymers such as PVP and PVA.

### 3.4 Electrochemical Characterization

#### 3.4.1 Galvanostatic Charging/Discharging Curves

Two different sets of half-cell were fabricated; one with PVA and the other one with PVP as polymer solvents. As discussed before, fabricated  $\text{V}_2\text{O}_5/\text{GO} + \text{PVA}$  half-cells reported the maximum specific capacity of  $102 \text{ mAhg}^{-1}$ . However, the reported Specific capacity for the  $\text{V}_2\text{O}_5/\text{GO} + \text{PVP}$  is  $342 \text{ mAhg}^{-1}$ . For the  $\text{V}_2\text{O}_5$  hydrogel, the large amount of water reacts with the lithium to form  $\text{Li}_2\text{O}$ , which deteriorates intercalation performance and is associated with the low capacity of  $\text{V}_2\text{O}_5/\text{GO} + \text{PVA}$ . It is worth to mention that water is the only known and popular solvent for PVA [116]. The initial capacity of  $342 \text{ mAhg}^{-1}$   $\text{V}_2\text{O}_5/\text{GO} + \text{PVP}$  is reported here. The following

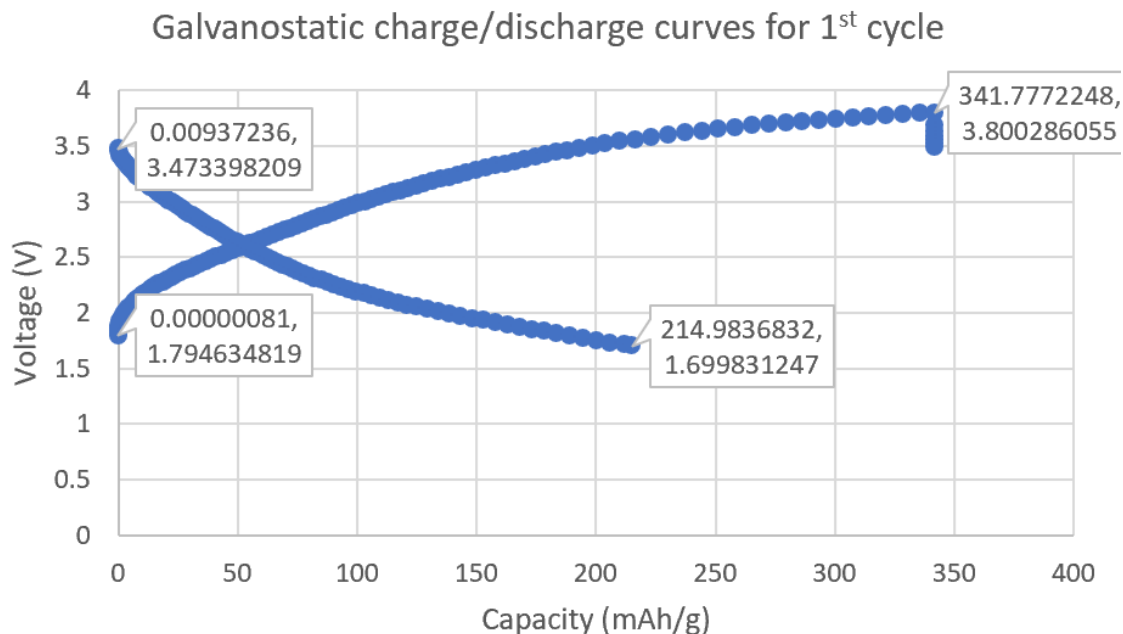


Fig. 3.13. Galvanostatic charge/discharge curve of  $V_2O_5/GO + PVP$  for the 1st cycle.

curves are the galvanostatic charge/discharge curve of  $V_2O_5/GO + PVP$  for the 1st, 2nd, and 10th cycles (Figure 3.11, Figure 3.12, Figure 3.13). The capacity plummets during the 1st cycle; however, for the following cycles, the capacity reduction decreases as the coulombic efficiency increases. The cells are charged between 1.7 V and 3.8 V at C/2 current rate.

### 3.4.2 Coulombic Efficiency

Coulombic efficiency (CE) measures the charge efficiency by providing the ratio of extracted charge to inserted charge within the battery over a full cycle. Li-ion has one of the highest CE ratings in rechargeable batteries [13]. This, however, depends on many factors such as the rate at which battery is charged, the ambient

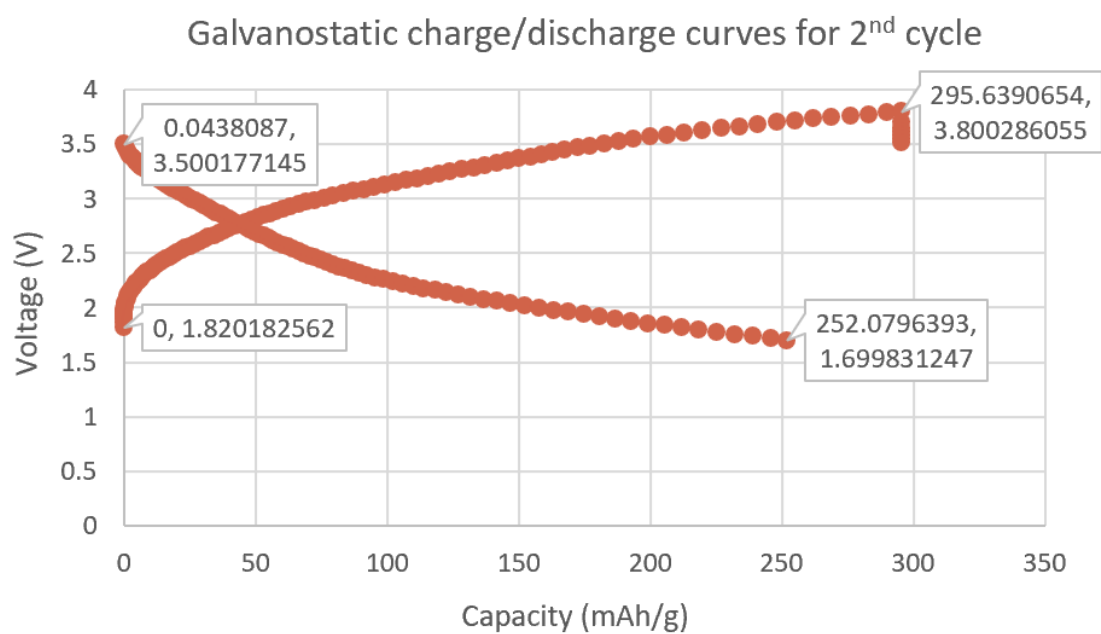


Fig. 3.14. Galvanostatic charge/discharge curve of  $V_2O_5/GO + PVP$  for the 2<sup>nd</sup> cycle.

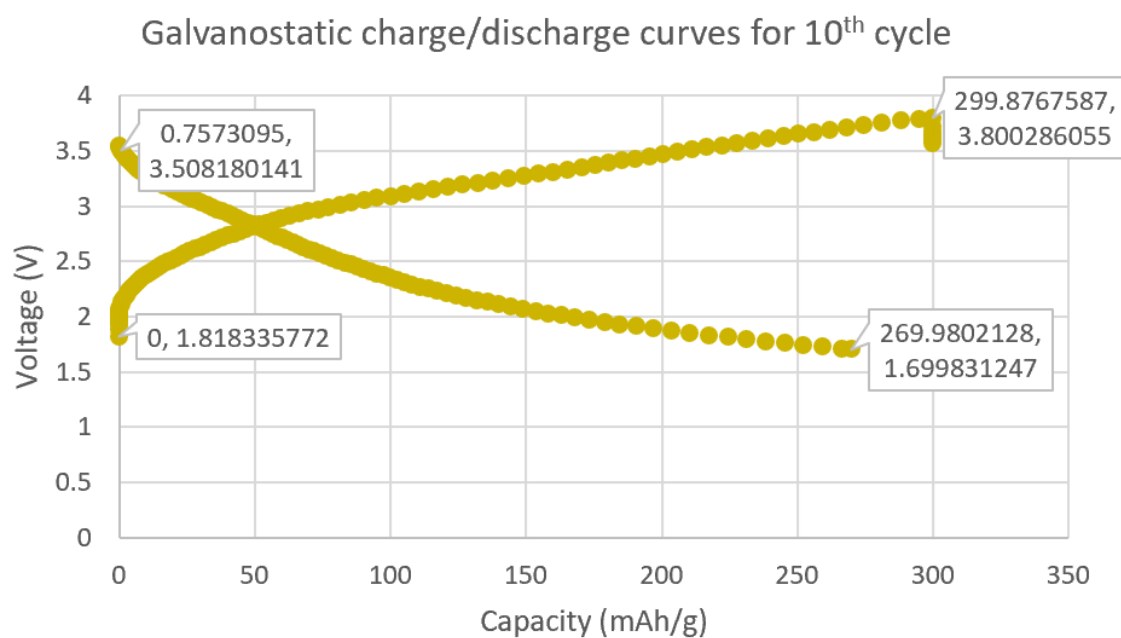


Fig. 3.15. Galvanostatic charge/discharge curve of  $V_2O_5/GO + PVP$  for the 10th cycle.

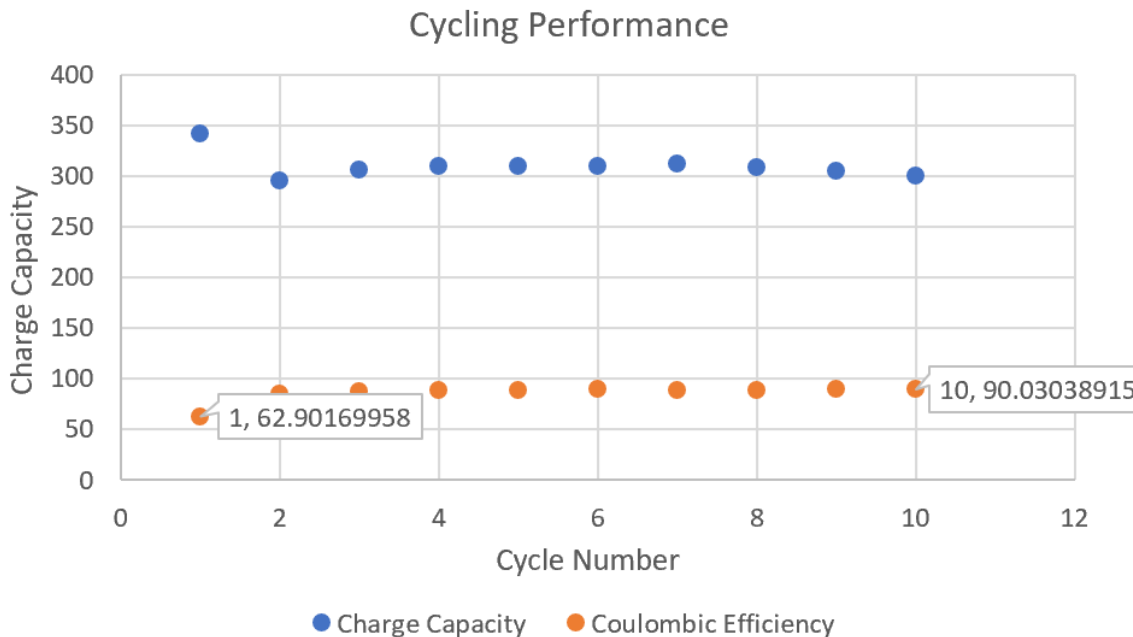


Fig. 3.16. Coulombic efficiency for  $V_2O_5/GO + PVP$  vs. charge capacity.

temperature etc. Fast charging of the batteries results in lower CEs. It is due to losses in charge acceptance and heat. The  $V_2O_5/GO + PVP$  cycling performance is reported here. First cycle charge capacity vs. coulombic efficiency is plotted (Figure 3.14). The coulombic efficiency rises from 62.90% to 90.030% in the 10th cycle. As explained before, coulombic efficiency above 90% is acceptable for such batteries. The coulombic efficiency of Li-ion improves with cycling as can be verified by the following results [179].

### 3.4.3 TGA Analysis

Thermogravimetric analysis (TGA) is a method of thermal analysis in which the weight loss of a sample is observed against temperature change. The TGA measurement was carried out for both pure PVA and PVP using a TA 2000 thermo-analyzer.

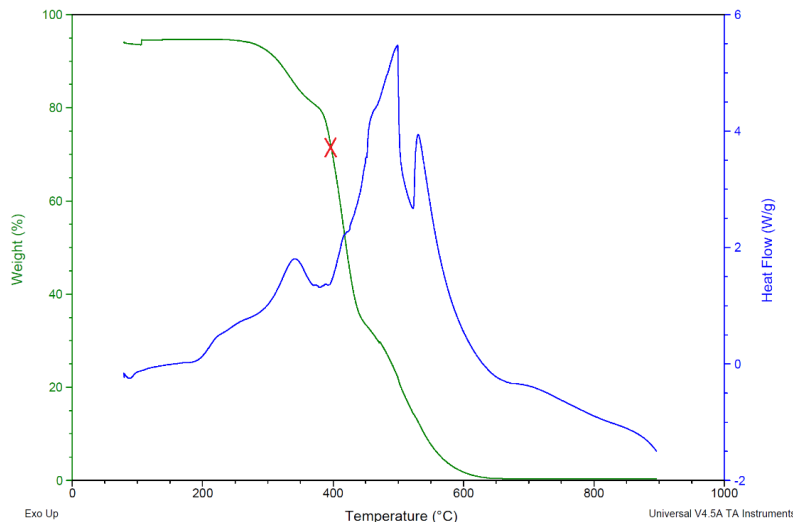


Fig. 3.17. TGA analysis of PVP (Sigma Aldrich,  $M_w = 1.3M$ ).

The annealed vs. regular TGA analysis was conducted for each polymer separately. It should be kept in mind that the maximum temperature limit for GO reduction is almost near 400 °C and at this temperature, almost 70% weight of the PVP is left, and almost 50% weight of the PVA remains (marked by cross sign in Figure 3.15 Figure 3.16). In this regard, for PVP annealing process, in some endeavours, the maximum temperature was increased up to between 450-500 °C in order to at least remove 50% weight of the PVP polymer.

#### 3.4.4 Mercury Porosimetry

The mercury porosimetry analysis technique is a method of porosity analysis in which mercury intrusion happens in a porous structure under severely controlled pressures. Mercury porosimetry is able to calculate handful of sample properties such as total pore volume, total pore surface area, median pore diameter, pore size distributions, and sample densities (bulk and skeletal) [180]. By selecting high surface area materials with carefully designed pore networks, as proved by electrospinning,

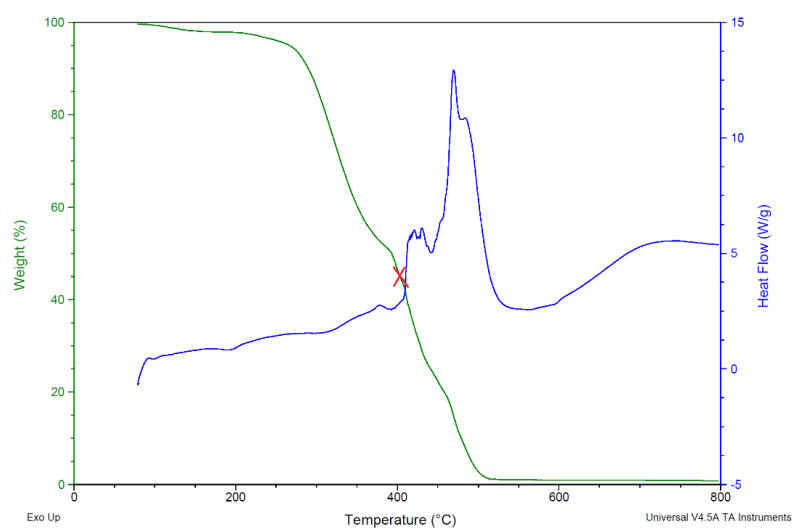


Fig. 3.18. TGA analysis of PVA (*Mowiol*<sup>R</sup> 8-88,  $M_w = 67k$ ).

<b>Total Intrusion Volume =</b>	<b>3.1353</b>	<b>mL/g</b>
<b>Total Pore Area =</b>	<b>-5.215</b>	<b>m<sup>2</sup>/g</b>
<b>Median Pore Diameter (Volume) =</b>	<b>1051363</b>	<b>A</b>
<b>Median Pore Diameter (Area) =</b>	<b>8992558</b>	<b>A</b>
<b>Average Pore Diameter (4V/A) =</b>	<b>-24050</b>	<b>A</b>
<b>Bulk Density at 0.20 psia =</b>	<b>0.0000</b>	<b>g/mL</b>
<b>Apparent (skeletal) Density =</b>	<b>1.0000</b>	<b>g/mL</b>
<b>Porosity =</b>	<b>1.0000</b>	<b>%</b>
<b>Stem Volume Used =</b>	<b>13</b>	<b>% ****</b>

Fig. 3.19. Powdered  $V_2O_5/GO$  mercury porosimetry results (prepared through sol-gel method).

<b>Total Intrusion Volume =</b>	<b>5.4014</b>	<b>mL/g</b>
<b>Total Pore Area =</b>	<b>-21.933</b>	<b>m<sup>2</sup>/g</b>
<b>Median Pore Diameter (Volume) =</b>	<b>300689</b>	<b>A</b>
<b>Median Pore Diameter (Area) =</b>	<b>8992558</b>	<b>A</b>
<b>Average Pore Diameter (4V/A) =</b>	<b>-9851</b>	<b>A</b>
<b>Bulk Density at 0.20 psia =</b>	<b>0.0000</b>	<b>g/mL</b>
<b>Apparent (skeletal) Density =</b>	<b>1.0000</b>	<b>g/mL</b>
<b>Porosity =</b>	<b>1.0000</b>	<b>%</b>
<b>Stem Volume Used =</b>	<b>6</b>	<b>% ****</b>

Fig. 3.20. Electro-spun  $V_2O_5/GO$  mercury porosimetry results (prepared through sol-gel method).

manufacturers of batteries and super-capacitors can minimize the use of costly raw materials while providing more exposed surface area for storage of charge. In this regard, total pore area and median pore of regular powdered  $V_2O_5/GO$  and electro-spun  $V_2O_5/GO$  have been compared.

As seen in the following figures (Figure 3.17, Figure 3.18), the total pore area after electrospinning is almost four times as the regular one. Also, the following results indicate that median pore diameter has decreased more than eight times as of the regular  $V_2O_5/GO$ . The as-prepared porous, hollow and interconnected  $V_2O_5$  is believed to provide more physical contact and space for lithium de/intercalation process.

### 3.4.5 BET Specific Surface Area

The BET (Brunauer, Emmett and Teller) surface area analysis is used to measure and evaluate the gas adsorption data which generates a specific surface area expressed in units of area per mass of sample (s/g). In this regard, a specific area of electro-spun  $V_2O_5/GO$  was measured, and the results were compared to the regular  $V_2O_5$  powder to observe the differences in the surface area changed. According to the results, the generated specific area for electro-spun  $V_2O_5/GO$  is 9.515 s/g.

### 3.4.6 XRD Analysis

To further understand the structure of  $V_2O_5/GO$ , phase analysis through XRD measurement was carried out measured for electro-spun  $V_2O_5/GO$ . Simply put, XRD results for both electro-spun  $V_2O_5/GO + PVP$ ,  $V_2O_5/GO + PVA$ , are displayed here (Figure 3.22, Figure 3.23). In order to quantify the intensity and compare different phases of vanadium oxides, XRD analysis was carried out. The formation of crystalline  $V_2O_5$  was confirmed by wide-angle  $90^\circ$  XRD analysis, as displayed in the following figures. Two distinct diffraction lines were identified in the XRD 95 profile, indicating two sharp peaks at  $38.1^\circ$  and  $44.6^\circ$  for electro-spun  $V_2O_5/GO + PVP$  (Figure 3.22) and at  $44.6^\circ$  for  $V_2O_5/GO + PVA$  (Figure 3.23).

The planes attributed to  $V_2O_5$  are marked. As seen in the figures, a sharp peak is observed attributed to the (0 0 1) plane of the formed  $V_2O_5$  in XRD patterns of  $V_2O_5/GO + PVP$ . Also, a sharp peak representing plane (4 0 1), is associated with the XRD patterns of  $V_2O_5/GO + PVA$ .

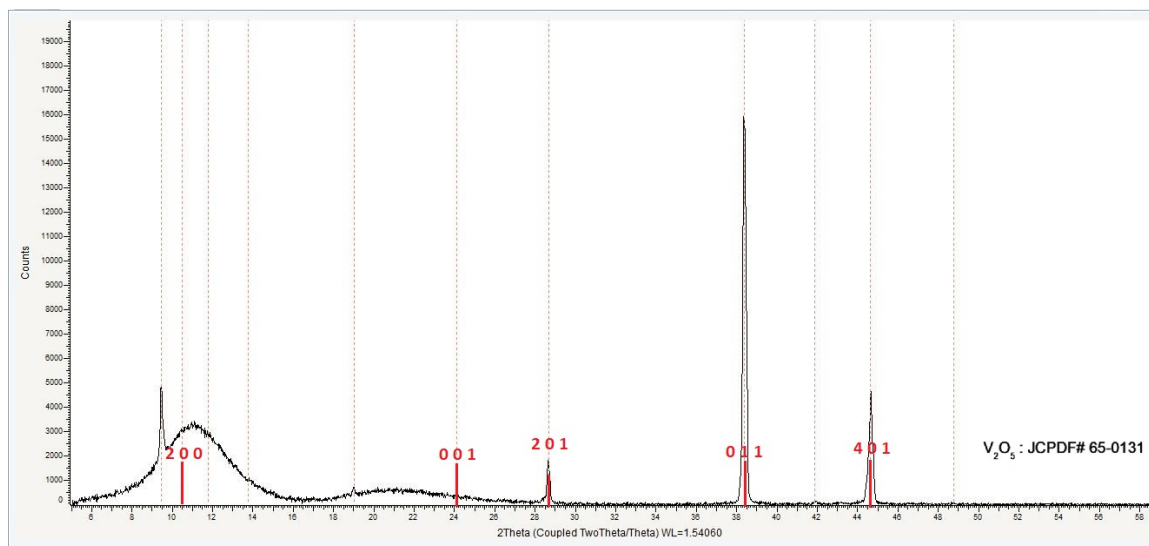


Fig. 3.21. XRD patterns of the  $V_2O_5/GO + PVP$

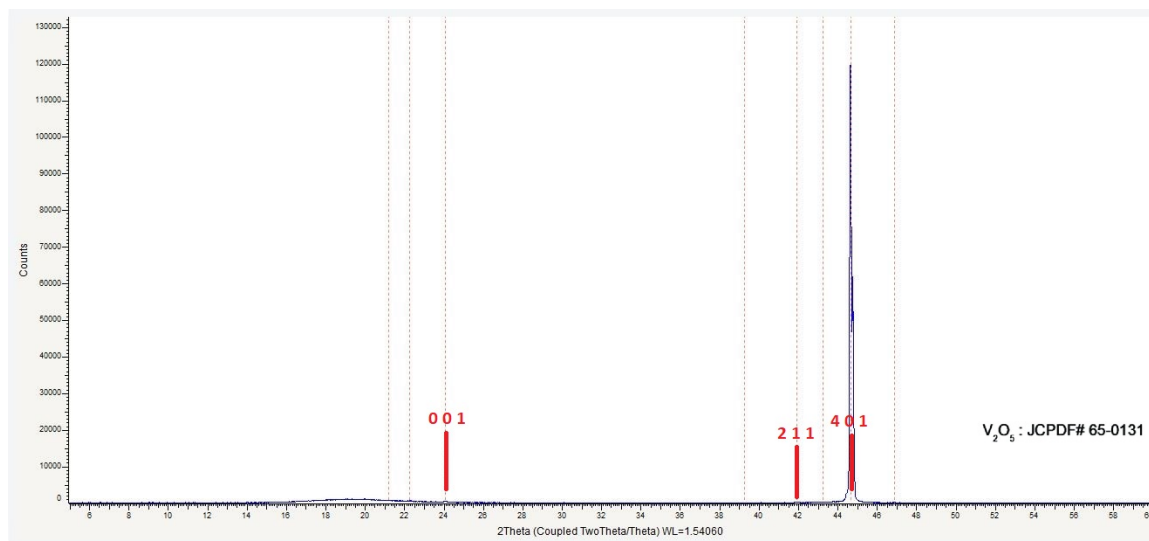


Fig. 3.22. XRD patterns of the  $V_2O_5/GO + PVA$

## 4. CONCLUSION

The ultra-fine fibers arising from electrospinning have two significant properties, such as a large surface to volume ratio and a structure that is relatively free from defects at a molecular level. A high surface to volume ratio makes electro-spun materials suitable for undertaking activities that require a higher physical contact, including providing a site for a chemical reaction as well as the filtration of small-sized physical materials. Also, minimal defects at a molecular level allow electro-spun fibers to attain maximum strength, thus can attain high mechanical performance for composite materials.

The electrospinning process produces fibers with diameters ranging from nanometers to micrometers [161]. The fibers provide sufficient storage space and also plays a critical role in converting the stored energy into electrical currents. Some of the advantages of electrospinning include flexible temperatures, short production cycle, and little pressure. Besides, nanofibers synthesized from the hydrothermal method have a lower aspect ratio, which is critical in the transfer of energy [165]. In other words, fibers made from electrospinning are likely to provide more efficient energy transfer compared to other methods such as electro-spun NWs [166]. However, electrospinning also has various limitations, including difficulties in preparing inorganic nanofibers and limited quantity or variety of polymers used in the process. Limited variety of polymers restricts manufacturers to the use of available materials which may not reach the desired energy capacities [167]. Besides, the performance of nanofibers made from the inorganic materials is likely to decline after calcination. Manufacturers are also silent about the aging process which renders many batteries inefficient. The aging process drains the energy capacity of various cells and reduces the performance of lithium-ion batteries. In this work,  $V_2O_5/GO$  as a layered crystal structure has been demonstrated to fabricate nanofibers formed by polymers such as Polyvinylpyrrolidone (PVP) and Polyvinyl alcohol (PVA), separately, as solvent polymers with electrospinning technique.

In this study, the synthesis of a graphene-modified nanostructured  $V_2O_5$  through optimized sol-gel method and electrospinning of  $V_2O_5/rGO$  hybrid is investigated. The as-prepared  $V_2O_5/GO$  has hollow, porous, and interconnected nanostructures. By controlling the electrospinning parameters, uniform nanorods with a diameter of within  $\sim 300$  nm were fabricated. Also, the graphene sheets sandwiched in between the  $V_2O_5$  layers create gaps between the  $V_2O_5$  layers. They improve the electron conduction also by creating proper gaps between the two layers of  $V_2O_5$ , they can facilitate the  $Li^+$  diffusion.

The results of this study showed that post-synthesis treatment of cathode material plays a an important role in electrochemical performance of the as prepared cells. By controlling the annealing and drying time and steps, a small amount of pyrolysis carbon can be retained, which could improve the conductivity of the  $V_2O_5$  nanorods. Also, controlled post-synthesis helped us to prevent aggregation of electrospun twisted nanostructured fibers which deteriorates the lithium diffusion process during charge/discharge of batteries. However, there are some limitations for the fabrication of this type of battery such as time-consuming sol-gel synthesis, difficult electrospinning process, and complicated annealing procedure.

As demonstrated, electrospinning has gained lots of interest in recent years due to its potential application in energy storage application. As the results have proved, the optimized sol-gel method, followed by the electrospinning of the cathode material achieved a high initial capacity of  $342 \text{ mAhg}^{-1}$  at a high current density of  $171 \text{ mA}g^{-1}$  (0.5C) and the capacity retention of 80% after 20 cycles. It was also shown that the prepared sol-gel method outperforms the pure  $V_2O_5$  cathode material, by reaching the capacity of two times higher.

## 5. FUTURE RECOMMENDATION

Polymer removal from the electro-spun samples is a critical part of this thesis. If the whole amount of the polymer (here PVP and PVA, electro-spun separately) remains in the electro-spun samples, it can act as an insulator during Lithium intercalation and deintercalation procedures. In this regard, as a future recommendation, PVP should be dried under vacuum to remove the remaining solvents including water, DMF, Ethanol, etc. and then it shall be transferred to a autoclave with deionized water maintained at 80°C. After drying the water-treated nanofibers under vacuum, the porous electro-spun nanofibers could be obtained. As a Next step, the as-prepared sample should be heat-treated inside furnace tube under  $N_2$  or air, starting from room temperature up to 380-400 °C at a rate of 1  $C.min^{-1}$ . Then it should be held there for 1-2 hours. By following this multi-step annealing process, crystallized water inside the  $V_2O_5$  xerogel will not result in collapse of the whole nanostructure.

In case of PVA, the same above heat-treatment method can be applied but with a slight difference. Firstly, PVA requires to be dispersed in hot water, i.e., 90 °C as the PVP and water mixture maintained at around waters boiling temperature for almost 3 hours. This will result in a homogeneous PVA mixture which later can be well mixed with  $V_2O_5$  xerogel. Although with PVA, not with PVP, 2-3 weeks old homogeneous vanadium oxide hydrogel could be spun, a large amount of water is required. For the  $V_2O_5$  xerogel, the large amount of water reacts with the lithium to form  $Li_2O$ , which deteriorates intercalation performance consequently lowers the capacity to around 102  $mAhg^{-1}$ . Therefore, electro-spun  $V_2O_5/GO + PVA$  has to be also freeze-dried to remove all the excess water from its structure.

In the end, nanofibers can be carbonized at a rate of 5  $C.min^{-1}$  up to 400 °C in a tubular furnace, which is the optimum temperature point for Graphene Oxide (GO) reduction. The maximum temperature for GO reduction is found to be 400 °C [39,181].

## REFERENCES

## REFERENCES

- [1] B. Scrosati, "History of lithium batteries," *Journal of solid state electrochemistry*, vol. 15, no. 7-8, pp. 1623–1630, 2011.
- [2] R. Marom, S. F. Amalraj, N. Leifer, D. Jacob, and D. Aurbach, "A review of advanced and practical lithium battery materials," *Journal of Materials Chemistry*, vol. 21, no. 27, pp. 9938–9954, 2011.
- [3] S. Passerini and B. Scrosati, "Lithium and lithium-ion batteries: challenges and prospects," *The Electrochemical Society Interface*, vol. 25, no. 3, pp. 85–87, 2016.
- [4] M. Li, J. Lu, Z. Chen, and K. Amine, "30 years of lithiumion batteries," *Advanced Materials*, vol. 30, no. 33, p. 1800561, 2018.
- [5] G. E. Blomgren, "The development and future of lithium ion batteries," *Journal of The Electrochemical Society*, vol. 164, no. 1, pp. A5019–A5025, 2017.
- [6] J.-M. Tarascon and M. Armand, *Issues and challenges facing rechargeable lithium batteries*. World Scientific, 2011, pp. 171–179.
- [7] P. Van den Bossche, F. Vergels, J. Van Mierlo, J. Matheys, and W. Van Autenboer, "Subat: An assessment of sustainable battery technology," *Journal of power sources*, vol. 162, no. 2, pp. 913–919, 2006.
- [8] V. Etacheri, R. Marom, R. Elazari, G. Salitra, and D. Aurbach, "Challenges in the development of advanced li-ion batteries: a review," *Energy Environmental Science*, vol. 4, no. 9, pp. 3243–3262, 2011.
- [9] A. K. Kushwaha, M. R. Sahoo, J. Nanda, and S. K. Nayak, "Engineering redox potential of lithium clusters for electrode material in lithium-ion batteries," *Journal of Cluster Science*, vol. 28, no. 5, pp. 2779–2793, 2017.
- [10] K. C. Kim, T. Liu, S. W. Lee, and S. S. Jang, "First-principles density functional theory modeling of li binding: Thermodynamics and redox properties of quinone derivatives for lithium-ion batteries," *Journal of the American Chemical Society*, vol. 138, no. 7, pp. 2374–2382, 2016.
- [11] G. Sun, L. Sun, H. Xie, and J. Liu, "Electrospinning of nanofibers for energy applications," *Nanomaterials*, vol. 6, no. 7, p. 129, 2016.
- [12] X. Shi, W. Zhou, D. Ma, Q. Ma, D. Bridges, Y. Ma, and A. Hu, "Electrospinning of nanofibers and their applications for energy devices," *Journal of Nanomaterials*, vol. 16, no. 1, p. 122, 2015.
- [13] T. B. Reddy, *Linden's handbook of batteries*. McGraw-hill New York, 2011, vol. 4.

- [14] M. Imran, S. Haider, K. Ahmad, A. Mahmood, and W. A. Al-Masry, "Fabrication and characterization of zinc oxide nanofibers for renewable energy applications," *Arabian Journal of Chemistry*, vol. 10, pp. S1067–S1072, 2017.
- [15] S. Mansouri, T. F. Sheikholeslami, and A. Behzadmehr, "Investigation on the electrospun pvdf/np-zno nanofibers for application in environmental energy harvesting," *Journal of Materials Research and Technology*, 2018.
- [16] S. Sahoo, S.-H. Bae, Y.-S. Lee, J.-M. Lee, J.-M. Ahn, C.-G. Kim, and I.-K. Oh, "Defect-engineered mesoporous ternary nanoarchitecture of zinc-cobalt-oxide/nitrogen-doped graphene as anode material in lithium ion batteries," *Carbon*, vol. 94, pp. 455–463, 2015.
- [17] S. Goutam, N. Omar, P. Van Den Bossche, and J. Van Mierlo, *Review of Nanotechnology for Anode Materials in Batteries*. Elsevier, 2017, pp. 45–82.
- [18] A. M. Stephan, "Review on gel polymer electrolytes for lithium batteries," *European polymer journal*, vol. 42, no. 1, pp. 21–42, 2006.
- [19] S. S. Zhang, "A review on the separators of liquid electrolyte li-ion batteries," *Journal of power sources*, vol. 164, no. 1, pp. 351–364, 2007.
- [20] H. Lee, M. Yanilmaz, O. Toprakci, K. Fu, and X. Zhang, "A review of recent developments in membrane separators for rechargeable lithium-ion batteries," *Energy Environmental Science*, vol. 7, no. 12, pp. 3857–3886, 2014.
- [21] P. Huang, Q. Wang, K. Li, P. Ping, and J. Sun, *The combustion behavior of large scale lithium titanate battery*, 2015, vol. 5.
- [22] J.-W. Jung, C.-L. Lee, S. Yu, and I.-D. Kim, "Electrospun nanofibers as a platform for advanced secondary batteries: a comprehensive review," *Journal of materials chemistry A*, vol. 4, no. 3, pp. 703–750, 2016.
- [23] H. Hou, L. Wang, F. Gao, G. Wei, B. Tang, W. Yang, and T. Wu, "General strategy for fabricating thoroughly mesoporous nanofibers," *Journal of the American Chemical Society*, vol. 136, no. 48, pp. 16 716–16 719, 2014.
- [24] Y.-S. Lee and K.-S. Ryu, "Study of the lithium diffusion properties and high rate performance of tinb 6 o 17 as an anode in lithium secondary battery," *Scientific reports*, vol. 7, no. 1, p. 16617, 2017.
- [25] S. Das, J. Li, and R. Hui, "Impact of electrode surface/volume ratio on lithium battery performance," in *Proceedings of the COMSOL Conference, Boston, MA, USA*, 2014, pp. 8–10.
- [26] J. Summerfield, "Modeling the lithium ion battery," *Journal of Chemical Education*, vol. 90, no. 4, pp. 453–455, 2013.
- [27] W. Luo, J.-J. Gaumet, and L. Mai, "Nanostructured layered vanadium oxide as cathode for high-performance sodium-ion batteries: a perspective," *MRS Communications*, vol. 7, no. 2, pp. 152–165, 2017.
- [28] J. Meng, H. Guo, C. Niu, Y. Zhao, L. Xu, Q. Li, and L. Mai, "Advances in structure and property optimizations of battery electrode materials," *Joule*, vol. 1, no. 3, pp. 522–547, 2017.

- [29] S. Gupta, B. Aberg, S. Carrizosa, and N. Dimakis, "Vanadium pentoxide nanobelt-reduced graphene oxide nanosheet composites as high-performance pseudocapacitive electrodes: Ac impedance spectroscopy data modeling and theoretical calculations," *Materials*, vol. 9, no. 8, p. 615, 2016.
- [30] H. Li, J. Wang, X. Liu, Q. Sun, A. B. Djurii, M. Xie, Y. Mei, C. Y. Tang, and K. Shih, "Template-free synthesis of hierarchical hollow  $\text{V}_2\text{O}_5$  microspheres with highly stable lithium storage capacity," *RSC Advances*, vol. 7, no. 5, pp. 2480–2485, 2017.
- [31] S. Beke, "A review of the growth of  $\text{V}_2\text{O}_5$  films from 1885 to 2010," *Thin Solid Films*, vol. 519, no. 6, pp. 1761–1771, 2011.
- [32] R. Moskalyk and A. Alfantazi, "Processing of vanadium: a review," *Minerals Engineering*, vol. 16, no. 9, pp. 793–805, 2003.
- [33] X. Liu, J. Zeng, H. Yang, K. Zhou, and D. Pan, " $\text{V}_2\text{O}_5$ -based nanomaterials: synthesis and their applications," *RSC advances*, vol. 8, no. 8, pp. 4014–4031, 2018.
- [34] N. Bahlawane and D. Lenoble, "Vanadium oxide compounds: structure, properties, and growth from the gas phase," *Chemical Vapor Deposition*, vol. 20, no. 7-8-9, pp. 299–311, 2014.
- [35] K. Kanamori and K. Tsuge, *Inorganic chemistry of vanadium*. Springer, 2012, pp. 3–31.
- [36] V. Sjöberg, K. Todd, L. Sartz, and S. Karlsson, "Impact of organic carbon in the release of vanadium from ld-slag," 2011.
- [37] B. Dunn, H. Kamath, and J.-M. Tarascon, "Electrical energy storage for the grid: a battery of choices," *Science*, vol. 334, no. 6058, pp. 928–935, 2011.
- [38] M. Ihsan, Q. Meng, L. Li, D. Li, H. Wang, K. H. Seng, Z. Chen, S. J. Kennedy, Z. Guo, and H.-K. Liu, " $\text{V}_2\text{O}_5$ /mesoporous carbon composite as a cathode material for lithium-ion batteries," *Electrochimica Acta*, vol. 173, pp. 172–177, 2015.
- [39] Q. Liu, Z.-F. Li, Y. Liu, H. Zhang, Y. Ren, C.-J. Sun, W. Lu, Y. Zhou, L. Stanciu, and E. A. Stach, "Graphene-modified nanostructured vanadium pentoxide hybrids with extraordinary electrochemical performance for li-ion batteries," *Nature communications*, vol. 6, p. 6127, 2015.
- [40] M. Rao, "Vanadium pentoxide cathode material for fabrication of all solid state lithium-ion batteries," *Res. J. Recent Sci*, vol. 2, pp. 67–73, 2013.
- [41] J. Li, L. Wang, C. Lyu, W. Luo, K. Ma, and L. Zhang, "A method of remaining capacity estimation for lithium-ion battery," *Advances in Mechanical Engineering*, vol. 5, p. 154831, 2013.
- [42] N. A. Chernova, M. Roppolo, A. C. Dillon, and M. S. Whittingham, "Layered vanadium and molybdenum oxides: batteries and electrochromics," *Journal of Materials Chemistry*, vol. 19, no. 17, pp. 2526–2552, 2009.

- [43] C. K. Chan, H. Peng, R. D. Twisten, K. Jarausch, X. F. Zhang, and Y. Cui, "Fast, completely reversible li insertion in vanadium pentoxide nanoribbons," *Nano letters*, vol. 7, no. 2, pp. 490–495, 2007.
- [44] R. Baddour-Hadjean, C. Navone, and J. Pereira-Ramos, "In situ raman microspectrometry investigation of electrochemical lithium intercalation into sputtered crystalline v2o5 thin films," *Electrochimica Acta*, vol. 54, no. 26, pp. 6674–6679, 2009.
- [45] Y. Zhang, Y. Li, X. Xia, X. Wang, C. Gu, and J. Tu, "High-energy cathode materials for li-ion batteries: a review of recent developments," *Science China Technological Sciences*, vol. 58, no. 11, pp. 1809–1828, 2015.
- [46] R. Guduru and J. Icaza, "A brief review on multivalent intercalation batteries with aqueous electrolytes," *Nanomaterials*, vol. 6, no. 3, p. 41, 2016.
- [47] J. Barbosa, J. Dias, S. Lanceros-Mndez, and C. Costa, "Recent advances in poly (vinylidene fluoride) and its copolymers for lithium-ion battery separators," *Membranes*, vol. 8, no. 3, p. 45, 2018.
- [48] H. Liu, X. Wang, C. Kuang, L. Li, and Y. Zhai, "Polyvinylidene fluoride/polystyrene hybrid fibers with high ionic conductivity and enhanced mechanical strength as lithium-ion battery separators," *Journal of Solid State Electrochemistry*, vol. 22, no. 11, pp. 3579–3587, 2018.
- [49] Q. Wei, J. Liu, W. Feng, J. Sheng, X. Tian, L. He, Q. An, and L. Mai, "Hydrated vanadium pentoxide with superior sodium storage capacity," *Journal of Materials Chemistry A*, vol. 3, no. 15, pp. 8070–8075, 2015.
- [50] A. Moretti, F. Maroni, I. Osada, F. Nobili, and S. Passerini, "V2o5 aerogel as a versatile cathode material for lithium and sodium batteries," *ChemElectroChem*, vol. 2, no. 4, pp. 529–537, 2015.
- [51] D. Liu and G. Cao, "Engineering nanostructured electrodes and fabrication of film electrodes for efficient lithium ion intercalation," *Energy Environmental Science*, vol. 3, no. 9, pp. 1218–1237, 2010.
- [52] Y. Wang, H. Shang, T. Chou, and G. Cao, "Effects of thermal annealing on the li+ intercalation properties of v2o5 n h2o xerogel films," *The Journal of Physical Chemistry B*, vol. 109, no. 22, pp. 11 361–11 366, 2005.
- [53] Y. Wang, K. Takahashi, K. H. Lee, and G. Cao, "Nanostructured vanadium oxide electrodes for enhanced lithiumion intercalation," *Advanced Functional Materials*, vol. 16, no. 9, pp. 1133–1144, 2006.
- [54] H. Wang, D. Ma, Y. Huang, and X. Zhang, "Electrospun v2o5 nanostructures with controllable morphology as highperformance cathode materials for lithium-ion batteries," *ChemistryA European Journal*, vol. 18, no. 29, pp. 8987–8993, 2012.
- [55] J. H. Roque-Ruiz, N. A. Medelln-Castillo, and S. Y. Reyes-Lpez, "Fabrication of -alumina fibers by sol-gel and electrospinning of aluminum nitrate precursor solutions," *Results in Physics*, vol. 12, pp. 193–204, 2019.

- [56] Q. An, Y. Li, H. D. Yoo, S. Chen, Q. Ru, L. Mai, and Y. Yao, "Graphene decorated vanadium oxide nanowire aerogel for long-cycle-life magnesium battery cathodes," *Nano Energy*, vol. 18, pp. 265–272, 2015.
- [57] G. Sudant, E. Baudrin, B. Dunn, and J.-M. Tarascon, "Synthesis and electrochemical properties of vanadium oxide aerogels prepared by a freeze-drying process," *Journal of The Electrochemical Society*, vol. 151, no. 5, pp. A666–A671, 2004.
- [58] Y. Wu, G. Gao, and G. Wu, "Self-assembled three-dimensional hierarchical porous  $v_2o_5$ /graphene hybrid aerogels for supercapacitors with high energy density and long cycle life," *Journal of Materials Chemistry A*, vol. 3, no. 5, pp. 1828–1832, 2015.
- [59] G. Chen, A. Zhamu, B. Z. Jang, and Z. Yu, "Graphene-enabled vanadium oxide cathode and lithium cells containing same," Jul. 1 2014, uS Patent 8,765,302.
- [60] Z. Chen and J. Dahn, "Improving the capacity retention of  $LiCoO_2$  cycled to 4.5 V by heat-treatment," *Electrochemical and Solid-State Letters*, vol. 7, no. 1, pp. A11–A14, 2004.
- [61] A. M. Kannan and A. Manthiram, "Surface/chemically modified  $LiMn_2O_4$  cathodes for lithium-ion batteries," *Electrochemical and Solid-State Letters*, vol. 5, no. 7, pp. A167–A169, 2002.
- [62] J. Xu, H. Zhang, T. Zhang, Q. Pan, and Y. Gui, "Influence of heat-treatment temperature on crystal structure, morphology and electrochemical properties of  $LiV_3O_8$  prepared by hydrothermal reaction," *Journal of Alloys and Compounds*, vol. 467, no. 1-2, pp. 327–331, 2009.
- [63] S.-H. Ng, T. J. Patey, R. Bchel, F. Krumeich, J.-Z. Wang, H.-K. Liu, S. E. Pratsinis, and P. Novk, "Flame spray-pyrolyzed vanadium oxide nanoparticles for lithium battery cathodes," *Physical Chemistry Chemical Physics*, vol. 11, no. 19, pp. 3748–3755, 2009.
- [64] S. Y. Chew, C. Feng, S. H. Ng, J. Wang, Z. Guo, and H. Liu, "Low-temperature synthesis of polypyrrole-coated  $LiV_3O_8$  composite with enhanced electrochemical properties," *Journal of The Electrochemical Society*, vol. 154, no. 7, pp. A633–A637, 2007.
- [65] N. Tran, K. Bramnik, H. Hibst, J. Prl, N. Mronga, M. Holzappel, W. Scheifele, and P. Novk, "Spray-drying synthesis and electrochemical performance of lithium vanadates as positive electrode materials for lithium batteries," *Journal of The Electrochemical Society*, vol. 155, no. 5, pp. A384–A389, 2008.
- [66] H. Liu, Y. Wang, K. Wang, Y. Wang, and H. Zhou, "Synthesis and electrochemical properties of single-crystalline  $LiV_3O_8$  nanorods as cathode materials for rechargeable lithium batteries," *Journal of Power Sources*, vol. 192, no. 2, pp. 668–673, 2009.
- [67] A. Sakunthala, M. Reddy, S. Selvasekarapandian, B. Chowdari, and P. C. Selvin, "Preparation, characterization, and electrochemical performance of lithium trivanadate rods by a surfactant-assisted polymer precursor method for lithium batteries," *The Journal of Physical Chemistry C*, vol. 114, no. 17, pp. 8099–8107, 2010.

- [68] A. Pan, J. Liu, J.-G. Zhang, G. Cao, W. Xu, Z. Nie, X. Jie, D. Choi, B. W. Arey, and C. Wang, "Template free synthesis of  $\text{Li}_3\text{V}_2\text{O}_8$  nanorods as a cathode material for high-rate secondary lithium batteries," *Journal of Materials Chemistry*, vol. 21, no. 4, pp. 1153–1161, 2011.
- [69] A. Pan, J.-G. Zhang, G. Cao, S. Liang, C. Wang, Z. Nie, B. W. Arey, W. Xu, D. Liu, and J. Xiao, "Nanosheet-structured  $\text{Li}_3\text{V}_2\text{O}_8$  with high capacity and excellent stability for high energy lithium batteries," *Journal of Materials Chemistry*, vol. 21, no. 27, pp. 10 077–10 084, 2011.
- [70] D. A. Semenenko, D. M. Itkis, E. A. Pomerantseva, E. A. Goodilin, T. L. Kulova, A. M. Skundin, and Y. D. Tretyakov, " $\text{Li}_2\text{V}_2\text{O}_5$  nanobelts for high capacity lithium-ion battery cathodes," *Electrochemistry communications*, vol. 12, no. 9, pp. 1154–1157, 2010.
- [71] A. Manthiram, "Materials challenges and opportunities of lithium ion batteries," *The Journal of Physical Chemistry Letters*, vol. 2, no. 3, pp. 176–184, 2011.
- [72] S. Gao, Z. Chen, M. Wei, K. Wei, and H. Zhou, "Single crystal nanobelts of  $\text{V}_3\text{O}_7 \cdot \text{H}_2\text{O}$ : A lithium intercalation host with a large capacity," *Electrochimica Acta*, vol. 54, no. 3, pp. 1115–1118, 2009.
- [73] H. Qiao, X. Zhu, Z. Zheng, L. Liu, and L. Zhang, "Synthesis of  $\text{V}_3\text{O}_7 \cdot \text{H}_2\text{O}$  nanobelts as cathode materials for lithium ion batteries," *Electrochemistry communications*, vol. 8, no. 1, pp. 21–26, 2006.
- [74] J. Xie, J. Li, H. Zhan, and Y. Zhou, "Low-temperature sol-gel synthesis of  $\text{Li}_1.2\text{V}_3\text{O}_8$  from  $\text{V}_2\text{O}_5$  gel," *Materials Letters*, vol. 57, no. 18, pp. 2682–2687, 2003.
- [75] J. Sun, L. Jiao, H. Yuan, L. Liu, X. Wei, Y. Miao, L. Yang, and Y. Wang, "Preparation and electrochemical performance of  $\text{Ag}_x\text{Li}_1-x\text{V}_3\text{O}_8$ ," *Journal of Alloys and Compounds*, vol. 472, no. 1–2, pp. 363–366, 2009.
- [76] G. d. N. Barbosa, C. F. d. O. Graeff, and H. P. Oliveira, "Thermal annealing effects on vanadium pentoxide xerogel films," *Ecltica Quimica*, vol. 30, no. 2, pp. 7–15, 2005.
- [77] E. A. Monyoncho, R. Bissessur, D. C. Dahn, and V. Trenton, "Intercalation of poly [oligo (ethylene glycol) oxalate] into vanadium pentoxide xerogel," *Alkali-ion batteries*, pp. 93–110, 2016.
- [78] G. Reina, J. M. Gonzalez-Domnguez, A. Criado, E. Vzquez, A. Bianco, and M. Prato, "Promises, facts and challenges for graphene in biomedical applications," *Chemical Society Reviews*, vol. 46, no. 15, pp. 4400–4416, 2017.
- [79] B. K. Poudel, K.-O. Doh, and J. H. Byeon, "Green and continuous route to assemble lateral nanodimensional graphitic oxide composites without process interruption," *Green Chemistry*, vol. 20, no. 13, pp. 2984–2989, 2018.
- [80] S. Korkmaz, F. M. Tezel, and I. Kariper, "Synthesis and characterization of  $\text{GO}/\text{V}_2\text{O}_5$  thin film supercapacitor," *Synthetic Metals*, vol. 242, pp. 37–48, 2018.
- [81] Q. Zhang, S. Tan, X. Kong, Y. Xiao, and L. Fu, "Synthesis of sulfur encapsulated 3d graphene sponge driven by micro-pump and its application in lithium battery," *Journal of Materiomics*, vol. 1, no. 4, pp. 333–339, 2015.

- [82] L. Wang, Y. Wang, and Y. Zhao, "Freeze-drying method to synthesize v2o5/graphene composites toward enhanced sodium ion storage," *Ceramics International*, vol. 44, no. 18, pp. 23 279–23 283, 2018.
- [83] R. Thangappan, S. Kalaiselvam, A. Elayaperumal, and R. Jayavel, "Synthesis of graphene oxide/vanadium pentoxide composite nanofibers by electrospinning for supercapacitor applications," *Solid State Ionics*, vol. 268, pp. 321–325, 2014.
- [84] M. Mao, J. Hu, and H. Liu, "Graphene-based materials for flexible electrochemical energy storage," *International Journal of Energy Research*, vol. 39, no. 6, pp. 727–740, 2015.
- [85] G. Du, K. H. Seng, Z. Guo, J. Liu, W. Li, D. Jia, C. Cook, Z. Liu, and H. Liu, "Graphene v2 o 5 n h 2 o xerogel composite cathodes for lithium ion batteries," *RSC Advances*, vol. 1, no. 4, pp. 690–697, 2011.
- [86] T. Lin and J. Fang, *Fundamentals of electrospinning and electrospun nanofibers*. DEStech Publications, 2017.
- [87] C. J. Angamma and S. H. Jayaram, "Fundamentals of electrospinning and processing technologies," *Particulate Science and Technology*, vol. 34, no. 1, pp. 72–82, 2016.
- [88] S. A. Harfenist, S. D. Cambron, E. W. Nelson, S. M. Berry, A. W. Isham, M. M. Crain, K. M. Walsh, R. S. Keynton, and R. W. Cohn, "Direct drawing of suspended filamentary micro-and nanostructures from liquid polymers," *Nano Letters*, vol. 4, no. 10, pp. 1931–1937, 2004.
- [89] T. Ondarcuhu and C. Joachim, "Drawing a single nanofibre over hundreds of microns," *EPL (Europhysics Letters)*, vol. 42, no. 2, p. 215, 1998.
- [90] X. Xing, Y. Wang, and B. Li, "Nanofiber drawing and nanodevice assembly in poly (trimethylene terephthalate)," *Optics express*, vol. 16, no. 14, pp. 10 815–10 822, 2008.
- [91] A. Tokarev, O. Trotsenko, I. M. Griffiths, H. A. Stone, and S. Minko, "Magnetospinning of nanoand microfibers," *Advanced Materials*, vol. 27, no. 23, pp. 3560–3565, 2015.
- [92] R. Baumgartner, A. Eitzlmayr, N. Matsko, C. Tetyczka, J. Khinast, and E. Roblegg, "Nano-extrusion: a promising tool for continuous manufacturing of solid nano-formulations," *International journal of pharmaceuticals*, vol. 477, no. 1-2, pp. 1–11, 2014.
- [93] J. Khinast, R. Baumgartner, and E. Roblegg, "Nano-extrusion: a one-step process for manufacturing of solid nanoparticle formulations directly from the liquid phase," *AAPS PharmSciTech*, vol. 14, no. 2, pp. 601–604, 2013.
- [94] Z. Bo, "Production of polypropylene melt blown nonwoven fabrics: Part iieffect of process parameters," 2012.
- [95] S. Grimm, R. Giesa, K. Sklarek, A. Langner, U. Gosele, H.-W. Schmidt, and M. Steinhart, "Nondestructive replication of self-ordered nanoporous alumina membranes via cross-linked polyacrylate nanofiber arrays," *Nano letters*, vol. 8, no. 7, pp. 1954–1959, 2008.

- [96] X. Dang, H. Yi, M.-H. Ham, J. Qi, D. S. Yun, R. Ladewski, M. S. Strano, P. T. Hammond, and A. M. Belcher, "Virus-templated self-assembled single-walled carbon nanotubes for highly efficient electron collection in photovoltaic devices," *Nature Nanotechnology*, vol. 6, no. 6, p. 377, 2011.
- [97] H. Jun, V. Yuwono, S. E. Paramonov, and J. D. Hartgerink, "Enzymemediated degradation of peptideamphiphile nanofiber networks," *Advanced Materials*, vol. 17, no. 21, pp. 2612–2617, 2005.
- [98] C. L. Haynes and R. P. Van Duyne, "Nanosphere lithography: a versatile nanofabrication tool for studies of size-dependent nanoparticle optics," 2001.
- [99] D. Pisignano, G. Maruccio, E. Mele, L. Persano, F. Di Benedetto, and R. Cingolani, "Polymer nanofibers by soft lithography," *Applied Physics Letters*, vol. 87, no. 12, p. 123109, 2005.
- [100] F. Dabirian, S. H. Ravandi, A. Pishevar, and R. Abuzade, "A comparative study of jet formation and nanofiber alignment in electrospinning and electrocentrifugal spinning systems," *Journal of Electrostatics*, vol. 69, no. 6, pp. 540–546, 2011.
- [101] K. Sarkar, C. Gomez, S. Zambrano, M. Ramirez, E. de Hoyos, H. Vasquez, and K. Lozano, "Electrospinning to forcespinning," *Materials Today*, vol. 13, no. 11, pp. 12–14, 2010.
- [102] G. Nagaraju, C. Tharamani, G. Chandrappa, and J. Livage, "Hydrothermal synthesis of amorphous mos 2 nanofiber bundles via acidification of ammonium heptamolybdate tetrahydrate," *Nanoscale research letters*, vol. 2, no. 9, p. 461, 2007.
- [103] G. Gorrasi and A. Sorrentino, "Mechanical milling as a technology to produce structural and functional bio-nanocomposites," *Green Chemistry*, vol. 17, no. 5, pp. 2610–2625, 2015.
- [104] M. R. Badrossamay, H. A. McIlwee, J. A. Goss, and K. K. Parker, "Nanofiber assembly by rotary jet-spinning," *Nano letters*, vol. 10, no. 6, pp. 2257–2261, 2010.
- [105] M. J. Bronikowski, "Cvd growth of carbon nanotube bundle arrays," *Carbon*, vol. 44, no. 13, pp. 2822–2832, 2006.
- [106] N. M. Neves, *Electrospinning for Advanced Biomedical Applications and Therapies*. Smithers Rapra, 2012.
- [107] M. K. Leach, Z.-Q. Feng, S. J. Tuck, and J. M. Corey, "Electrospinning fundamentals: optimizing solution and apparatus parameters," *JoVE (Journal of Visualized Experiments)*, no. 47, p. e2494, 2011.
- [108] S. Agarwal, J. H. Wendorff, and A. Greiner, "Use of electrospinning technique for biomedical applications," *Polymer*, vol. 49, no. 26, pp. 5603–5621, 2008.
- [109] D. Li and Y. Xia, "Electrospinning of nanofibers: reinventing the wheel?" *Advanced materials*, vol. 16, no. 14, pp. 1151–1170, 2004.

- [110] A. Greiner and J. H. Wendorff, "Electrospinning: a fascinating method for the preparation of ultrathin fibers," *Angewandte Chemie International Edition*, vol. 46, no. 30, pp. 5670–5703, 2007.
- [111] C. Luo, S. D. Stoyanov, E. Stride, E. Pelan, and M. Edirisinghe, "Electrospinning versus fibre production methods: from specifics to technological convergence," *Chemical Society Reviews*, vol. 41, no. 13, pp. 4708–4735, 2012.
- [112] W. Li and R. S. Tuan, "Fabrication and application of nanofibrous scaffolds in tissue engineering," *Current protocols in cell biology*, vol. 42, no. 1, pp. 25.2.1–25.2.12, 2009.
- [113] T. D. Brown, P. D. Dalton, and D. W. Hutmacher, "Melt electrospinning today: An opportune time for an emerging polymer process," *Progress in Polymer Science*, vol. 56, pp. 116–166, 2016.
- [114] M. Yousefzadeh, *Modeling and simulation of the electrospinning process*. Elsevier, 2017, pp. 277–301.
- [115] U. Ali, H. Niu, A. Abbas, H. Shao, and T. Lin, "Online stretching of directly electrospun nanofiber yarns," *RSC advances*, vol. 6, no. 36, pp. 30564–30569, 2016.
- [116] M. N. Shuakat and T. Lin, "Recent developments in electrospinning of nanofiber yarns," *Journal of nanoscience and nanotechnology*, vol. 14, no. 2, pp. 1389–1408, 2014.
- [117] T. Subbiah, G. Bhat, R. Tock, S. Parameswaran, and S. Ramkumar, "Electrospinning of nanofibers," *Journal of applied polymer science*, vol. 96, no. 2, pp. 557–569, 2005.
- [118] F. Anton, "Process and apparatus for preparing artificial threads," Oct. 2 1934, uS Patent 1,975,504.
- [119] G. Davino, L. Muccioli, F. Castet, C. Poelking, D. Andrienko, Z. G. Soos, J. Cornil, and D. Beljonne, "Electrostatic phenomena in organic semiconductors: fundamentals and implications for photovoltaics," *Journal of Physics: Condensed Matter*, vol. 28, no. 43, p. 433002, 2016.
- [120] K. Xiao, Y. Zhou, X.-Y. Kong, G. Xie, P. Li, Z. Zhang, L. Wen, and L. Jiang, "Electrostatic-charge-and electric-field-induced smart gating for water transportation," *ACS nano*, vol. 10, no. 10, pp. 9703–9709, 2016.
- [121] J. Hughes and H. Schaub, "Effects of charged dielectrics on electrostatic force and torque," in *International Workshop on Spacecraft Formation Flying*, 2017.
- [122] N. Bhardwaj and S. C. Kundu, "Electrospinning: a fascinating fiber fabrication technique," *Biotechnology advances*, vol. 28, no. 3, pp. 325–347, 2010.
- [123] T. J. Sill and H. A. von Recum, "Electrospinning: applications in drug delivery and tissue engineering," *Biomaterials*, vol. 29, no. 13, pp. 1989–2006, 2008.

- [124] B. Dmuth, A. Farkas, H. Pataki, A. Balogh, B. Szab, E. Borbs, P. L. Sti, T. Vigh, . Kiserdei, and B. Farkas, "Detailed stability investigation of amorphous solid dispersions prepared by single-needle and high speed electrospinning," *International journal of pharmaceutics*, vol. 498, no. 1-2, pp. 234–244, 2016.
- [125] H. Susanto, A. Samsudin, M. Faz, and M. Rani, "Impact of post-treatment on the characteristics of electrospun poly (vinyl alcohol)/chitosan nanofibers," in *AIP Conference Proceedings*, vol. 1725. AIP Publishing, Conference Proceedings, p. 020087.
- [126] F. Zhou, R. Gong, and I. Porat, "Mass production of nanofibre assemblies by electrostatic spinning," *Polymer International*, vol. 58, no. 4, pp. 331–342, 2009.
- [127] X. Wang, H. Niu, T. Lin, and X. Wang, "Needleless electrospinning of nanofibers with a conical wire coil," *Polymer Engineering Science*, vol. 49, no. 8, pp. 1582–1586, 2009.
- [128] M. S. Cosio, S. Benedetti, M. Scampicchio, and S. Mannino, *Electroanalysis in food process control*. John Wiley Sons, Ltd Chichester, UK, 2015, pp. 421–441.
- [129] A. L. Yarin, S. Koombhongse, and D. H. Reneker, "Taylor cone and jetting from liquid droplets in electrospinning of nanofibers," *Journal of applied physics*, vol. 90, no. 9, pp. 4836–4846, 2001.
- [130] H. F. Guo and B. G. Xu, "Numerical study of taylor cone dynamics in electrospinning of nanofibers," in *Key Engineering Materials*, vol. 730. Trans Tech Publ, Conference Proceedings, pp. 510–515.
- [131] J. Guerrero, J. Rivero, V. R. Gundabala, M. Perez-Saborid, and A. Fernandez-Nieves, "Whipping of electrified liquid jets," *Proceedings of the National Academy of Sciences*, vol. 111, no. 38, pp. 13 763–13 767, 2014.
- [132] D. Sadeghi, S. Karbasi, S. Razavi, S. Mohammadi, M. A. Shokrgozar, and S. Bonakdar, "Electrospun poly (hydroxybutyrate)/chitosan blend fibrous scaffolds for cartilage tissue engineering," *Journal of Applied Polymer Science*, vol. 133, no. 47, 2016.
- [133] N. Aliheidari, A. Ameli, and P. Potschke, "Solvent sensitivity of smart 3d-printed nanocomposite liquid sensor," in *Behavior and Mechanics of Multifunctional Materials and Composites XII*, vol. 10596. International Society for Optics and Photonics, Conference Proceedings, p. 105960V.
- [134] C. M. Hansen, *Hansen solubility parameters: a user's handbook*. CRC press, 2002.
- [135] Z.-M. Huang, Y.-Z. Zhang, M. Kotaki, and S. Ramakrishna, "A review on polymer nanofibers by electrospinning and their applications in nanocomposites," *Composites science and technology*, vol. 63, no. 15, pp. 2223–2253, 2003.
- [136] O. Jirsak, F. Sanetnik, D. Lukas, V. Kotek, L. Martinova, and J. Chaloupek, "Method of nanofibres production from a polymer solution using electrostatic spinning and a device for carrying out the method," Sep. 8 2009, uS Patent 7,585,437.

- [137] A. Luzio, E. Canesi, C. Bertarelli, and M. Caironi, “Electrospun polymer fibers for electronic applications,” *Materials*, vol. 7, no. 2, pp. 906–947, 2014.
- [138] R. Khajavi and M. Abbasipour, *Controlling nanofiber morphology by the electrospinning process*. Elsevier, 2017, pp. 109–123.
- [139] R. Erdem, I. Usta, M. Akalin, O. Atak, M. Yuksek, and A. Pars, “The impact of solvent type and mixing ratios of solvents on the properties of polyurethane based electrospun nanofibers,” *Applied Surface Science*, vol. 334, pp. 227–230, 2015.
- [140] T. Lin, H. Wang, H. Wang, and X. Wang, “Effects of polymer concentration and cationic surfactant on the morphology of electrospun polyacrylonitrile nanofibres,” *Journal of materials science technology*, vol. 21, no. Supplement 1, pp. 1–4, 2005.
- [141] M. Bercea, S. Morariu, C. Ioan, S. Ioan, and B. C. Simionescu, “Viscometric study of extremely dilute polyacrylonitrile solutions,” *European polymer journal*, vol. 35, no. 11, pp. 2019–2024, 1999.
- [142] P. Gupta, C. Elkins, T. E. Long, and G. L. Wilkes, “Electrospinning of linear homopolymers of poly (methyl methacrylate): exploring relationships between fiber formation, viscosity, molecular weight and concentration in a good solvent,” *Polymer*, vol. 46, no. 13, pp. 4799–4810, 2005.
- [143] S. L. Shenoy, W. D. Bates, H. L. Frisch, and G. E. Wnek, “Role of chain entanglements on fiber formation during electrospinning of polymer solutions: good solvent, non-specific polymerpolymer interaction limit,” *Polymer*, vol. 46, no. 10, pp. 3372–3384, 2005.
- [144] S. L. Shenoy, W. D. Bates, and G. Wnek, “Correlations between electrospinnability and physical gelation,” *Polymer*, vol. 46, no. 21, pp. 8990–9004, 2005.
- [145] A. Moriya, P. Shen, Y. Ohmukai, T. Maruyama, and H. Matsuyama, “Reduction of fouling on poly (lactic acid) hollow fiber membranes by blending with poly (lactic acid)polyethylene glycolpoly (lactic acid) triblock copolymers,” *Journal of membrane science*, vol. 415, pp. 712–717, 2012.
- [146] M. Estanqueiro, H. Vasconcelos, J. M. S. Lobo, and H. Amaral, *Delivering miRNA modulators for cancer treatment*. Elsevier, 2018, pp. 517–565.
- [147] C.-M. Hsu and S. Shivkumar, “Nano-sized beads and porous fiber constructs of poly (-caprolactone) produced by electrospinning,” *Journal of Materials Science*, vol. 39, no. 9, pp. 3003–3013, 2004.
- [148] Y.-K. Wu, L. Wang, J. Fan, W. Shou, B.-M. Zhou, and Y. Liu, “Multi-jet electrospinning with auxiliary electrode: The influence of solution properties,” *Polymers*, vol. 10, no. 6, p. 572, 2018.
- [149] X. Li, J. Lin, and Y. Zeng, “Electric field distribution and initial jet motion induced by spinneret configuration for molecular orientation in electrospun fibers,” *European Polymer Journal*, vol. 98, pp. 330–336, 2018.

- [150] C. Meechaisue, R. Dubin, P. Supaphol, V. P. Hoven, and J. Kohn, "Electrospun mat of tyrosine-derived polycarbonate fibers for potential use as tissue scaffolding material," *Journal of Biomaterials Science, Polymer Edition*, vol. 17, no. 9, pp. 1039–1056, 2006.
- [151] A. Balogh, R. Cselk, B. Dmuth, G. Verreck, J. Mensch, G. Marosi, and Z. K. Nagy, "Alternating current electrospinning for preparation of fibrous drug delivery systems," *International journal of pharmaceutics*, vol. 495, no. 1, pp. 75–80, 2015.
- [152] A. Balogh, B. Farkas, . Plvlgyi, A. Domokos, B. Dmuth, G. Marosi, and Z. K. Nagy, "Novel alternating current electrospinning of hydroxypropylmethylcellulose acetate succinate (hpmcas) nanofibers for dissolution enhancement: The importance of solution conductivity," *Journal of pharmaceutical sciences*, vol. 106, no. 6, pp. 1634–1643, 2017.
- [153] P. Pokorny, E. Kostakova, F. Sanetnik, P. Mikes, J. Chvojka, T. Kalous, M. Bilek, K. Pejchar, J. Valtera, and D. Lukas, "Effective ac needleless and collectorless electrospinning for yarn production," *Physical Chemistry Chemical Physics*, vol. 16, no. 48, pp. 26 816–26 822, 2014.
- [154] R. Kessick, J. Fenn, and G. Tepper, "The use of ac potentials in electro spraying and electrospinning processes," *Polymer*, vol. 45, no. 9, pp. 2981–2984, 2004.
- [155] S. Theron, E. Zussman, and A. Yarin, "Experimental investigation of the governing parameters in the electrospinning of polymer solutions," *Polymer*, vol. 45, no. 6, pp. 2017–2030, 2004.
- [156] R. Srivastava, *Electrospinning of patterned and 3D nanofibers*. Elsevier, 2017, pp. 399–447.
- [157] L. Wang and A. Ryan, *Introduction to electrospinning*. Elsevier, 2011, pp. 3–33.
- [158] S. De Vrieze, T. Van Camp, A. Nelvig, B. Hagström, P. Westbroek, and K. De Clerck, "The effect of temperature and humidity on electrospinning," *Journal of materials science*, vol. 44, no. 5, pp. 1357–1362, 2009.
- [159] J. Pelipenko, J. Kristl, B. Jankovi, S. Baumgartner, and P. Kocbek, "The impact of relative humidity during electrospinning on the morphology and mechanical properties of nanofibers," *International journal of pharmaceutics*, vol. 456, no. 1, pp. 125–134, 2013.
- [160] G.-Z. Yang, H.-P. Li, J.-H. Yang, J. Wan, and D.-G. Yu, "Influence of working temperature on the formation of electrospun polymer nanofibers," *Nanoscale research letters*, vol. 12, no. 1, p. 55, 2017.
- [161] H. Abdollahi, M. Samkan, and M. M. Hashemi, "Facile and fast electrospinning of crystalline zno 3d interconnected nanoporous nanofibers for ammonia sensing application," *Microsystem Technologies*, vol. 24, no. 9, pp. 3741–3749, 2018.
- [162] Y. Park, H. Lim, J.-H. Moon, H.-N. Lee, S. Son, H. Kim, and H.-J. Kim, "High-yield one-pot recovery and characterization of nanostructured cobalt oxalate from spent lithium-ion batteries and successive re-synthesis of licoo<sub>2</sub>," *Metals*, vol. 7, no. 8, p. 303, 2017.

- [163] L. Singh, A. Kumar, H. Lee, J. Lee, M. Ji, and Y. Lee, "Ultrafast auto flame synthesis for the mass production of licoo 2 as a cathode material for li-ion batteries," *Journal of Solid State Electrochemistry*, vol. 22, pp. 2561–2568, 2018.
- [164] O. Chiscan, I. Dumitru, V. Tura, and A. Stancu, "Pvc/fe electrospun nanofibers for high frequency applications," *Journal of Materials Science*, vol. 47, no. 5, pp. 2322–2327, 2012.
- [165] X. Huang, D. Bahrolloomi, and X. Xiao, "A multilayer composite separator consisting of non-woven mats and ceramic particles for use in lithium ion batteries," *Journal of Solid State Electrochemistry*, vol. 18, no. 1, pp. 133–139, 2014.
- [166] R. Kumar, R. K. Sharma, and A. P. Singh, "Grafted cellulose: a bio-based polymer for durable applications," *Polymer Bulletin*, vol. 75, no. 5, pp. 2213–2242, 2018.
- [167] C. Shi, J. Dai, C. Li, X. Shen, L. Peng, P. Zhang, D. Wu, D. Sun, and J. Zhao, "A modified ceramic-coating separator with high-temperature stability for lithium-ion battery," *Polymers*, vol. 9, no. 5, p. 159, 2017.
- [168] Z. Li, G. Liu, M. Guo, L.-X. Ding, S. Wang, and H. Wang, "Electrospun porous vanadium pentoxide nanotubes as a high-performance cathode material for lithium-ion batteries," *Electrochimica Acta*, vol. 173, pp. 131–138, 2015.
- [169] D. Yu, C. Chen, S. Xie, Y. Liu, K. Park, X. Zhou, Q. Zhang, J. Li, and G. Cao, "Mesoporous vanadium pentoxide nanofibers with significantly enhanced li-ion storage properties by electrospinning," *Energy Environmental Science*, vol. 4, no. 3, pp. 858–861, 2011.
- [170] Y. L. Cheah, R. von Hagen, V. Aravindan, R. Fiz, S. Mathur, and S. Madhavi, "High-rate and elevated temperature performance of electrospun v2o5 nanofibers carbon-coated by plasma enhanced chemical vapour deposition," *Nano Energy*, vol. 2, no. 1, pp. 57–64, 2013.
- [171] Y. L. Cheah, N. Gupta, S. S. Pramana, V. Aravindan, G. Wee, and M. Srinivasan, "Morphology, structure and electrochemical properties of single phase electrospun vanadium pentoxide nanofibers for lithium ion batteries," *Journal of Power Sources*, vol. 196, no. 15, pp. 6465–6472, 2011.
- [172] D. Wang, L. Cao, J. Huang, and J. Wu, "Synthesis and electrochemical properties of liv3o8 via an improved solgel process," *Ceramics International*, vol. 38, no. 4, pp. 2647–2652, 2012.
- [173] M. Nasir, H. Matsumoto, M. Minagawa, A. Tanioka, T. Danno, and H. Horibe, "Preparation of porous pvdf nanofiber from pvdf/pvp blend by electrospray deposition," *Polymer journal*, vol. 39, no. 10, p. 1060, 2007.
- [174] T. E. Newsome and S. V. Olesik, "Electrospinning silica/polyvinylpyrrolidone composite nanofibers," *Journal of Applied Polymer Science*, vol. 131, no. 21, 2014.
- [175] S. Peng, L. Li, J. K. Y. Lee, L. Tian, M. Srinivasan, S. Adams, and S. Ramakrishna, "Electrospun carbon nanofibers and their hybrid composites as advanced materials for energy conversion and storage," *Nano Energy*, vol. 22, pp. 361–395, 2016.

- [176] E. Tavakkol, H. Tavanai, A. Abdolmaleki, and M. Morshed, "Production of conductive electrospun polypyrrole/poly (vinyl pyrrolidone) nanofibers," *Synthetic Metals*, vol. 231, pp. 95–106, 2017.
- [177] C. Zhu, J. Shu, X. Wu, P. Li, and X. Li, "Electrospun v2o5 micro/nanorods as cathode materials for lithium ion battery," *Journal of Electroanalytical Chemistry*, vol. 759, pp. 184–189, 2015.
- [178] N. Aliahmad, M. Agarwal, S. Shrestha, and K. Varahramyan, "based lithium-ion batteries using carbon nanotube-coated wood microfibers," *IEEE Transactions on Nanotechnology*, vol. 12, no. 3, pp. 408–412, 2013.
- [179] A. Magasinski, P. Dixon, B. Hertzberg, A. Kvit, J. Ayala, and G. Yushin, "High-performance lithium-ion anodes using a hierarchical bottom-up approach," *Nature materials*, vol. 9, no. 4, p. 353, 2010.
- [180] H. Giesche, "Mercury porosimetry: a general (practical) overview," *Particle & particle systems characterization*, vol. 23, no. 1, pp. 9–19, 2006.
- [181] Z. Zhang, X. Li, C. Wang, S. Fu, Y. Liu, and C. Shao, "Polyacrylonitrile and carbon nanofibers with controllable nanoporous structures by electrospinning," *Macromolecular Materials and Engineering*, vol. 294, no. 10, pp. 673–678, 2009.